

Alma Mater Studiorum – Università di Bologna

DOTTORATO DI RICERCA IN

Ingegneria elettronica, telecomunicazioni e tecnologie
dell'informazione

Ciclo XXXI

Settore Concorsuale: 09/E3 - ELETTRONICA

Settore Scientifico Disciplinare: ING-INF/01 – ELETTRONICA

EEG system design for VR viewers and
emotions recognition

Presentata da: ANDREA VERDECCHIA

Coordinatore Dottorato

ALESSANDRA COSTANZO

Supervisore

BRUNO RICCO'

Esame finale anno 2019

Abstract

BACKGROUND: Taking advantage of virtual reality today is within everyone's reach and this has led the large commercial companies and research centers to re-evaluate their methodologies. In this context the interest in proposing the Brain Computer Interfaces (BCIs) as an interpreter of the *personal* experience induced by virtual reality viewers is increasing more and more.

OBJECTIVE: The present work aims to describe the design of an electroencephalographic system (EEG) that can easily be integrated with virtual reality viewers currently on the market. The final applications of such system are several, but our intention, inspired by Neuromarketing, wants to analyze the possibility of recognize the mental state of *like* and *dislike*.

METHODS: The design process involved two phases: the first relating to the development of the hardware system that led to the analysis of techniques to obtain the most possible *clean* signals; the second one concerns the analysis of the acquired signals to determine the possible presence of characteristics which belong and distinguish the two mental states of like and dislike, through basic statistical analysis techniques.

RESULTS: Our analysis shows that differences between the like and dislike state of mind can be found analyzing the power in the different frequencies band relative to the brain's activity classification (Theta, Alpha, Beta and Gamma): in the like case the power is slightly higher respect the dislike one. Moreover we have found through the use of logistic regression that the EEG channels F7, F8 and Fp1 are the most determinant component in the detection, along with the frequencies in the Beta-high band (20-30 Hz).

CONCLUSIONS: At the end of this work we have obtained a system completely integrable in virtual reality viewers and fully functional. However, it is necessary to continue with a more in-depth analysis regarding the recognition of the mental states of like and dislike because, given the vastness of the relative theoretical field, it is certainly possible to arrive at better results.

Contents

Introduction	iii
1 The <i>VeeRg</i>: an EEG system for VR	1
1.1 Neuromarketing and virtual shops	2
1.2 Medical rehabilitation and virtual reality	6
1.3 How the brain works	7
1.3.1 Brain's waves classification	9
1.4 Electrodes' placement	10
1.5 The prototype idea	12
2 The <i>VeeRg</i> design: deals and choices	15
2.1 Hardware design	15
2.1.1 Analog power supply and input referred noise	18
2.1.2 The common mode noise and the feedback loop	20
2.1.2.1 CM2DM in electrodes mismatch	31
2.1.2.2 CM2DM in input stages mismatch	33
2.1.2.3 Limits for stability	38
2.2 Firmware design	43
2.2.1 Filtering	46
2.2.1.1 FIR and IIR	47
2.2.1.2 The high-pass filter	50
2.2.1.3 Filtering effect	51
3 Like and dislike recognition	61
3.1 Related research	64
3.2 Test definition and data recording	67
3.3 Analysis of data	69
Conclusion	79

A Schematics and Code	81
A.1 Schematics	81
A.2 Code	94
A.2.1 Biquad filters	94
A.2.2 Commands decoder	95
List of figures	99
Bibliography	101

Introduction

Many things have changed since Ivan Edward Sutherland in 1968 introduced the first prototype virtual reality (VR) viewer. Perhaps, it would be better to specify that there have been many progresses made since that day in the technological field, but few have been made in the cultural one. Virtual reality has always aroused great curiosity in the imagination of us all. Curiosity often contaminated by the countless stories that literature and cinema have given us over the years and that have brought virtual relativity to be seen with a look of wonder and at the same time concern. This until 2014, when it can be said that the era of virtual reality available to anyone actually began. In that year a new company, the Oculus VR, puts on the market the first development kit based on a wearable virtual reality viewer. The product boom was imminent and at least inevitable, attracting to itself the interest of those who until then thought that virtual reality belonged to a distant future. Let's be clear that we are talking about a relative young technology that currently involves only the sight and the hearing, still far from that described by literature and cinema, and still characterized by the impossibility of completely immersing oneself in an artificial world that simultaneously involves *all* our senses. But if we consider that the dominant sense is the sight, then it is clear that among the various types of settings that can be proposed through virtual reality, are those 3D (and therefore visual) to receive and to convey a greater interest today. This is the reason why virtual environments must be characterized first of all by excellent visual qualities, therefore able of propose themselves as substitutes for reality, while the other senses seem to have a less influential weight, at least until nowadays since that technological progress is aiming to fill this gap (see, for example, haptic sensors).

It is quite normal to think that virtual reality has as its main application field the recreational one or, more generally, the entertainment, given its high commercial potential. Some companies in the sector have put their own viewers on the market for a few years to try and get their market share. Consequence of this is that currently you can find virtual reality viewers of various brands that meet the needs of everyone. And the really interesting thing is that they satisfy

especially the need of the world of scientific research. For example, the medical is one of those areas where the use of virtual reality viewers is currently having very interesting and satisfying results. In fact, medical devices are being released that, for example, allow patients suffering from severe deficit due to stroke to accelerate their rehabilitation through sessions in which, immersed in a virtual world, they have to complete what apparently may appear to be games but which in reality they are used to stimulate and restore the injured part of the body. Another example, this time belonging to the field of psychology, is the use of the viewers to put in certain mental conditions the patients who suffer from pathologies such as anxiety, depression, phobias etc. : bring the patient in state of stress recreating a virtual environment that represents the cause of his pathology allows to keep under control the triggering stimuli and go deeper in the therapeutic investigation.

Another example of the use of VR viewers that we want to describe is the one which allows us to introduce more effectively the reason of present work. Example that regards a new branch of marketing aimed at investigating the interests of consumers, studying their behavior during their shopping times, through the use of new technologies made available by the progress: this branch is called Neuro-marketing. The idea for our work arose from the request of a company that was interested in the creation of a virtual reality system that re-proposed a common investigatory test to analyze what was the best arrangement of a product on the supermarket shelves. This test was and still is carried out through the analysis of the behavior of physical peoples placed inside a real shop: the tester is asked to perform normally shopping, then they takes note of his behavior and at the end of the shopping session he is asked what were the most interested products and which were not. Given the lack of practicality of the test and the time needed to prepare different scenarios to analyze (products arranged differently on the shelves), the company requested to transpose everything in virtual reality. In this way there would not have been any need of ample space to recreate a real supermarket and especially it would have drastically reduced the setting time. Leaving aside all the problems related to the creation of such virtual environments, what has been extremely interesting was to consider the possibility of integrating the final phase of the test (asking if a product had been appreciated or not) directly during the session of shopping without being interrupted in any way. At first it was thought to use the technique of tracking the pupil to understand what the tester was actually observing, but this alone could not give clear information on its real intentions and also there would be problems at the implementation level. The idea then was to use an electroencephalographic (EEG) system that, in order to make everything as practical as possible, would go to integrate discretely into the virtual reality viewer

already available for use and applied only on the front of the face.

The main question at this point was: is it possible through electroencephalography to understand if someone is liking something or not? The answer was not difficult to find, given that at the moment there are many researches carried out especially in the neurological field on the analysis of the brain's activity in the phases of liking and not. Numerous articles have highlighted certain characteristics in the brain wave trends, taken through the use of electroencephalographic systems made for medical investigation, which have led to the possibility of discriminating these two states of mind. These characteristics are very different and concern both the trend in time and frequency domain. The results of these studies, however, do not fully meet our demand because in them it has been normally used a *complete* electroencephalographic systems, i.e. with electrodes that cover the entire area of the brain which means the whole head. A question then remained: can the two states of like and dislike be discerned through the use of the frontal electrodes only? Hence the idea of our project.

It's undoubtedly the applicative utility of a viewer that, in addition to bringing the user into a virtual environment, simultaneously analyzes his emotional state. Big companies for the shopping on-line are currently starting to invest in the development of their virtual stores; the intention is to bring users to be able to make purchases at home in virtual environments built ad hoc. If the system were to be able to know what is being felt during use, then the whole virtual store could be adapted to the user's wishes at that precise moment. And this for companies certainly means increasing sales. The application field of this system is not limited only to that of Neuromarketing, but would also extend to those previously described, such as the medical. Having a virtual device able to perform an electroencephalographic acquisition in real-time and eventually specific elaborations on them can represent the key point to get that extra information which can be determinant in a certain type of medical investigation. If the user's emotional state could be detected, the virtual environment could consequently adapt itself to the best in order to recreate the optimal conditions and increase its effectiveness.

Then, the present work is intended to design and implement an electroencephalographic system (EEG) specially for the use in the virtual reality viewer (VR), that could be seen as an hardware plug-in. The final target is to recognize the *like* and/or *dislike* state of mind, specially for Neuromarketing purpose, starting from the information coming from the brain's waves acquisition. We named our prototype system *VeeRg* which is a merge between EEG and VR acronyms.

In the first chapter we'll introduce the reader to the main conceptual arguments relate to the design of such system: we'll come back to the neuromarketing and

medical arguments, we'll show how the brain works and the way we can read information from it, and finally we'll show the taken choices for our VeeRg system.

In the second chapter we'll see the main problem a designer of electroencephalographic systems is used to deal with. In the first part an hardware point of view of the design will be proposed, focusing on the most important target reached to obtain an high quality electroencephalographic signal: the implementation of perfect analog references for the analog to digital conversion and the analysis of *Common Mode Rejection* (CMR) which is a fundamental technique in such systems. In the second part, the VeeRg design will be analyzed from a software point of view, where the choices about the signals post-processing will be treated.

In the third and last chapter we'll introduce the state of the art of the emotional recognition through the description of two research made on the detection of the like and dislike state of mind in commercial field. Then we'll present our test implementation to acquire the data from a sample of ten subjects and finally we'll analyze them following the method proposed by one previous research to find the most discriminative frequencies and EEG channels in the like/dislike recognition.

Chapter 1

The *VeeRg*: an electroencephalographic system for the virtual reality

The *Brain-Computer Interface* (BCI) concept steams from the older *Human-Computer Interface* (HCI). The reasonable difference is that the BCI are born necessarily when the HCI become useless in particular contexts. Take as example a patient unable to command his electrical wheelchair through the common joystick (seen as HCI) because his illness affected the hands; in this particular, but not so unusual, case what is used to do is to interface the patient to the machine through the acquisition of the bio-electrical signals which can derive from the arm's muscles or directly from the brain. With the BCI term then we intend a wide type of system that have all the characteristic to acquire informations from the brain, useful to help the user in all kinds of ways. From this point of view it's easy understand the importance of the BCI application in the medical aid environment, but in the last years the interest on this systems has grown also in other fields, like the commercial one.

The purpose of the present research is born right from the growing request by many commercial companies of a system which simplifies the investigation test to improve own proceeds. Take for example a supermarket chain which want to analyzes the better solution in the product's disposition on the shelves. There are a lot of studies that describe the influence of disposal and visual impact of products inside a store, but the most effective test is to recreate *in vitro* a similar environment in which real people can make shopping under the attention of commercial researchers which analyze their behaviors relative to different disposition of products. But reproduce such test is so expensive in terms of money and time that they

begin to use the virtual reality as substitute. In this case the tester is asked to wear a VR viewer which brings him in a virtual store where move and reproduce a shopping session. And if we could know automatically what the tester is liking or disliking without ask to him through a *simple* and *discrete* electroencephalographic acquisition, that would be gold for all the companies which want to improve their own proceeds. This kind of strategies belong to a new branch of marketing which use all the informations coming from the unconscious (but unaffected) signals of the customer: the *Neuromarketing*.

Also in the medical field the interest for the virtual reality grew up in the last years thanks to the power of its immersive characteristic useful to speed up the rehabilitation of patients affected by illness like strokes, phobias, motion issue and so on. And again, in this medical contest, featuring an virtual reality viewer with an electroencephalographic system could bring to a deeper investigation of illness in the diagnosis phase or rehabilitation session.

Anyway, the two cases above should be enough to understand the importance of the growing use of virtual reality systems in both the medical and commercial fields, and the usefulness to integrate an electroencephalographic system in them as a generic BCI, creating in this way a powerful device for deep investigation (specifically for the marketing).

The present work is intended to design and implement an electroencephalographic system (EEG) specially for the use in the virtual reality viewer (VR); it should be seen as an hardware plug-in. The final target is to recognize the *like* and/or *dislike* state of mind, specially for Neuromarketing purpose, starting from the information coming from the brain's waves acquisition. We named our prototype system *VeeRg* which is a merge between EEG and VR acronyms. In the next sections of the present chapter, we'll introduce the reader to the main conceptual arguments relate to the design of such system: we'll come back to the Neuromarketing and medical arguments, we'll show how the brain works and the way we can read information from it, and finally we'll show the taken choices for our *VeeRg*.

1.1 Neuromarketing and virtual shops

The Neuromarketing is a powerful instrument available to marketers which allow them to "enter in consumer's minds" in order to discover what kind of emotion drive purchase decisions. By definition, the Neuromarketing can also be described as a place where Neurosciences, which study the functioning mechanisms of our brain, meet marketing. Since several years it is used by brands with the aim of

increasing publicity effects on consumers, to create successful new products and brands, to find new methods able to convince people in doing or buying things. But understanding the human mind's mechanisms has always been a complex mysterious work so that marketing experts, in the last ten years, became always more passionate about man's brain. In this context, Neuromarketing became helpful for our study.

We are constantly overwhelmed by the information and also if we are convinced about our rational decision, actually, the choice is always also emotive. There's no choice in life which disregards emotions. Therefore, in the company's creative departments, the research focuses on the ability to create an emotional response to an advertisement or a promotion. During the last decades, marketing's studies researched different methods to comprehend and measure those emotional responses in order to determine advertisers' messages efficiency. The Neuromarketing studies created and offer tools able to predict the performance of the product on the market. In a certain level, it represents the evolution of *focus group*¹, apart from the fact that it requires more effort for the brain trying to lie or to give an uncertain answer because of the suffering from colleagues' pressure. Indeed, the rational response of consumers to surveys or questionnaires is often conditioned by various factors, whether they are more or less aware of it. From one side, often individuals try to give "the right" answer because, being social for nature, they continuously seek other people approval, and that factor influences their choices and behaviors. On the other side, what individuals think to feel doesn't correspond to the reality.

"It is not possible to ask people their impression on a smell or a tactile sensation or a flavor. It is difficult to verbalize a sensation because we don't have the right vocabulary to do that. In 2008, I conducted the biggest Neuro-marketing experiment in the world using the functional magnetic resonance to scan customer's brain in order to understand what really happened in the unconscious part of the brain. The idea of the experiment is based on the fact that if we are able to give a sense to the unconscious part of the brain – which manages the 85% of what we do every day – we will be closer to discover what we really feel when we daily buy something. Basing on that

¹A focus group is a small, but demographically diverse group of people and whose reactions are studied especially in market research or political analysis in guided or open discussions about a new product or something else to determine the reactions that can be expected from a larger population. It is a form of qualitative research consisting of interviews in which a group of people are asked about their perceptions, opinions, beliefs, and attitudes towards a product, service, concept, advertisement, idea, or packaging. Questions are asked in an interactive group setting where participants are free to talk with other group members. During this process, the researcher either takes notes or records the vital points he or she is getting from the group. Researchers should select members of the focus group carefully for effective and authoritative responses. (*Wikipedia*)

Neuromarketing Tools		
Metabolic Brain's Activities	Electrical Brain's Activities	Without Brain's Activities
<ul style="list-style-type: none"> • Position Emission Tomography (PET) • Functional Magnetic Resonance Imaging (fMRI) 	<ul style="list-style-type: none"> • Electroencephalography (EEG) • Magnetoencephalography (MEG) • Steady State Topography (SST) • Transcranial Magnetic Stimulation (TMS) 	<ul style="list-style-type: none"> • Eye tracking • Skin conductance • Facial coding • Facial electromyography

Table 1.1: Classification of Neuromarketing tools.

fact, we could maybe search advertising campaigns a little more successful than the ones which are present nowadays."²

In order to better understand the growing importance of the Neuromarketing, it is enough to point out the example of the *Associazione Italiana di Neuromarketing* (AINEM), association born in 2016, which propose to develop the culture and the practice of the marketing into the Italian companies, universities and professionals³. It's vice president, Francesco Gallucci, confirm the constant increase of the interest on this matter, affirming that in 2017 has been created all over the world more than three thousand of agencies which offer Neuromarketing's services⁴. Such agencies have at their disposal a very large quantity of tools in order to carry out their studies, but it is not difficult to understand the reason why the major part of them come from the medical field. In Tab. 1.1 are indicated different methods of investigation, divided depending on the typology of the source of information, has described from [1].

The viewer for virtual reality begins to enter into the present context from the moment that important agencies which operate on the market, most of all on-line, began slowly to interest on proposing their products to customers who are sitting comfortably at their home. Web agencies such as Amazon or eBay, but

²Martin Lindstrom, expert for Neuromarketing and for both corporate and consumer branding.

³Web site of AINEM: [HTTP://www.ainem.it/](http://www.ainem.it/)

⁴<http://www.ainem.it/news/notizie/intervista-del-prof-francesco-gallucci-a-pubblicita-italia-per-il-corso-neurobranding/>

also *physical* companies as the American Walmart, which shops are all over the U.S. area, are pushing in creating what is going to be their virtual shop, where customers can access simply wearing a virtual viewer. But is not such an easy matter as it can seem, because if the idea is to use the viewer as a means to recreate a conventional shop, then it will be completely lost the fundamental point under which such technologies, together, can radically change the way people use to shop, and not only that: entering into a place where products adapt to your interest in that specific moment, interact with shop workers who understand what you really search, enter into the recording studio with the musician who shows the process he lived until the creation of his last album which you would like to buy, etc. This is the reason we need to change the concept of interactivity, which until nowadays is characterized by the conscious willing of the customer to make use of a physical tool to interface to the web and virtual worlds. It is exactly at this point that became useful the Neuromarketing tools, described in Tab. 1.1. This is the starting point of the process which brought to the realization of the VeeRg: recognize if what we are observing is to your liking or not, under certain points of view, is an invaluable information, as it would allow to automatically adapt the virtual experience (whatever it is, A/N) to its own interests of the moment.

It is necessary to specify that although the interest toward the virtual viewer is constantly increasing, their technologies are relatively young and there are still many problems related to them. It is known, for example, that during the first sections of tests, wearing the virtual mask can bring into an uncomfortable state which can also lead to nausea and vomit. For example, into a virtual experience where the subject can move walking through a controller when actually the body is still, the player brain get destabilized, causing the sensation of vertigo. Everything is strictly linked to the typology of experience and to the ability of the virtual reality programmers to reduce this nausea effect. That defects also represents the reason why the market of AR (Augmented Reality) viewer is still competitive, as they make use of common transparent and not focused glasses on which advanced technologies project the information about the surrounding environment. In this way, the consumer never loses completely the connection with the reality, avoiding that the brain goes haywire. Although if with a high level of quality, these systems of increased reality have also very high costs⁵ and obviously they will never be able to give the sense of a complete immersion into a totally artificial world.

⁵At present the state of the art of AR viewers is represented by the *Magic Leap*.

1.2 Medical rehabilitation and virtual reality

As for Neuromarketing, virtual reality offers an innovative approach in supporting the functional recovering of the physical skills in patients affected by cognitive disorders (during the initial phases), motor disorders caused by medical conditions like strokes or Parkinson, psychological disorders like anxiety, stress, or phobias. This methodology consists of the execution of specific virtual programs aimed to improve the exercise upon the compromised body functions, in order to manage, reduce, overcome, or compensate the deficit. The recovering program is based on the execution of activities with a gradual level of difficulty within an immersive device which simulates in a realistic and interactive way different situation taken from the daily life context. Big medical companies already began to approach this kind of therapies creating specific recovering areas fitted with virtual environments, using their own denomination: for example, in Italy, they talk about the *Telepresenza Immersiva Virtuale* (TIV)⁶, in America it has been implemented the *Virtual Reality Exposure Therapy* (VRET), and other examples can be listed. Different names with a common objective: the immersion into a virtual environment which allows patients to feel certain sensations and to live situations as they would happen in the real place, facing their phobias or anxieties due to certain traumas lived in the past which created psychological difficulties in present life.

The physical therapy could offer a huge number of examples of potential applications of virtual reality for medical purposes, and all of them are characterized by the necessity to give to the subject the sensation of total immersion into an environment specifically created for the therapy which doctors are taking in consideration. Often the aim is to push the patient toward the boundaries of his pathology; in case of paralysis due to an stroke, for example, what should be better to do is to put the patient into a context where he is brought to make determined movements which born spontaneously on an unconscious level, because of the specific environment proposed it. Another field where the virtual reality is already considered is Psychology⁷. An emblematic example is represented by a patient who developed a form of acute anxiety which blocked him in driving the car in the place where he made an accident. This patient was hilled through the (VRET): doctor and patient came back on the specific place of the accident making use of virtual reality and

⁶The TIV recovering programs bases on the execution of activities with a gradual level of difficulty within an immersive device (CAVE) which simulates in an extremely realistic and interactive way different situation taken from the daily life context. The CAVE is a system achieved in dialogue with the Italian Ministry of Helth and with the support of *Forge Reply*, agency expert in the implementation on innovative hardware and software.

⁷Is to notice the Limbix system.

the doctor could guide the patient into this emotional experience. Other emblematic cases can be represented by therapies which took care of those pathologies due to traumas coming from the war [24] or particular terrifying events like the World Trade Center attempt [4][23]. The virtual reality could become a valid help to afford not only the fear of driving, as the previous example, or the fear of high, or the one of talking in front of a public, or of spider, just to mention some examples; it can also create a calm and relaxing environments when patients live a moment of anxiety.

Also in the medical environment is not difficult to note the increasing help which virtual reality can and will bring. It is consequently easy to come to the conclusion that a virtual system already equipped with electroencephalographic functions can represent an interesting product to facilitate the process of therapy of a patient, whatever is his pathology. As is known, on the market are already present solutions to integrate the electroencephalography into the virtual viewers. This solutions have all got a good level of quality, but integrate a viewer with the electroencephalographic functions means work to improve its comfortableness and its size because, the more the patient will be unaware about the presence of the mask, the more he will concentrate on the action, improving the results coming from its use. And even if some companies already began to try to produce such all-in-one system, we must observe that this kind of production is still at the beginning of its process of growth.

1.3 How the brain works and which informations we are dealing with

The electroencephalography is a medical inspection technique which reads the distributed electrical activity (or potential) on scalp's area of the patient, generated by the particular structure of the brain. Unlike electrocorticogram, which requires the use of electrodes on the cerebral cortex, or even electrogram, which makes use of probes pushed deep inside different brain's areas, the electroencephalography is a completely non-invasive practice since it utilizes electrodes softly leaned against the head surface. This is a fundamental characteristic, which allows the practice to be safe, reproducible and practically without limitations.

How can the superficials potentials related to the internal activity of the brain be created?

As soon as the brain's cells (neurons) are activated, local electrical flows start to be generated. The EEG measures the currents related to the synaptic excitation

of many pyramidal neurons' dendrites located on the cerebral cortex. Electrical potential differences arise from the sum of the post-synaptic potentials of the pyramidal cells, which create electrical dipoles between the soma (neuronal body) and the apical dendrites (neural branches).

The electrical current generated into the brain is composed by Na^+ , K^+ , Ca^{++} e Cl^- ions, which are transferred through specific channels within the neuronal membrane. The microscopic detailed image is illustrated in Fig. 1.1. Only a big amount of active neurons can generate electrical activity revealed on the head surface. From the neuronal layers to the electrodes, the electrical current needs to pass through the skin, the skull and different other layers. The weakest electric signals detected from the electrodes on the scalp has to be conveniently amplified in order to visualize them on the paper (or medical device's monitor) and maybe to save them.

From the anatomical point of view, the brain can be divided into three sections: the brain, the cerebellum and the brain stem. The brain is composed by the left and the right hemispheres enveloped by a superficial layer called cerebral cortex. The cortex is a dominant element of the central nervous system. Into the brain there are centers dedicated to the initial phases of body movements, to the conscious awareness of sensations, to complex analysis and to the expression of emotions and behaviours. The cerebellum coordinates the volunteer muscular movements and the maintenance of the body balance. The brain stem controls the breathing, heart regulation, the biorhythm, the hormonal secretion, etc. Due to its superficial position, the cerebral cortex plays a fundamental role in the detection

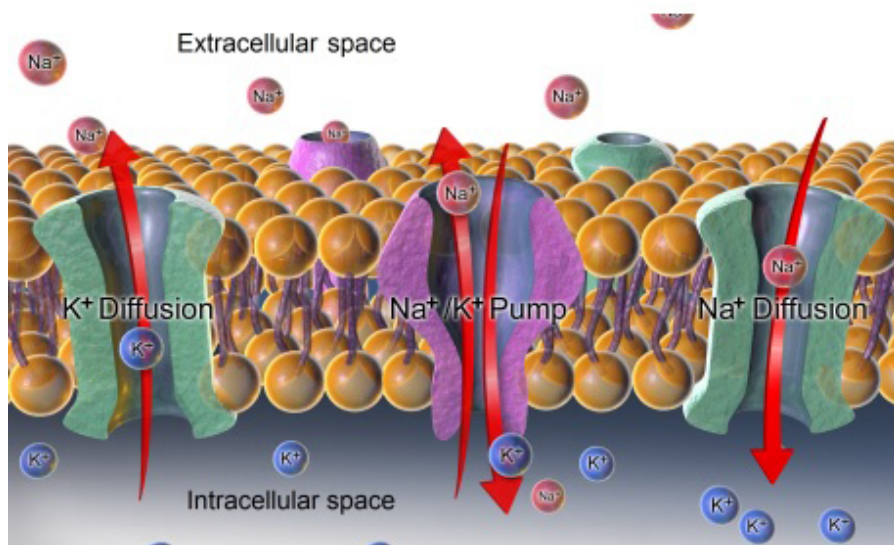


Figure 1.1: Flux of Na^+ , K^+ , Ca^{++} e Cl^- ions through neural membrane, which is the source of so called *membrane potential*.

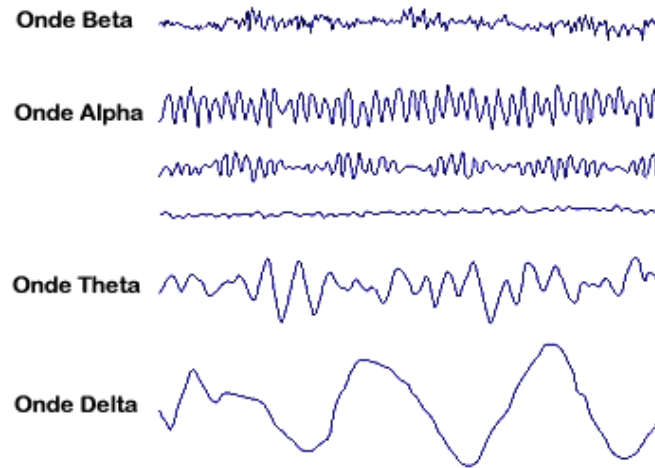


Figure 1.2: Brain's waves classification. Starting from lower frequencies we find the *Delta* waves, then *Theta*, *Alpha* and last *Beta*.

of the neurological activity through EEG.

1.3.1 Brain's waves classification

The EEG potentials, resulting from the activity of the neurons, are in the range of about 1-150 μV . Although there are a lot of analysis based on the time-domain response to specific sensory stimuli (*evoked potentials*, EP), the main information is still their frequency characteristic with the band between about 0.4-80 Hz.

The most significant frequencies discovered in the medical field are divided into four bands related to the different states of mind:

- *Delta*: the band from 1 to 3 Hz. Detectable in children's temporoparietal areas, they often appear in adults exposed to emotional stresses.
- *Theta*: the band from 4 to 7 Hz. They are indicators of the deep sleep of an individual and have an amplitude between 1 μV and 200 μV .
- *Alpha*: the band from 8 to 12 Hz. They have an amplitude of around 50 μV and are detectable mostly in the occipital area of the cerebral cortex. They correspond to an awake state with eyes closed or to a resting state; for this reason, this typology of waves completely disappear as the individual switch into an attentive and concentrated state of mind.
- *Beta*: the band from 13 to 30 Hz. They can be classified into three subcategories: low-Beta waves (13-16 Hz, *Beta 1*), Beta waves (16-20 Hz, *Beta 2*) and high-Beta waves (20-30 Hz, *Beta 3*). These typologies of waves are strictly connected to a conscious state of mind. That is the reason why they are the

most interesting for our analysis but, at the same time, they are the most complex as they appear during different phases of general active thought: focusing in the resolution of a problem or concentrating in the study or carrying out a particular activity or simply thinking on specific thing.

- *Gamma*: the band from 30 to around 100 Hz. Involved in the formation of percepts and memory, linguistic processing, and other behavioral and perceptual functions. Increased gamma-band activity is also involved in associative learning.

Basing on the description of the main brainwaves, it is easy to understand why the VeeRg system, object of the present work, has been implemented focusing on the Beta waves. Their engagement in almost the totality of the action that an individual can perform in daily activities, make them particularly interesting in the design of a digital systems able to detect the intentions and the different states of mind of the user who is wearing it. Furthermore, this typology of waves is concentrated mostly in the frontal part of the cortex, which makes them an optimal object of analysis as soon as our system's electrodes will be positioned exactly in that area of the cerebral cortex (see Par. 1.4).

The fact that Beta waves are basically associated with awake actions does not necessarily rule out the presence involved by the other typologies of waves; actually, in an EEG acquisition during an awake state of mind, it's easy to notice the Delta, Theta waves appearing, or even Alpha waves, which are usually positioned in the occipital part of the cerebral cortex. Then we have to keep in mind that the final information will result from a combination of all that waves, technically speaking from all the band ranging in 0.4-80 Hz, no matter of which signals are going to be acquired.

1.4 Electrodes' placement

There is an international Standard for the placement of the electrodes, which name is characterized by a couple of numbers (e.g. the 10-20 system, Fig. 1.3a). These numbers referred to the distance, expressed in percentage, between two contiguous electrodes, referred to the total one between the point of the skull named *inion* (protrusion located at the base of the occipital bone) and the starting point of the nose bone (a total of around twenty electrodes in the 10-20 system). It needed to keep in mind that it is not a strict rule for electroencephalographic measurement; anyone can place the electrodes in his own way, but following the standard helps

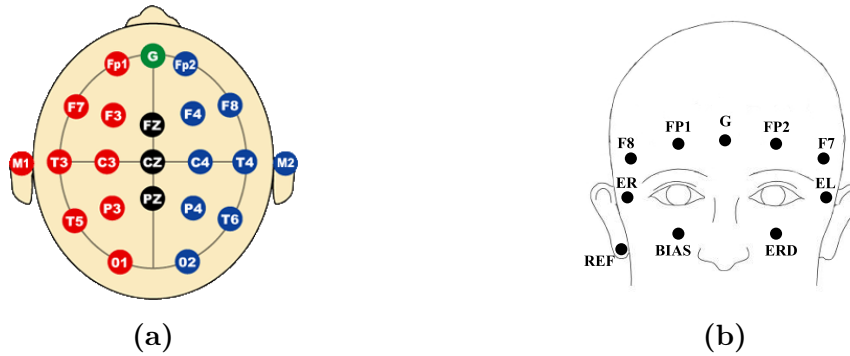


Figure 1.3: Electrodes' placement in the 10-20 standard configuration (a) and the placement's in the VeeRg system (b).

to indicate and recognize specific electrode connected to specific areas of head without ambiguity. Then, each electrode is marked by an abbreviation (commonly one or a couple of characters) which identifies the region of the cerebral cortex (Fp = Frontal-Parietal, F = Frontal, C = Central, P = Parietal, T = Temporal e O = Occipital) and a number which refers to one hemispheres (odd number = left hemisphere, even number = right hemisphere) or a "z" in case the electrode is placed on the midline saggital plane of skull.

The electroencephalographic data recording use a couple of electrodes; each couple represents a specific channel for the reading device, corresponding to the potentials difference between the two electrodes. Consequently, there can be different EEG lectures, but all of them starts from the basic assumption that each electrode placed on the head has a specific reference. That reference can be chosen based on the type of test we are going to perform; for example, it can be related to the electrode signal coming from the top of the skull (Cz in 10-20); it can result from the average of all signals coming from all electrodes (*average reference*); it can refer to a specific electrode placed on the orbit of the eye or on the mastoid (only two electrodes each mastoid/ear can be used) or even on the nose. Once that the electrode has been chosen, there can be the possibility to interpret the single electrode signals (*single-ended* system acquisition) or the difference between a couples of electrodes signals (*differential* system acquisition).

The VeeRg consist of a ski mask properly modified in order to host the electrodes and an acquisition/processing board. For this reason, it became necessary to take in consideration, for our study, the area of the cerebral cortex where the mask is placed, namely the frontal (F) and the frontal-parietal (Fp) zones. In particular, there had been placed four electrodes related to Fp1, Fp2, F7 and F8 in the system 10-20, and one another electrode in the center of the cortex which we called G. Thanks to the versatility of the mask, there had been introduced also

three different channels, added in order to reach the electro-ocular signals: ER = right eye, EL = left eye, ERD = right low eye; the fourth electrode, necessary to complete the electro-oculographic system, is the same Fp2 used for EEG. These additional electrodes could be useful to add some specific features to the system like eye tracking or eye's blink removal. In Fig. 1.3b is illustrated the system just explained above.

1.5 The prototype idea

In Fig. 1.4 it is shown how the VeeRg was thought when we started to think about it. Wanting to make it invisible to the user, it came to us naturally to choose to placing the electrodes along the thickness of the sponge of the viewer that rests on the face. The ADS1299 front-end provides 8 acquisition channels for EEG signals, one channel for the reference electrode and one channel for correcting the common potential due to the isolation of the body from the earth (common mode CM, see Par. 2.1.2). There are overall ten electrodes to be disposed. Regarding those intended for electroencephalography, it was not a big deal to understand what their position was, as already cited in the previous paragraph, we have complied with the standard arrangement 10-20 for the electrodes Fp1, Fp2, F7 and F8. However, we have introduced a fifth electrode, not provided for by the standard, we have called G and which we have placed right in the middle of the front; the usefulness of this electrode is twofold: on the one hand it can very well act as a normal encephalographic electrode by using signals that can be useful in the analysis of the cerebral activity; on the other, it can be considered a reference electrode for the remaining four, allowing to calculate the potential of the frontal points with respect to the point placed along the midline saggital plane of skull. The remaining three channels are dedicated to the electrodes for the oculographic signals useful in the moment we want to implement an algorithm for removing artifacts due to the movement of the eye or, even more interestingly, implement an algorithm that is able to trace their movements. The last electrode to put on the display, is the bias for the elimination of the common mode signal. Regarding the reference, a clip was constructed with an electrode to be placed on the earlobe.

The rest of the system made up of the cards and the battery doesn't represent a big problem about the positioning but we must however take into account the type of viewer on which it will be applied since not all of them give the same freedom. In Fig. 1.4 for example the model represents an Oculus Rift viewer, which has a large area in the upper part on which the VeeRg can be placed (represented by the

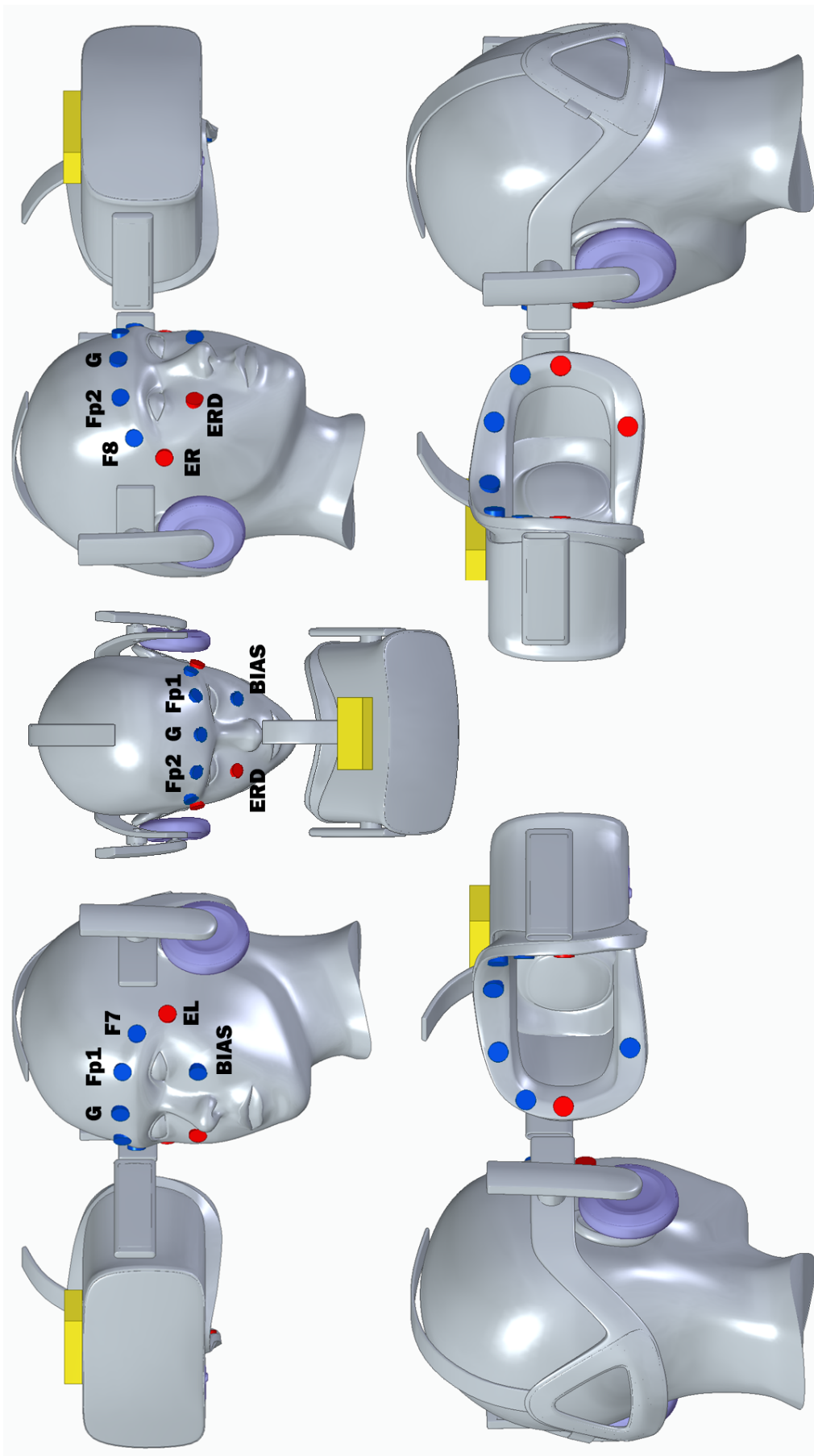


Figure 1.4: The 3D model shows how the VeeRg is integrated into the virtual reality viewer. To make everything as discreet as possible, the electrodes are placed along the sponge of the viewer that rests on the face of the user and connected with appropriate wiring to the VeeRg placed on the top of the viewer (yellow box).

yellow box in the figure).

Obviously for the creation of a prototype it is not necessary to use, at least in the first versions, a real virtual reality viewer. Rather, it is more practical to use a mask for generic use, such as those used for skiing, for more freedom of action. In the first phase, in fact, it will be necessary to understand if the system actually works correctly and if the position of the electrodes is right or must be corrected. Following, the basic idea is to provide the users having already a viewer, a practice hardware plug-in that can easily integrate with it. Only then can we think of developing a new product that integrates both the functions of virtual visor and electroencephalography.

Chapter 2

The *VeeRg* design

The intent of this chapter is to describe the main steps that have characterized the design of the VeeRg system. The contents we are going to talk about are the most common challenges that a designer can encounter during the design of such systems. These challenges do not depend on the use of particular circuit components or particular programming techniques, which we preferred to omit given their relative lack of scientific interest, but they represent a higher conceptual level and for this reason they become the fundamental bases for a good design. Anyway, a little description of the devices used on the boards will be done in next paragraph.

The milestones we have fixed in our mind during the design of such kind of system are essentially two, the second of which is strictly dependent from the first one. The first step was to obtain an acquired signal, representative of the brain activity coming from the electrodes, as accurate and clear as possible; the second step was to clean and isolate the frequency bands relative to the common brain activity's classification (*Alpha*, *Beta*, etc. . .) seen in the Chap 1, to extract all the useful informations.

From this point of view, two different phases of workflow could be defined, the hardware and the software ones, and so we've done in the description of the VeeRg system in the following sections. In Fig. 2.1 is shown the whole work process which will lead to the final results.

2.1 Hardware design

An overview on how the our electroencephalographic system is composed is given by the Fig. 2.2. The basic idea was to divide the strictly *analogue* part, for the acquisition and digitalization of the signals coming from the electrodes placed

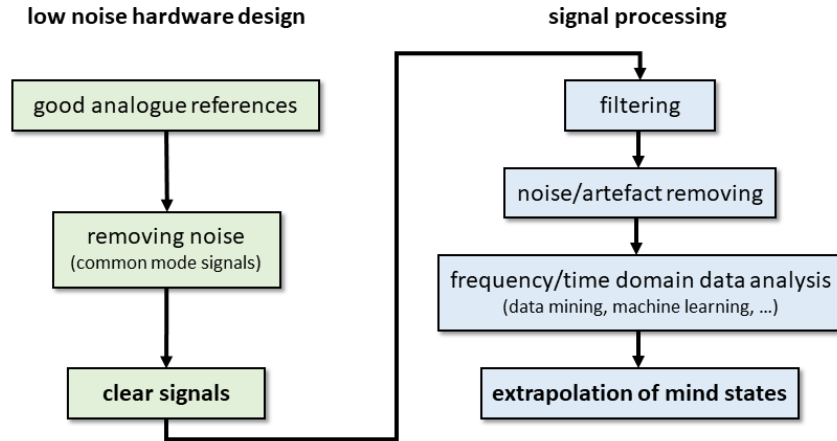


Figure 2.1: The main steps of workflow that, from an hardware design focused on low-noise features to obtain signals as clean as possible, leads to the software processing for the correct analysis trying to extrapolate the states of mind.

on the head, from the *processing* one, the purpose of which is to clean up the information and prepare it to the further phase of mental state recognition that will run on the terminal that the VeeRg is connected to.

The first board (Fig. 2.2b), the analogue one, from a components point of view is not particularly interesting, if not for the ADS1299 device which is a specific front-end developed for bio-signal acquisition, and for particular voltage regulators with the purpose of generating the references for the analog-to-digital conversion. For this reason its conceptual scheme is relatively simple, being composed only of the conversion block and the one for generating the references. The most interesting part designing this board concerns the techniques used to obtain signals as clean as possible. On one side, although we are dealing with signals characterized relatively by low frequencies, we had to be careful in the routing of the printed circuit board in order to avoid errors that would bring, even at its most ordinary, to the presence of unwanted background noise. The results of this attention will be illustrated in the Par 2.1.1 where the quality of the references and the input referred noise of the ADS1299 front-end will be measured. On the other side, we had to analyze and go into the details of the most common techniques in bio-signals acquisition to reduce all interferences due to the body isolation respect to a reference potential and subject to electromagnetic fields of the surrounding environment, nowadays omnipresent. The reason and implementation of these techniques will be developed in the Par 2.1.2.

The second board (Fig. 2.2a) differs significantly from the first one if compared on the design complexity. In this case we dealt with a purely digital sub-system and

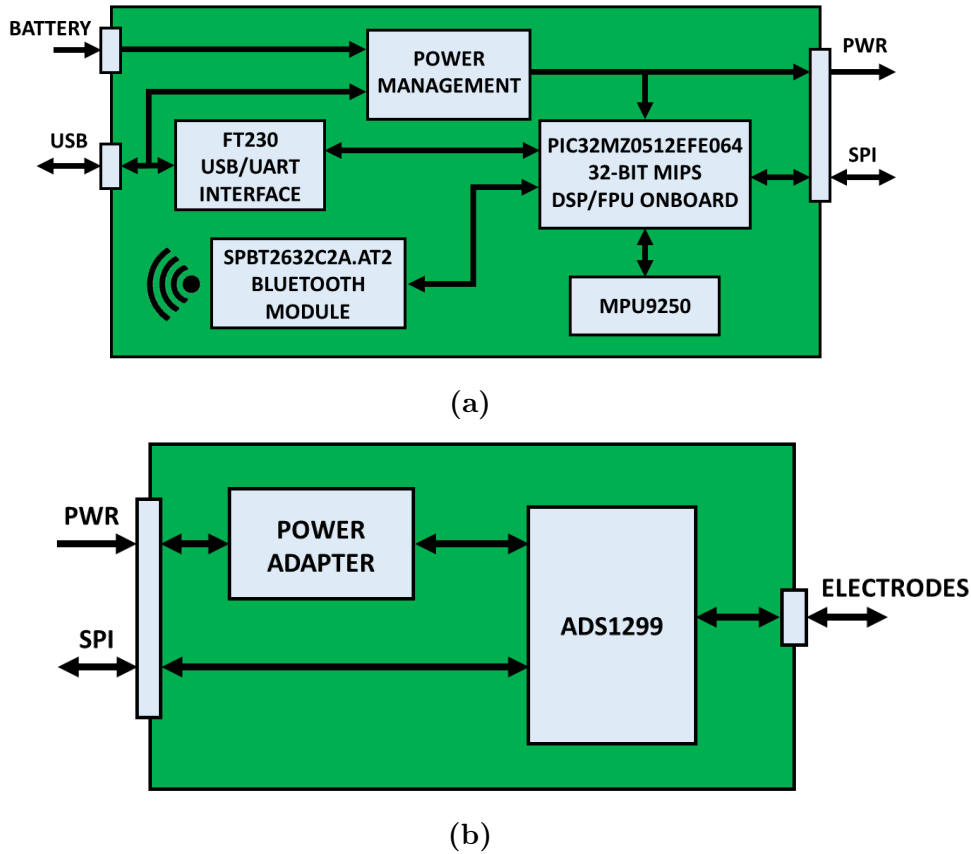


Figure 2.2: An overview of the system boards. In a) the elaboration board which receives and processes the digitalized data coming from the analog-to-digital conversion. In b) the acquisition board which is strictly analogue and has the specific front-end for bio-electrical signal acquisition, the ADS1299.

therefore techniques to keep the noise under control were not required. However, since the desire is to provide a system as complete and practical as possible, it was necessary the use of numerous integrated circuits for the management of various functionalities, increasing the complexity of the routing. The heart of processing is represented by a 32-bit *Microchip* micro-controller model PIC32MZ0512EFE064, device that offers a MIPS M-Class core, superset of the microAptiv one, which can reach up to 415 DMIPS in terms of performance (252 MHz of clock speed); for this particular MCU family, a 32 and 64 bit Floating Point Unit (FPU) and a DSP core have been integrated to increase the performance during particularly heavy elaborations in floating point[19], feature very useful since the idea to perform filtering of digital signals directly on-board to select and clean up the band of our interest for the analysis of brain's waves coming from the electrodes. In this way we also want to create a system as independent as possible, leaving the analysis of the information concerning the mental activity to the software interface that runs on the work station to which the system is connected. Although the micro-controller

has the ability to manage a USB OTG communication, in order to reduce the computational load we have considered the use of the FTD232 from FTDI company, an USB/UART interpreter that independently manages all the stack layer necessary for communication through the USB standard. The same was done for the wireless bluetooth communication with the use of the SPBT2632C2A.AT2 module by *ST Microelectronics* which integrates a Cortex core for the independent management of the bluetooth stack layer and for the communication with the micro-controller through UART. Finally, to complement the *processing* board, we have the block for the management of power supplies and the charge/discharge of the 900mAh battery, which with the present elaboration load guarantees an autonomy of approximately 5 hours of continuous acquisition, and the block consisting of an IMU (inertial measurement unit) MPU9250 by InvenSense that provides the ability to implement an AHRS (attitude and heading reference system) if the system was not used with a virtual reality viewer but still wanted to have information on the movements of the head in 3D space.

Both the boards and the complete final system prototype are shown in the Fig. 2.26 at the end of this chapter. The schematics of the VeeRg system are available in App. A.1.

2.1.1 Analog power supply and input referred noise

In Par. 1.3.1 we introduced the classification of the different brain waves according to their frequency band (*Delta, Theta, Alpha, Beta* and *Gamma*). We have also mentioned that these waves have a very small amplitude, of the order of microvolt (μV). Being dealing with signals so small it's essential try to not introduce any noise through wrong design choices. From this point of view, the ADS1299 front-end gives us already some good low-noise features, but if the designer doesn't enter into this perspective, then the situation may be worse. The choice about separating the digital part from the analogue part in the VeeRg into two different PCB essentially stems from these points. We wanted to isolate the analogue part to avoid a priori the additional noise due to possible coupling with the digital signals of the communication interfaces. Moreover, the board has been designed following the practice of the shielding through the use of an external metallic box and a suitable plane placed in an inner layer of the board, both connected to the system ground (Fig. 2.26c).

In Fig: 2.2b the *Power Adapter* block plays a fundamental role in keeping the background noise of the whole system as low as possible. In fact this block is the one that generates the analog power supplies for the ADS1299 front-end and the voltage

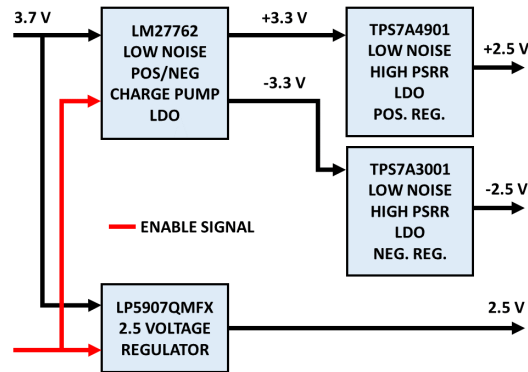


Figure 2.3: Model of body used in the analysis of common mode noise. The feedback-loop (or right-leg driver) is the most effective method to reduce it.

references to perform the analog to digital conversion. Inside of it we find some voltage regulators specifically chosen to obtain the double power supply ($V_{dd} = +2.5V$ and $V_{ss} = -2.5V$), characterized by a low noise on the output and, most important, by a very high *Power Supply Ripple Rejection* (PSRR) that guarantees the stability of the output even in the presence of a noisy input signal. The Fig. 2.3 shows the internal structure of the *Power Adapter* block. The first component that takes in input the battery voltage from 3.7 V is the LM27762 [10], regulator that makes it possible to generate a double and opposite voltage power supplies through its integrated charge pump. This component generates voltages at ± 3.3 V which become the inputs for the second regulation stage in which an TPS7A4901 [11] is used to generate the +2.5 V and an TPS7A3001 [7] to generate the -2.5 V. The choice of using this second regulation stage instead of directly generate the ± 2.5 V from the LM27762 is due to the fact that we wanted to minimize the possible noise on the power supplies due to the regulator’s charge pump. Being components with a very low leakage current, their apparently redundant use doesn’t represent at all a problem from the point of view of consumption nor area occupation.

The ADS1299 front-end has special functions that make it possible to carry out measurements of the power supplies and, most important, of the input referred noise through the shorting of both the differential inputs of a channel. Through these features we were able to measure the *Power Supply Noise* (PSN) of the system¹ and its *Input Referred Noise* (IRN). The recorded values are indicated in the Tab. 2.1.

If we compare the our values registered with those listed in [8, Tab. 1] we can immediately see that the ones referring to the IRN with unitary gain ($G=1$) are

¹Given that the measurement carried out by the ADS1299 is given by the formula $V_s = \frac{V_{dd} - V_{ss}}{2}$, the final value of the PSN refers to the differential case.

	μV_{rms}	μV_{pp}
PSN	7.04	39.08
IRN	0.97	5.79

Table 2.1: The final Power Supply Noise (PSN) and the Input Referred Noise (IRN) of the system.

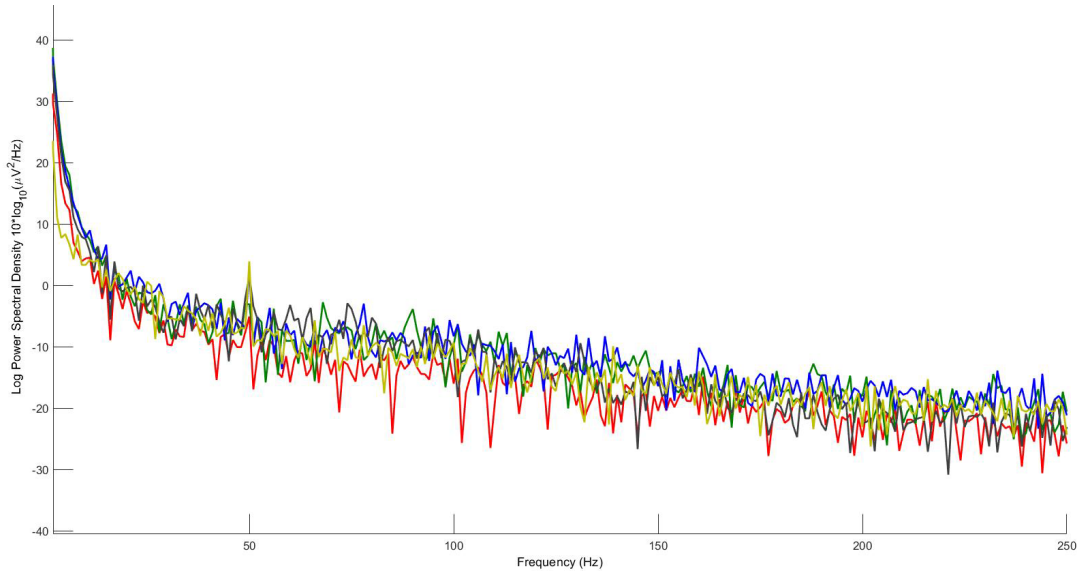


Figure 2.4: Model of body used in the analysis of common mode noise. The feedback-loop (or right-leg driver) is the most effective method to reduce it.

significantly higher than our: we have an improvement of 10% for the root mean square (V_{rms}) and 22% for the peak-to-peak value (V_{pp}).

Fig. 2.4 wants to represent the final result of all the techniques aimed at reducing the background noise of the system. The graph represents the spectral power density of all 8 channels with the VeeRg worn, in a state of vigilant rest and a time window of about 10 seconds. It can be seen a small component at 50 Hz that represents the coupling of the body with the electric line (argument completely explored in Par. 2.1.2), but overall the system presents a background noise with a density lower than $1\mu V^2/Hz$ (this means an high signal-to-noise ratio S/N), which makes it very competitive if we try to compare it with the current electroencephalographic systems on the market.

2.1.2 The common mode noise and the feedback loop

When the recording of a bio-electrical signal is performed, the main source of noise are the electromagnetic interferences (EMI) that surround the patient's body. The most powerful contribute results from the main power line ($220V_{rms}@50Hz$ in

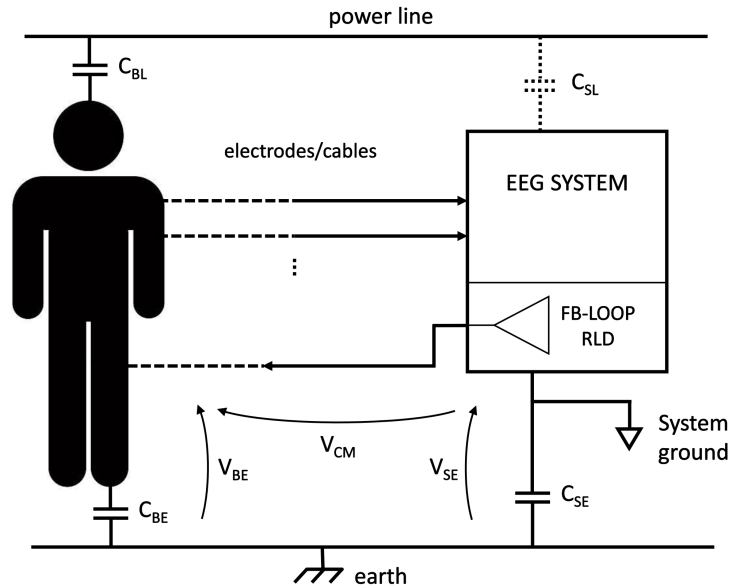


Figure 2.5: Model of body used in the analysis of common mode noise. The feedback-loop (or right-leg driver) is the most effective method to reduce it.

Europe) which supplies all the devices around us: a common ballast in office's neon lamp can produce a huge interferences that are reached by the body which acts like an antenna due to its isolation from the earth's ground potential reference. This type of noise is called *common mode* (CM) signal since it's present in all system's channels connected to body and the capability to be insensitive to it is defined *common mode rejection* (CMR). Although our system, like the most ones, catches the information from bio-electrical signals referring each channel to one chosen as reference (the right ear lobe, A2 in the 10-20 system), the common mode noise isn't rejected simply by the differential nature of system cause the not so perfect matching in the input channels' stages; this issue is well known as *common mode to differential mode conversion* (CM2DM) and it will be discussed in 2.1.2.1 and 2.1.2.2. Furthermore the CM, if large enough, could lead the active stages of the channels to saturate and then cut off information of the signal acquired (see Fig. 2.6). Therefore, the need for find an optimal approach to reduce the common mode noise is still necessary to obtain a final useful system.

In the order to design our VeeRg system, a body's model (Fig. 2.5) was implemented to perform all the necessary simulations to understand the main causes which lead to an improvement or worsening of the overall common mode rejection. For the sake of simplicity, the coupling between the power line and the system and between the power line and the electrodes' cables were not taken into account, keeping the focus on the most relevant contribute which affect the common mode

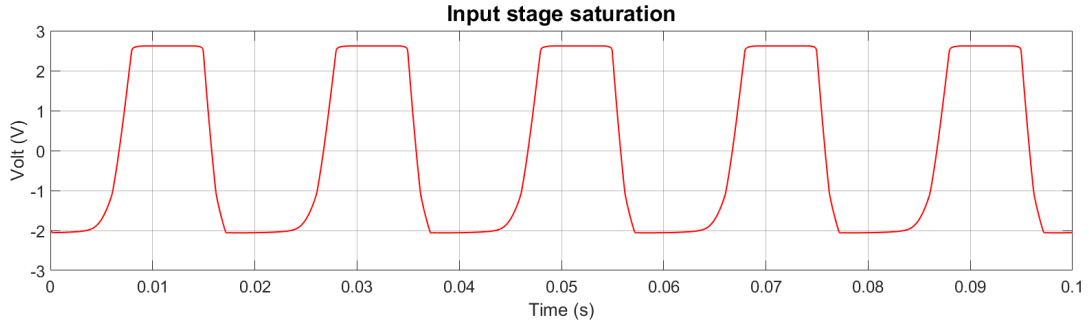


Figure 2.6: Example of the common mode signal effect on the output of active input stage system supplied with ± 2.5 V.

noise.

In Fig. 2.5, C_{bl} represents the coupling between the power line (or EMI in general) and the body, C_{be} between the body and the earth ground, C_{se} between the earth ground and the VeeRg system ground and C_{sl} between the power line and the VeeRg system. The main source of the common mode signal (CM) is the coupling represented by C_{bl} , C_{be} and, most important due to its contribute, C_{se} . In fact, the CM noise can be seen as results of the body's polarization and the isolation of the system both referred to the earth' ground, in a direct and inverse proportional ratio respectively:

$$V_{cm} = V_{be} - V_{se} \quad (2.1)$$

This means that if we want to reduce the CM we need to cut down the body-earth impedance or increase the system-earth one. This is the reason because wearable systems have notoriously an high rejection to CM since their ground is *totally* disconnected to the earth which means a very large impedance.

In the following analysis, since we are dealing with not so well defined entities which depend all by the particular context or circumstance, we guess that it is necessary, where is impossible to find numerical values for the variables involved, reduce the study of the worst case. In this way we can obtain some values which guarantee to us keep the CMR under defined limits.

In the simulations, we have chosen for the model's capacitance the values $C_{bl} = 20pF$, $C_{be} = 300pF$ and $C_{se} = 300fF$ (if otherwise indicated). These values are just for example and are taken from some research articles [18][21]. But they can vary widely from some femtofarad to hundreds picofarad, depends to circumstance (e.g. if the user touch a metal objects C_{bl} change drastically).

The most effective solution to reduce the effect of body's isolation from the

signal ground, is the use of so called Right Leg Driver (RLD); this term stems from his first use in the ECG recording but now we could refer to this technique with different names like Feedback Loop (FL), Ground Electrode or Bias Electrode. In this context we'll use the term Feedback Loop (FL from here).

The principle of FL is simple: polarize the body with a signal opposite to the common mode (this the reason for the Bias Electrode name). From another point of view, the FL provide to create a path from the body to the system's ground to eliminate the potential difference between these two parts, letting the the system sensible only to the bio-electrical signals.

This connection between the body and the system thus reduces its isolation leading to a considerable reduction of the common mode signal; but if on one hand it helps to reduce noise on the other it can put the user in a danger state. In fact, if the voltage potential applied to the body finds a return path (i.e. the user somehow accidentally touches the mass of the system), can be created currents which, depending on the case, can flow through very sensitive organs. Suffice it to say that currents of a few hundred microampere can seriously interfere with the correct physiological functioning of the heart. For this reason, over the years it has come to set a limit to the current that a medical device can, in the event of a fault, deliver through the user's body. Although the debate is still open on the effectiveness of this limit, the AAMI and IEC set it at $50 \mu\text{A}$ in the case of multiple faults (more restrictive limit) [26] [27]. To ensure that this limit is respected, it is mandatory to place a limiter in the FL which in practice is a simple series resistance. As we will see, the presence of this resistance will be significant in the attempt to improve the CMR and the stability of the system.

The Fig. 2.7 shows a typical implementation of the FL. The schematic, although simplified to just two electrodes, includes the model of the body for the simulation and the study of all the variables that contribute or not to the CMR and shows all the main features of the method. The common mode signal is generated by making a simple mean of all the input signals coming from the electrodes using a passive averaging network formed by resistors of the same value. Once obtained, the common mode signal is given to the input of an active filter composed of an operational amplifier in inverting low-pass configuration. The output of this stage is the voltage which is finally applied to the user's body through a dedicated electrode, but not before being passed through the protection resistance (R_p in Fig. 2.7), previously discussed to limit any current that it can flow through the body in case of fault. The reason for the inverting characteristic of the filter is logical in that, as already mentioned, the technique is based on polarizing the body with a voltage opposite to the one of the common-mode signal to be eliminated;

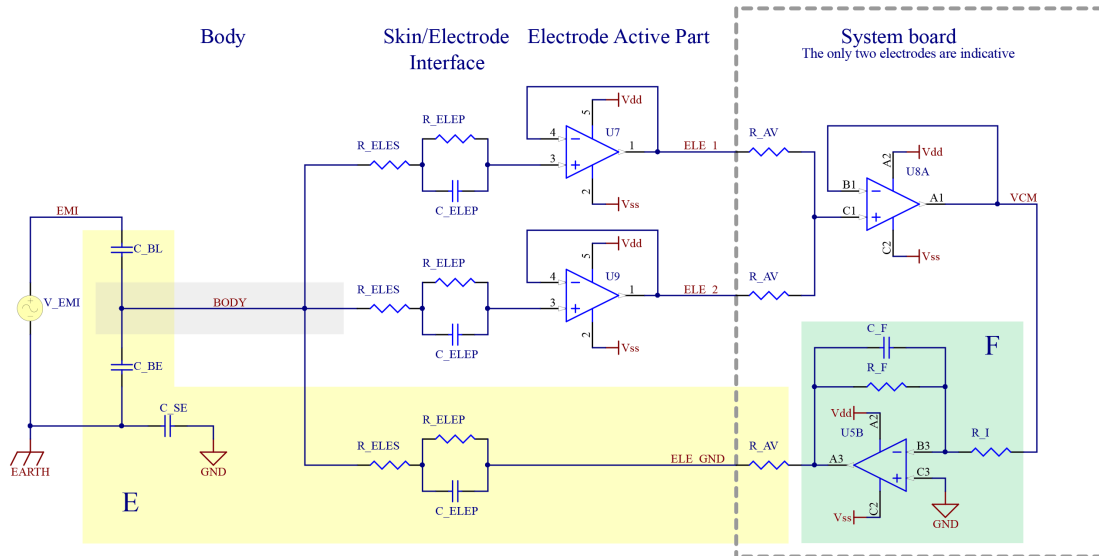


Figure 2.7: The simplified schematic for the body's model and the FL. The block E and the block F represent the two main contribute in CMR which can analyzed separately, since they are independent. The block F refers to the effect of the active filter while the block E refers to the contributes of the skin/electrode interface and the coupling between the body and the earth ground; in this one, the only thing that we can menage with good approximation is the protection resistor R_p .

the low-pass feature, on the other hand, is essential to manage and control the stability of the entire system, since we are basically managing a feedback system. These concepts will be discussed in detail in Par 2.1.2.3.

From the simulations carried out with our model, we were able to define the effects of its various elements on the final CMR. Let's just say that unfortunately, given the nature of the context, a little remains to the designer to try increasing the CMR, since most of the variables involved are of a completely random nature; it is in practice impossible to define correct values for the coupling between the body and electromagnetic interferences to be used in its own favor, just as it is impossible to define the values of the intrinsic components of the electrode model. If you look at Fig. 2.7 you will see two highlighted circuit blocks called E ad F ; these blocks represent the two independent contributions in the final expression of the CMR that we have found and which we are going to analyze. But while for the F block it is possible to modify its characteristics in the design phase, for the E block there is little to do but modify the value of the protection resistance R_p or try to reduce the negative effects of the body and the electrode due to the components that can not be defined a priori.

However, we can understand how these random elements affect the final CMR so that try at least to reduce the effects with appropriate measures. The contributions

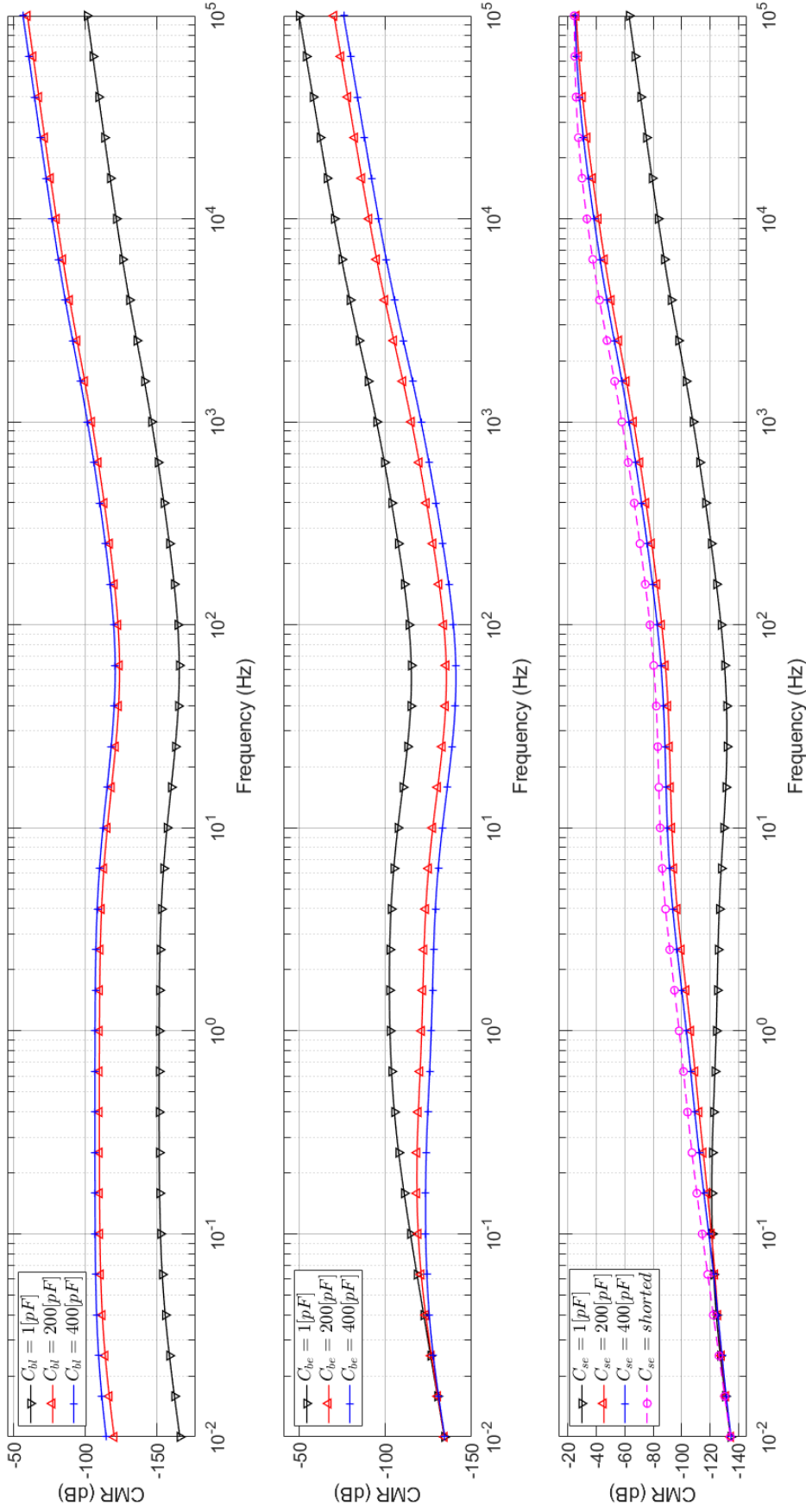


Figure 2.8: Dependence of common mode signal for different values of variables C_{bt} , C_{be} and C_{se} . For the first one, C_{bt} , the relation is linear as expected. Very interesting is the effect of C_{se} when it's very high, which means the system's ground and the earth shorted: in this case the frequency characteristic of common mode signal reach an maximum limit which means the worst case of CMR.

related to the isolation of the body are particularly interesting in this sense and therefore the couplings represented by the capacities C_{bl} , C_{be} and C_{se} . For this purpose we performed a simulation maintaining an unity gain for the FL filter and a cutoff frequency of about 1.6 kHz; a frequency analysis was performed on a band ranging from 10 mHz to 100 kHz. Keep in mind that in this analysis the CMR is expressed in negative form, so an increase in it results in a decrease in the value of the expressions found.

In Fig. 2.8 we have the results of the analysis. With regard to the capacitance C_{bl} the inversely proportional dependence between its value and the final CMR can be immediately noticed; this behavior is easily understandable since an increase in capacity corresponds to a reduction in the impedance seen between the noise source and the body. It is a different matter for C_{be} , given the fact that its value is linked to the CMR by a relationship of inverse proportionality: the higher its value, the lower the impedance between body and earth and therefore less *isolation* of the body from a reference potential (non floating body). Of particular interest is the case of C_{se} related to the CMR by an inverse proportionality ratio; this explains why battery-powered systems have a notoriously better rejection to the common mode signal due to electromagnetic interference since the coupling between the system ground and the earth has a very small value. The interest in this parameter increases if we observe the case in which $C_{se} \rightarrow \infty$, i.e. when the two ground and earth references are shorted together: the CMR in this case reaches an upper limit value that represents the worst case for the C_{se} parameter. This can be very useful in simplifying the analysis of the whole system considering already from begin the two masses shorted and focusing on the other parameters, knowing however that any change related to C_{se} can only lead to an improvement of the Final CMR. As we will see shortly, removing from the calculations C_{se} , the final formulas describing the CMR (poles and zeros also) will be simplified.

Fixed to mind the effects of the parameters which are parts of *body* system, we can now move the attention to an deeper analysis of the CMR and in particular of its two independent components that previously in the schematic we have indicated as block F , representing the active filter part, and block E , representing the total impedance seen by the F block. We have to keep in mind that the validity of this analysis is limited to the use of active electrodes or, at least, characterized by a very high input impedance.

Fig. 2.8 gives a general idea of CMR trend vs. frequency. During the calculation of its general expression, the possibility of separate the two independent blocks F and E was noticed. The relationship found is thus expressible as:

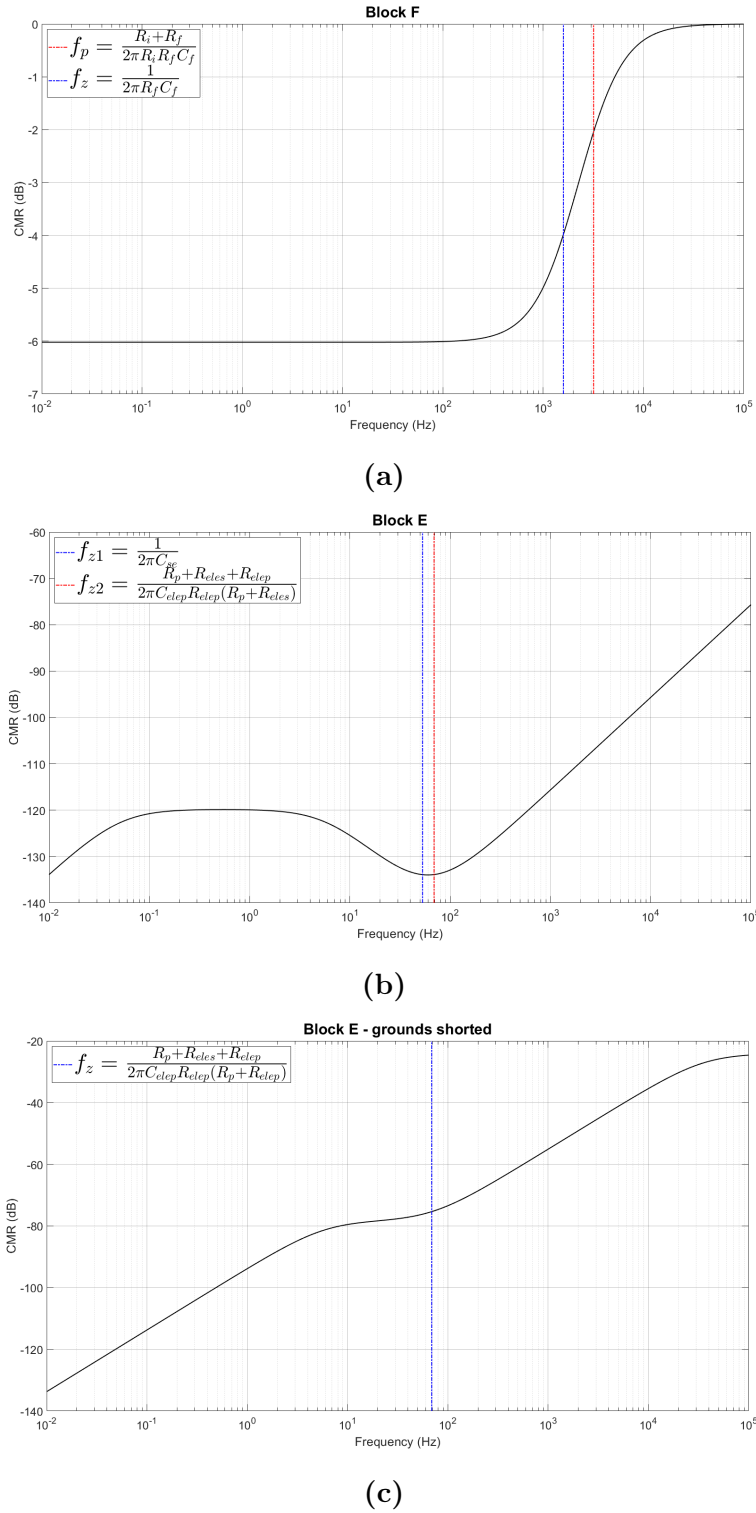


Figure 2.9: The CM characteristic (c) disjoined into the two contributions F and E . In (a) the frequency characteristic of the contribution $F(\omega)$ with the presence of one pole and one zero. In (b) the $E(\omega)$ and two of its three zeros. Unlike $F(\omega)$, it was not possible to find clear and simple analytical expressions of the poles given the complexity of the calculations.

$$\frac{V_{cm}}{V_{emi}}(\omega) = F(\omega)E(\omega) = \frac{Z_i}{Z_f + Z_i} \frac{Z_e Z_{be}}{Z_{bl}(Z_e + Z_{se} + Z_{be}) + Z_{be}(Z_e + Z_{se})} \quad (2.2)$$

that in decibel becomes

$$\left| \frac{V_{cm}}{V_{emi}} \right|_{dB}(\omega) = 20 \log \left(\left| \frac{Z_i}{Z_i + Z_f} \right| \right) + 20 \log \left(\left| \frac{Z_e Z_{be}}{Z_{bl}(Z_e + Z_{se} + Z_{be}) + Z_{be}(Z_e + Z_{se})} \right| \right) \quad (2.3)$$

with

$$\begin{aligned} Z_i &= R_i \\ Z_f &= R_f \parallel C_f = \frac{R_f}{1 + j\omega R_f C_f} \\ Z_{be} &= \frac{1}{j\omega C_{be}} \\ Z_{bl} &= \frac{1}{j\omega C_{bl}} \\ Z_{se} &= \frac{1}{j\omega C_{se}} \\ Z_e &= R_p + R_{eles} + (R_{elep} \parallel C_{elep}) = \frac{R_p + R_{eles} + R_{elep} + j\omega R_{elep} C_{elep} (R_p + R_{eles})}{1 + j\omega R_{elep} C_{elep}} \end{aligned} \quad (2.4)$$

Note that the impedance Z_e is no more that the result of electrode in series with the protection resistance.

In Fig. 2.9a the frequency characteristic of the contribution $F(\omega)$ is depicted, also highlighting the presence of one pole and one zero. We have already mentioned that this contribution, even if it can theoretically lead to an infinite CMR, is limited by the condition of stability of the system (see Par 2.1.2.3). Its expression as a function of ω is

$$F(\omega) = \frac{Z_i}{Z_i + Z_f} = R_i \frac{1 + j\omega R_f C_f}{R_i + R_f + j\omega R_i R_f C_f} \quad (2.5)$$

and his analysis shows the presence of two limits for $\omega \rightarrow \pm\infty$, of a pole f_p and of a zero f_z . Their expressions are as follows:

$$|F|(\omega \rightarrow 0) = \frac{R_i}{R_i + R_f} \quad (2.6)$$

$$|F|(\omega \rightarrow \infty) = 1 \quad (2.7)$$

$$f_z = \frac{1}{2\pi R_f C_f} \quad (2.8)$$

$$f_p = \frac{R_i + R_f}{2\pi R_i R_f C_f} \quad (2.9)$$

Regard the contribution $E(\omega)$, its characteristic is shown in Fig. 2.9b with expression given by

$$E(\omega) = \frac{Z_e Z_{be}}{Z_{bl}(Z_e + Z_{se} + Z_{be}) + Z_{be}(Z_e + Z_{se})} \quad (2.10)$$

Like for $F(\omega)$, the analysis of $E(\omega)$ leads to find the characteristic values of its trend vs. frequency for $\omega \rightarrow \pm\infty$ and the values of its three zeros f_{z0} , f_{z1} and f_{z2} . Unlike $F(\omega)$ however, it was not possible to find clear and simple analytical expressions of the poles given the complexity of the calculations. The results are

$$|E|(\omega \rightarrow 0) = 0 \quad (2.11)$$

$$|E|(\omega \rightarrow \infty) = \infty \quad (2.12)$$

$$f_{z0} = 0 \quad (2.13)$$

$$f_{z1} = \frac{1}{2\pi C_{se}} \quad (2.14)$$

$$f_{z2} = \frac{R_p + R_{eles} + R_{elep}}{2\pi R_{elep} C_{elep} (R_p + R_{eles})} \quad (2.15)$$

Although we only have the expressions of the zeros, we can however say that to optimize the final CMR we should try to have such points at the highest possible frequencies; this would guarantee that with the increase of the frequency the relative decrease of the CMR happens with greater delay. To move the zeros f_{z1} and f_{z2} at high frequencies means, observing their expressions, to decrease the capacity C_{se} and to decrease the resistance R_p (for the latter we will see shortly how its value affects the position of zero f_{z2}).

Consider now the much simpler case in which $C_{se} \rightarrow \infty$ i.e. with the mass of the system and the earth shorted. We have already found how this particular context turns out to be a worst case limit for what concerns this parameter such that every possible random variation could only lead to an improvement of the CMR. The general expression resulting from this change is

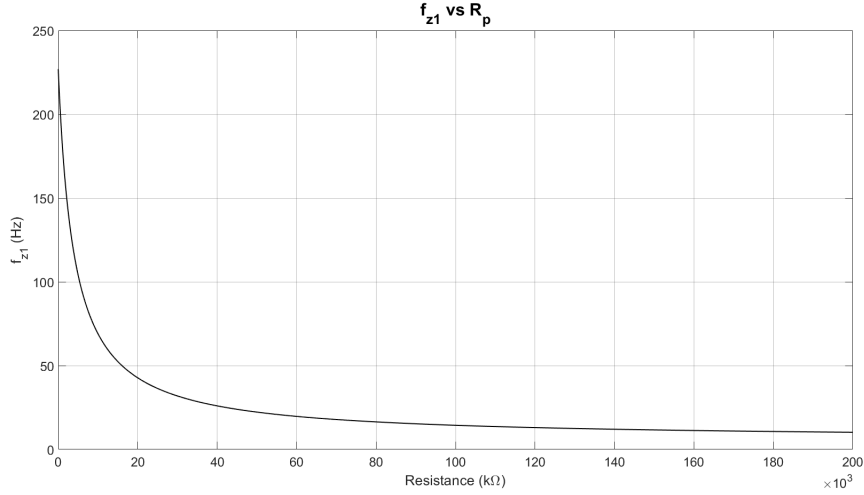


Figure 2.10: The relation between the values of R_p and f_{z1} is inversely proportional. The graph has been drawn as example with $R_{eles} = 4kH_z$, $R_{elep} = 150kH_z$ and $C_{elep} = 180nF$ [16][3].

$$\frac{V_{cm}}{V_{emi}}(\omega) = F(\omega)E(\omega) = \frac{Z_i}{Z_f + Z_i} \frac{Z_e Z_{be}}{Z_{bl}(Z_e + Z_{be}) + Z_{be}Z_e} \quad (2.16)$$

with $F(\omega)$ as the previous case. It changes only $E(\omega)$ which become

$$E(\omega) = \frac{Z_e Z_{be}}{Z_{bl}(Z_e + Z_{be}) + Z_{be}Z_e} \quad (2.17)$$

with its new values for $\omega \rightarrow \pm\infty$ and the missing of one zero:

$$|E|(\omega \rightarrow 0) = 0 \quad (2.18)$$

$$|E|(\omega \rightarrow \infty) = \frac{C_{bl}}{C_{bl} + C_{be}} \quad (2.19)$$

$$f_{z0} = 0 \quad (2.20)$$

$$f_{z1} = \frac{R_p + R_{eles} + R_{elep}}{2\pi R_{elep} C_{elep} (R_p + R_{eles})} \quad (2.21)$$

The graph of the new contribution $E(\omega)$ is shown in Fig. 2.9c, where the zero f_{z1} is highlighted (note that it has the same expression as the previous f_{z2}). Also in this case the concept is the same: to improve the overall CMR we need to move f_{z1} at high frequencies. But the only parameter that we can change is just the value of the resistance R_p , related to the found formula of f_{z1} through an inverse proportionality ratio (Fig. 2.10).

The results just obtained so far want to highlight the strong random component in the final value of the CMR of our system and, more generally, in a system for

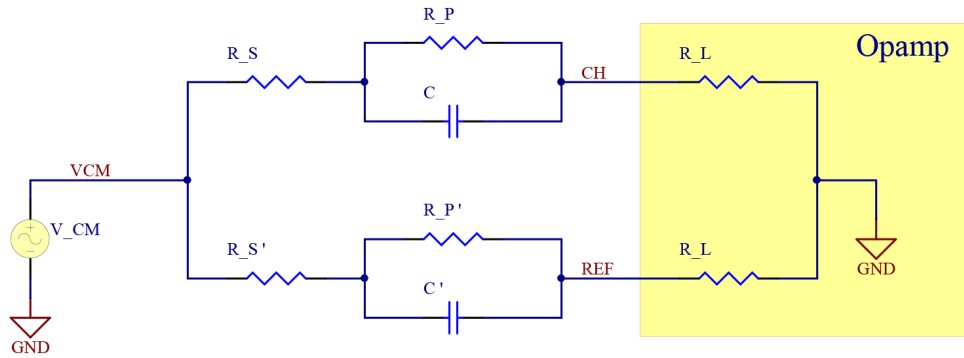


Figure 2.11: The electrodes model and their mismatching.

acquisition of bio-electrical signals using superficial electrodes. However, although there are very few degrees of freedom that allow us to improve it, it's essential to have clear in mind and under control all the characteristics involved and all the causes from which they derives. In the next paragraphs we are going to analyze how the presence of the common mode signal can turn into differential mode and then pass through the whole acquisition stages arriving at the digital analysis camouflaged by a normal signal.

2.1.2.1 Common mode to differential mode conversion in electrodes mismatch

The Fig. 2.11 shows the model for two electrodes seen as a common electrode-electrolyte interfaces, method used in all researches relatives to the bio-electrical signals acquisition [3][2][16]. In this case the components are bind to the intrinsic characteristic of the physical electrode: R_p represent the charge transfer resistance of the contact, C his double-layer capacitance² and R_s the resistance of the electrolyte/sweat. Under these conditions, is easy to understand how is very common reach a mismatching between the whole impedance of electrodes: just a little movement can change significantly the values of R_p and/or C while R_s can even change in time. Although these effects are not under our control, it's useful to get the effect of this changes on the overall CMR, since they lead to a common mode to differential mode signal conversion (CM2DM). In the schematic, R'_s , R'_p and C' have the same value of R_s , R_p and C with the addition of mismatching value δR or δC :

²In this analysis we referred to the model known as the Randles circuit for an electrode-electrolyte interfaces. We've not considered the Warburg element.

$$\begin{aligned}
R'_s &= R_s + \delta R \\
R'_p &= R_p + \delta R \\
C' &= C + \delta C
\end{aligned} \tag{2.22}$$

with $\frac{\delta R}{R}$ and $\frac{\delta C}{C}$ the entity of mismatching in percentage. For simplicity, these values are the same in following analysis.

From the schematic in Fig. 2.11 we can find the relation

$$\begin{aligned}
&\left| \frac{V_{ch1} - V_{ch2}}{V_{cm}} \right| (\omega) = \\
&R_l \frac{\sqrt{\omega^4 \tau^4 \beta^2 (1 + E)^2 + \omega^2 \tau^2 ((\gamma (1 + E) + \delta)^2 - 2\alpha\beta (1 + E)) + \alpha^2}}{\sqrt{\omega^4 \tau^4 \theta^2 (1 + E)^2 + 2\omega^2 \tau^2 ((\phi (1 + E) + \rho)^2 - 2\eta\theta (1 + E)) + \eta^2}} \tag{2.23}
\end{aligned}$$

with

$$\begin{aligned}
\tau &= RC \\
E &= \frac{\delta R}{R} + \frac{\delta C}{C} \\
\alpha &= \frac{\delta R}{R} (R_s + R_p) \\
\beta &= \frac{\delta R}{R} R_s \\
\gamma &= \frac{\delta R}{R} R_s - R_p \\
\delta &= \frac{\delta R}{R} (R_s + R_p) + R_p \\
\eta &= R_l^2 + R_l \left(2 + \frac{\delta R}{R} \right) (R_s + R_p) + \left(1 + \frac{\delta R}{R} \right) (R_s + R_p)^2 \\
\theta &= R_l^2 + R_l \left(2 + \frac{\delta R}{R} \right) R_s + \left(1 + \frac{\delta R}{R} \right) R_s^2 \\
\rho &= R_l^2 + R_l \left(\left(1 + \frac{\delta R}{R} \right) (R_s + R_p) + R_s \right) + \left(1 + \frac{\delta R}{R} \right) (R_s^2 + R_s R_p) \\
\phi &= R_l^2 + R_l \left(\left(2 + \frac{\delta R}{R} \right) R_s + R_p \right) + \left(1 + \frac{\delta R}{R} \right) (R_s^2 + R_s R_p)
\end{aligned} \tag{2.24}$$

The 2.23 and the 2.24 describe the effect of these mismatches in the electrodes when they are feed by the same common signal: even if we perform the difference between the values on input channels (CH1 and CH2 in the Fig. 2.11), the common

signal remains as noise. The parameters values are: $R_s = 4k\Omega$, $R_p = 140k\Omega$, $C = 180nF$, $R_l = 10M\Omega$ and $\delta R/R = 0.1$ (10% tolerance). The analysis of 2.23 gives us some important characteristics of this conversion from the common mode and the differential mode: the presence of two horizontal asymptotes for $\omega \rightarrow 0$ and $\omega \rightarrow \infty$, the first one of them represents the absolute maximum which could help us to keep under control the CM2DM effect (Fig. 2.12). Its value is

$$\left| \frac{V_{ch} - V_{ref}}{V_{cm}} \right| (\omega \rightarrow 0) = R_l \frac{\alpha}{\eta} \approx \frac{\delta R R_s + R_p}{R R_l} \quad (2.25)$$

, while for $\omega \rightarrow \infty$ we have

$$\left| \frac{V_{ch} - V_{ref}}{V_{cm}} \right| (\omega \rightarrow \infty) = R_l \frac{\beta}{\theta} \approx \frac{\delta R R_s}{R R_l} \quad (2.26)$$

To complement the analysis of 2.23, the expressions of the two poles and two zeros were found. The poles are at lower frequency respect the zeros, which can become complex conjugates depending on the values of the parameters involved, changing significantly the trend of the CM2DM in the frequencies domain. In Fig. 2.12b we can see the effect of complex conjugates zeros. However, the presence of the asymptotes remains for both $\omega \rightarrow 0$ and $\omega \rightarrow \infty$, the first of which continues to represent the absolute maximum. For the poles and for the zeros we found the following expressions:

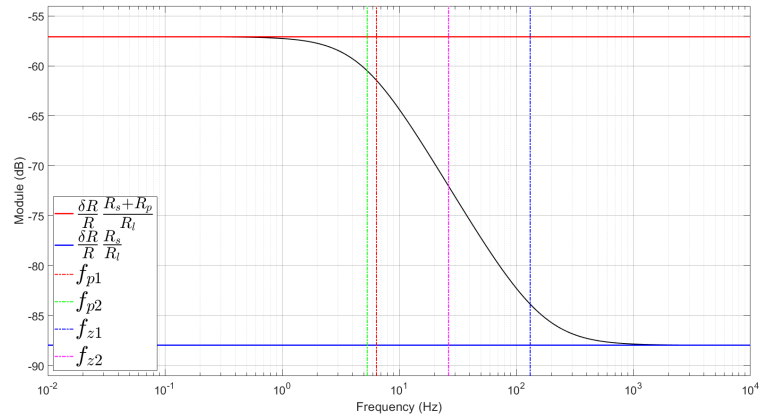
$$f_{p1} = \frac{R_l + R_s + R_p}{2\pi R_p C (R_l + R_s)} \quad (2.27)$$

$$f_{p2} = \frac{R_l + (R_s + R_p)(1 + \frac{\delta R}{R})}{2\pi R_p C (1 + E)[R_l + R_s(1 + \frac{\delta R}{R})]} \quad (2.28)$$

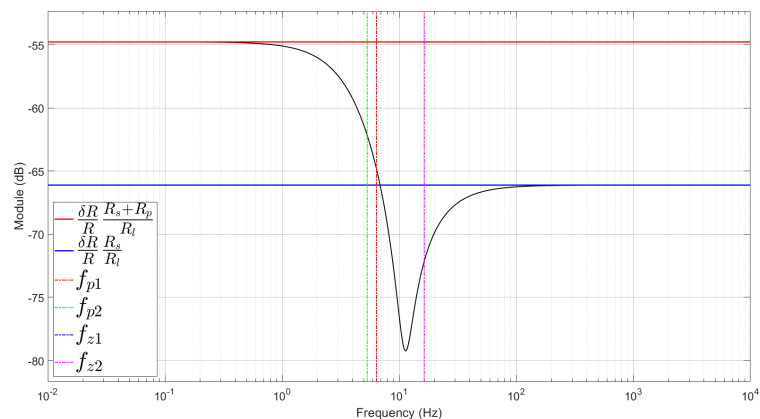
$$f_{z1,z2} = \frac{-R_p C (\gamma(1 + E) + \delta) \pm \sqrt{R_p^2 C^2 (\gamma(1 + E) + \delta)^2 - 4R_p^2 C^2 (1 + E)\beta\alpha}}{2\pi R_p^2 C^2 (1 + E)\beta} \quad (2.29)$$

2.1.2.2 Common mode to differential mode conversion in input stages mismatch

Designing an input stage for analog pre-processing signals could represent a serious deal due to the odd to introduce additional noise, or unwanted new signals, which degrade the final $\frac{S}{N}$ ratio of EEG information. Let's take just for example the choice to use an low-pass RC filter before the inputs of the ADC, like shown in



(a)



(b)

Figure 2.12: The frequency response of CM2DM in the case of mismatching in the intrinsic components of electrodes model. The parameters values are: $R_s = 4k\Omega$, $R_p = 140k\Omega$, $C = 180nF$, $R_l = 10M\Omega$ and $\delta R/R = 0.1$ (10% tolerance). The presence of a horizontal asymptote as absolute maximum value lets to keep the effect under a specific value. The graphs show the difference between regular zeros (a) and complex conjugate zeros (b).

Fig. 2.13a. This is a common practice in the EEG system design and the most of times it's a good solution, but you must have in mind a good perspective of what you are doing. The main problem using an RC stage as input stems from the non ideal nature of the real components which compound all the stages. In fact, it's well known that all the passive parts of a circuit are characterized by a value which is not perfect but carries a little relative error. This error is well known as value's tolerance of component and it is represented by percentage. This non ideal condition leads always to a mismatching between the different input stages, the RC filters in our example. And the presence of mismatching means different behaviors respect to what we are expecting. So if we put the same signal in two

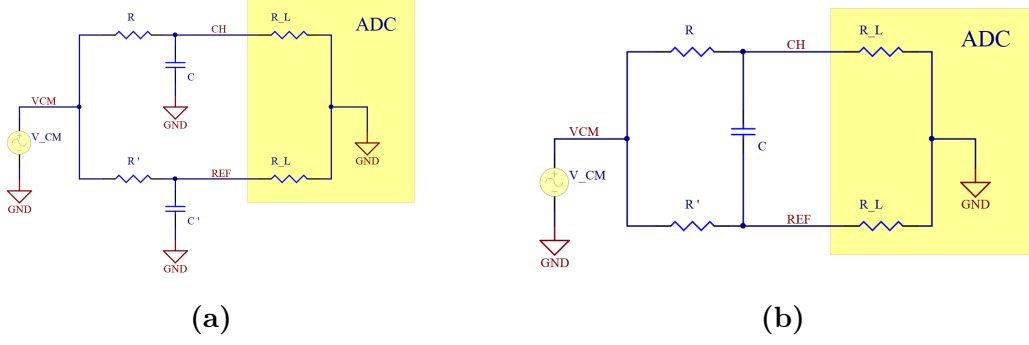


Figure 2.13: In this example, two different choices to implement the low-pass input pre-processing stages. In (a) is shown the common mode configuration, where the signal are individually filtered; in this case the designed must keep in mind the common-mode to differential transformation due to the mismatching between the real components values. In (b) the case of differential low-pass configuration; this kind of filter compensates the mismatch, leading to a common mode signal insensitivity.

mismatched stages, on the output we'll have two different signal with a different frequency spectrum. In a differential system this create an unwanted signal that in a ideal condition should be null. Then, as seen for the electrodes mismatching, we have again an CM2DM issue which degrades the final CMR of the whole system.

We made a simple simulation to show up and well understanding the conversion. In [9] the simplified formula which describes the relation between the differential output and the common input, in the simplest case of a passive low-pass filter, is

$$CMR = 20 \log \left(\frac{\delta R}{R} + \frac{\delta C}{C} \right) + 20 \log \left(\frac{f}{f_c} \right) \quad (2.30)$$

where f_c is the cut frequency of the RC filter. The 2.30 is a good starting point to understand the consequences of mismatching, but we have found a more accurately expression which describes the frequency characteristic of the phenomena:

$$\left| \frac{V_{ch} - V_{ref}}{V_{cm}} \right| (\omega) = \frac{R_l \sqrt{R_d^2 + \omega^2 \tau^2 R_l^2 E^2}}{\sqrt{\omega^4 \tau^4 R_l^4 (1 + E)^2 + \omega^2 \tau^2 R_l^2 \left((R_s (1 + E) + R_s')^2 - 2R_p (1 + E) \right) + R_p^2}} \quad (2.31)$$

with

$$\begin{aligned}
R' &= R + \delta R \\
C' &= C + \delta C \\
\tau &= RC \\
E &= \frac{\delta R}{R} + \frac{\delta C}{C} \\
R_s &= R + R_l \\
R'_s &= R' + R_l \\
R_d &= R'_s - R_s \\
R_p &= R'_s R_s
\end{aligned} \tag{2.32}$$

Although the 2.31 could seem more complex and unclear, a deep analysis of it leads to know some useful attribute of function. Taking a look to the graph in Fig. 2.14 we can see the presence of an asymptote for $\omega \rightarrow 0$ with value

$$\left| \frac{V_{ch} - V_{ref}}{V_{cm}} \right| (\omega \rightarrow 0) = \frac{R_l (R'_s - R_s)}{R'_s R_s} \tag{2.33}$$

and an absolute maximum for a frequency that we call ω_{max} ,

$$\omega_{max} \approx \frac{1}{\sqrt{\tau^2 (1 + E)}} \tag{2.34}$$

which help us to find the maximum value of module as

$$\left| \frac{V_{ch} - V_{ref}}{V_{cm}} \right| (\omega_{max}) \approx \frac{E}{E + 2} \tag{2.35}$$

These formulas allow to find the better components in order to keep the degradation of CMR under a specific limit. Keep in mind that the case described above is particular and simple but its easy for a designer to reach a worst condition since the complexity of the issue grows as much as the number of the passive components involved (adding an high-pass CR filter to the example should be enough to understand).

Fortunately, we can reduce this kind of problem since in the our case the acquisition is purely differential, that is every channels (the electrodes) is referred to one, the reference on ear lobe. The improvement comes with the use of filters in differential configuration (and so called differential filters); in Fig. 2.13b the low-pass of these kind of filters is shown. The main differences between the common mode

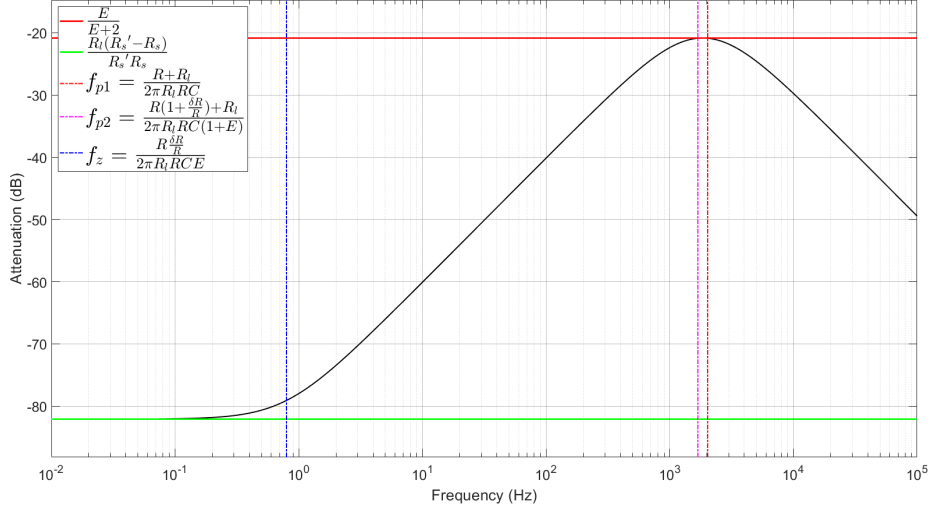


Figure 2.14: Frequency response for CM2DM in the low-pass RC filter with $R_l = 100K\Omega$, $R = 78.8\Omega$, $C = 1\mu F$ and 0.1% of tolerance.

configuration respect to the differential one is that here the value of time-constant parameter is $\tau = (R + R)C$, since the frequency response is

$$H_{diff} = \frac{1}{1 + j\omega(R + R)C} \quad (2.36)$$

, and the filtering is applied exclusively to the differential signal among channels.

The analysis of CM2DM for this new configuration bring us to find a different formula which describe the its characteristics:

$$\left| \frac{V_{ch} - V_{ref}}{V_{cm}} \right|(\omega) = \frac{R_l R \frac{\delta R}{R}}{\sqrt{\omega^2 \tau^2 R_l^2 (R_l E_2 + 2R E_1)^2 + R_l^4 + R_l^2 R^2 (2E_1 + E_2^2) + R^4 E_1^2 + 2R_l^3 R E_2 + 2R_l R^3 E_1 E_2}} \quad (2.37)$$

with

$$\begin{aligned} E_1 &= \left(1 + \frac{\delta R}{R} \right) \\ E_2 &= \left(2 + \frac{\delta R}{R} \right) \end{aligned} \quad (2.38)$$

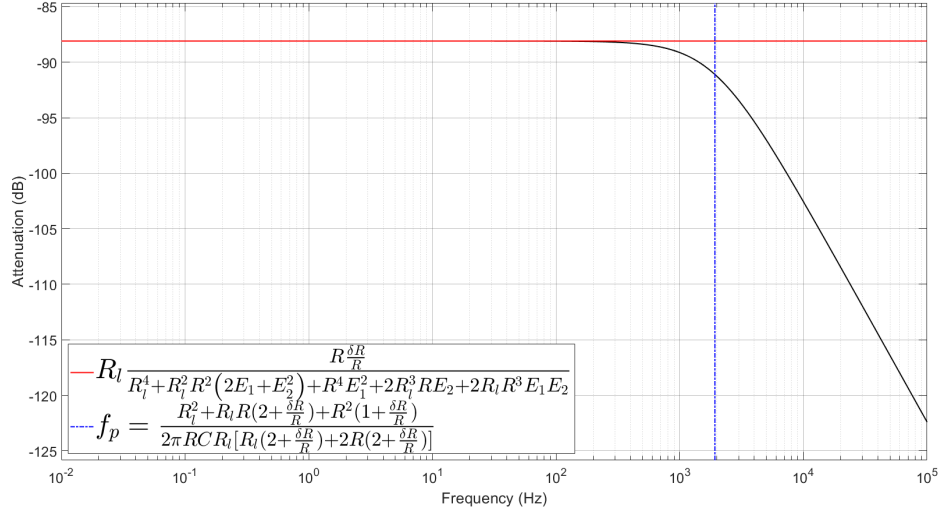


Figure 2.15: Frequency response for CM2DM in the differential low-pass RC filter with $R_l = 100K\Omega$, $R = 78.8\Omega$, $C = 1\mu F$ and 0.1% of tolerance.

In Fig. 2.15 the frequency response of the CM2DM shows again the presence of an horizontal asymptote for $\omega \rightarrow 0$ as in the case of common mode filter configuration, but now it represents even the maximum values reached:

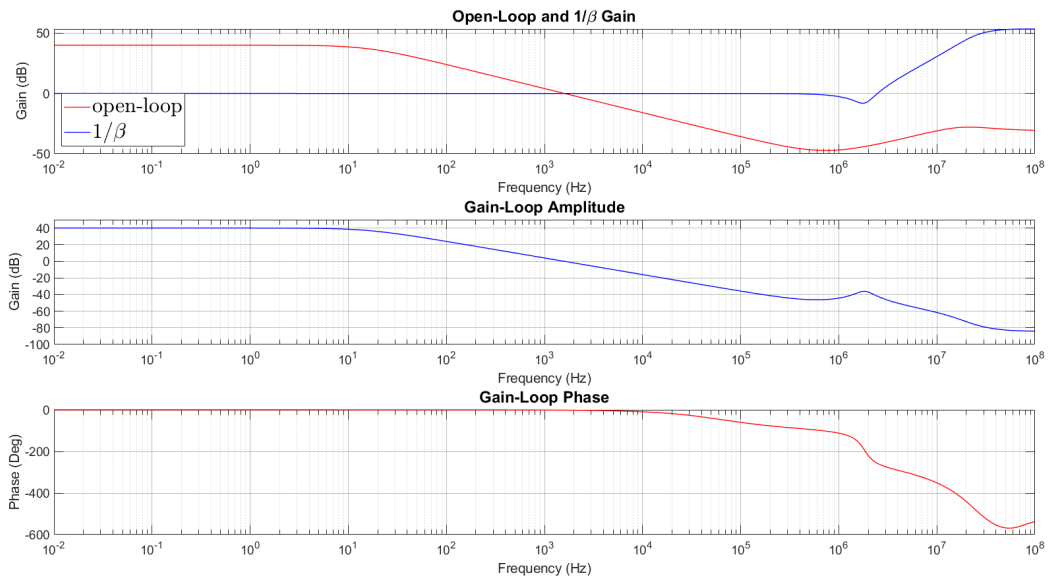
$$\left| \frac{V_{ch} - V_{ref}}{V_{cm}} \right| (\omega \rightarrow 0) = \frac{R_l R \frac{\delta R}{R}}{R_l^4 + R_l^2 R^2 (2E_1 + E_2^2) + R^4 E_1^2 + 2R_l^3 R E_2 + 2R_l R^3 E_1 E_2} \quad (2.39)$$

Comparing Fig. 2.14 with Fig. 2.15 we easily get the benefit using in our system filters in differential configuration, as the nature of acquisition lets us to do it.

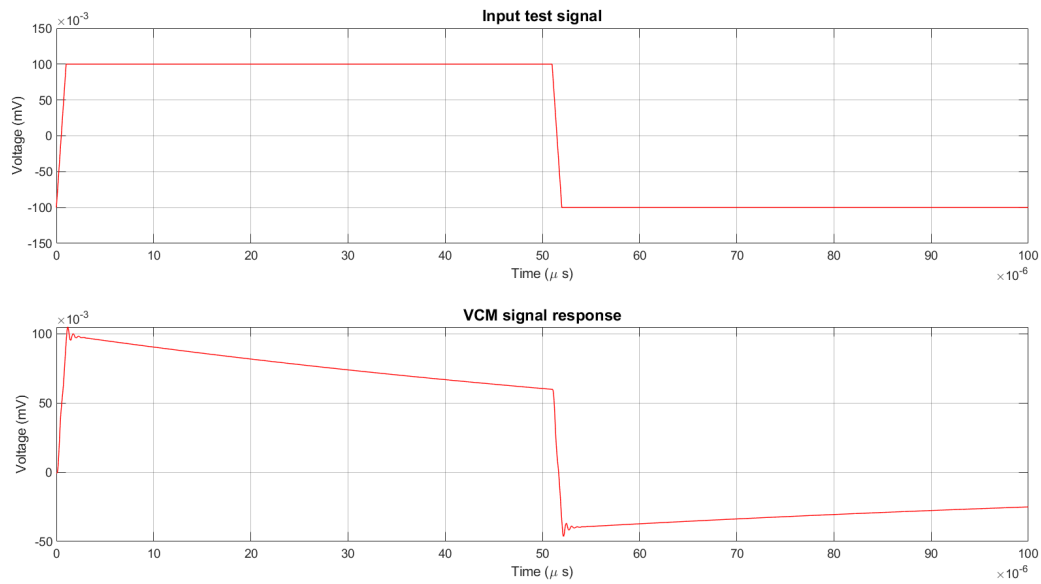
2.1.2.3 Limits for stability

As said in Par 2.1.2, the CMR improvement requires a feedback in the system and therefore an accurate analysis it's necessary to ensure its stability. For this reason, we had to break the loop before the active low-pass filter to be able to study the trend of open-loop gain A (active filter) and β gain (electrodes) in the frequency domain. Rather than calculate the loop-gain $A\beta$ to analyze the phase margin, the simplest method to ensure the system's stability is to look at the *Rate Of Closure* (ROC) between the open-loop gain A and the $1/\beta$ curves: the stability is guaranteed when the ROC is less or equal to $20dB$ per decade, in the other case instability occurs. A look to Fig. 2.16 and Fig. 2.17 gives a first overview of the concept.

The curve A and the curve $1/\beta$ respectively represent the transfer function of

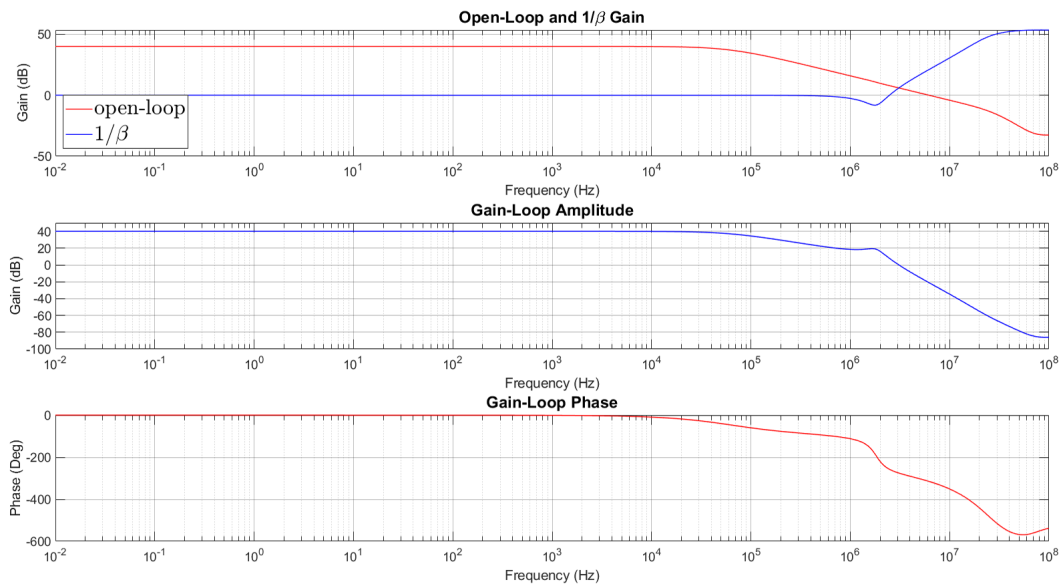


(a)

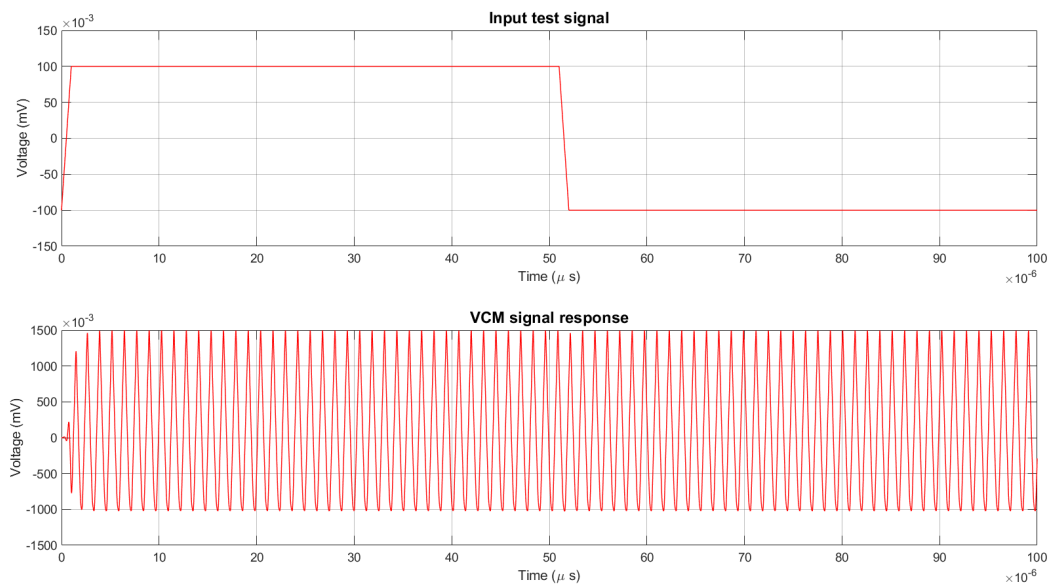


(b)

Figure 2.16: The stability is guaranteed when the *rate of closure* (ROC) between the open-loop gain A and the $1/\beta$ curves is less or equal to 20 dB per decade. In this example we have a ROC equal to 20 dB/decade near 1 kHz which guarantees the stability (a). As proof, we tested the system applying a step signal on one electrode and control the common mode response; the result is shown in (b).



(a)



(b)

Figure 2.17: The instability is reached when the *rate of closure* (ROC) between the open-loop gain A and the $1/\beta$ curves is more than $20dB$ per decade. In this example we have a ROC equal to about $40dB/decade$ near 30 MHz which means instability (a). As proof, we tested the system applying a step signal on one electrode and control the common mode response; the result is shown in (b).

the low pass filter and the inverse of the transfer function of the FL electrode, i.e. the whole section from the filter output to the user body (skin/electrode interface included). In general, in the expression of the β curve should also come into play the characteristics of paths relative to the electrodes of acquisition channels, which together bring the common mode signal to the buffer (U8A in the schematic of Fig. 2.7), but in our case the most significant contributions end at the inputs of the operational amplifiers mounted the individual active electrodes. Thus, if we want simplify, in the expression of β we will find only the input impedance value of the active electrode (usually very high). Taking these concepts into account we find the following expressions for A and β :

$$A(\omega) = -\frac{Z_f}{Z_i} \quad (2.40)$$

$$\beta(\omega) \approx \frac{Z_{iop}}{Z_{iop} + 2Z_e + Z_p} \quad (2.41)$$

with

$$\begin{aligned} Z_i &= R_i \\ Z_f &= \frac{R_f}{1 + j\omega R_f C_f} \\ Z_{iop} &= \frac{R_{iop}}{1 + j\omega R_{iop} C_{iop}} \\ Z_e &= R_{es} + \frac{R_{elep}}{1 + j\omega R_{elep} C_{elep}} \\ Z_p &= R_p \end{aligned} \quad (2.42)$$

where R_{iop} and C_{iop} represent the generic parallel of the input impedance of electrodes' operational amplifier.

To study the stability of the system we must therefore analyze the characteristics of 2.40 and 2.41 and in particular their dominant poles. This is because the ROC between A and $1/\beta$ necessarily depends on the relative position of their poles. To clarify the concept, we have to look at Fig. 2.18 in which the two curves are represented. As can be seen, the condition necessary for the ROC to not exceed $20dB/decade$ is that the zero $f_{z\beta}$ of the curve $1/\beta$ (which is nothing more than the β pole³) is as far as possible from the point f_{A0dB} where the curve A goes at $0dB$, value that $1/\beta$ keeps constant until its zero $f_{p\beta}$, point from which it begins to rise.

We can therefore define useful relationships that allow us to keep these points

³The curve $1/\beta$ is the inverse of β , so in the transition the poles and zeros exchange roles.

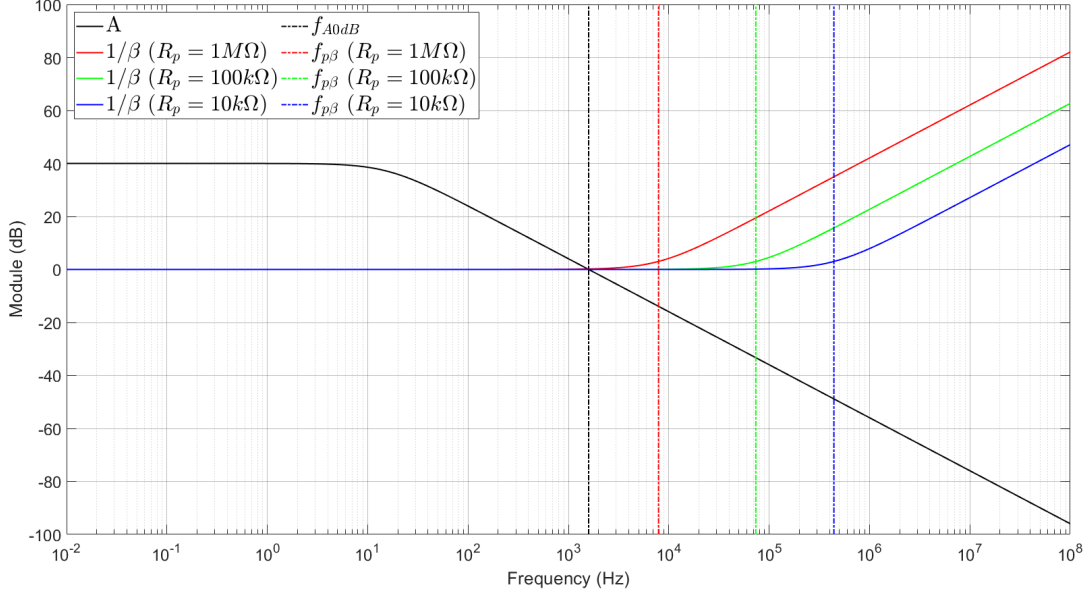


Figure 2.18: To study the stability of the system we must therefore analyze the characteristics of open-loop gain and the $1/\beta$ curves. In this simplified representation, the condition necessary for the ROC to not exceed $20\text{dB}/\text{decade}$ is that the zero of the curve $1/\beta$ is as far as possible from the point f_{A0dB} where the curve A goes at 0dB .

far enough to guarantee stability. We express the values of f_{A0dB} and $f_{p\beta}$:

$$f_{A0dB} = \frac{1}{2\pi} \sqrt{\frac{G(0)^2 - 1}{\tau^2}} \quad (2.43)$$

with

$$G(0) = \frac{R_f}{R_i} \quad (2.44)$$

$$\tau = R_f C_f$$

,

$$f_{p\beta} = \frac{R_{t1} + R_{t2} + \sqrt{[R_{t1} - R_{t2}]^2 - 4R_{ep}C_e R_{iop}C_{iop}R_{ep}R_{iop}}}{2R_{ep}C_e R_{iop}C_{iop}(R_p + 2R_{es})} \quad (2.45)$$

with

$$R_{t1} = R_{elep}C_{elep}(R_p + 2R_{eles} + R_{iop}) \quad (2.46)$$

$$R_{t2} = R_{iop}C_{iop}(R_p + 2R_{elep} + 2R_{eles})$$

.

As you can see, the only main constraint is represented by $f_{p\beta}$. Can we manage its value? Not entirely since in our model it is characterized by the protection resistance R_p , which we remember to be bound by international standards, and by various parameters that, by their random nature, cannot be known a priori (these parameters represent the contact quality between electrode and skin). However, it is interesting to see in Fig. 2.18 the effect of changing the value of R_p on the whole trend of the curve $1/\beta$: the more the resistance decreases, more the point $f_{p\beta}$ moves to higher frequencies guaranteeing the stability condition. It is important to note that this concept doesn't concern only R_p but the overall resistance seen by the active low pass filter. In fact, if we succeed in some way to reduce the impedance that characterizes the entire electrode, including the interface with the epidermis, the previous point continues to be valid (to check it is enough to solve the 2.45 at varying of parameters).

At the end, however, it is always wise try to keep the value of f_{A0dB} low; this is because it is the only parameter on which we can actually act. This in practice means not being able to set the gain and cutoff frequency of the filter as you want, but choose them appropriately so that

$$f_{A0dB} \ll f_{p\beta} \quad (2.47)$$

2.2 Firmware design

Once the hardware prototype of the VeeRg was implemented, the next phase involved the design of the firmware that will run on the on-board PIC32. Being a prototype, the attitude adopted all the time was to define an environment as flexible as possible since we didn't know what types of processing should have been implemented.

The development environment used is MPLABX IDE by Microchip, available with its XC32 compiler. In some cases, this environment has become very useful thanks to the recent implementation of the Harmony framework, but only with regard to the configuration of microcontroller peripherals; for the rest, we decided to implement the libraries necessary for their management in order to keep everything under control and streamline the code as much as possible.

The starting point was to create a communication standard to allow the system to communicate with any device in total transparency. Keeping this point, has been defined a command package, used to inform the system about what to do,

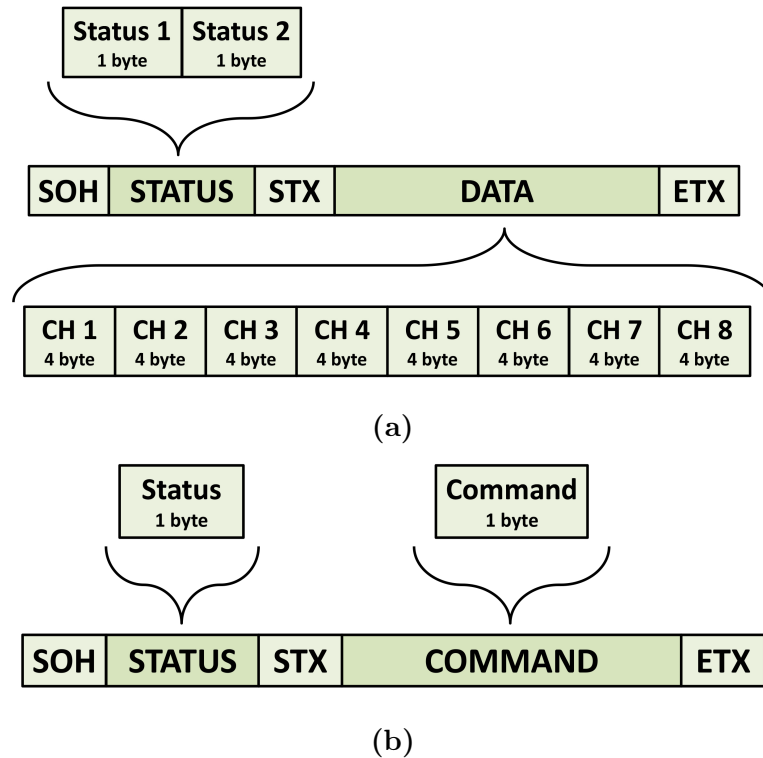


Figure 2.19: The definition of data (a) and command (b) packets.

and a data package, used to send the acquisition data and the internal status of the VeeRg.

In Fig. 2.19 the two configurations of data (a) and command (b) packets are shown. The SOH, STX and ETX⁴ represent markers for check the correct transmission of information. These markers delimit the status bytes and data/command bytes.

Once it has been defined the way in which the system communicates with the terminal connected to, the firmware has been developed from the lowest processing level, the one of the relevant drivers useful for the correct communication between the peripheral devices and the microcontroller. In Fig. 2.20 we show the overall structure of the implemented code, whose layered layout wants to underline the hierarchy of the libraries (every individual box) each developed for a particular processing level that increases in complexity from the bottom towards up. The dashed boxes represent those functionalities implemented but which currently have been disabled as not useful for the purposes of our work (in particular the management of the IMU and the AHRS system) or cause has yet to be optimized (the removal of eye's artifacts); this means that their functionality it can be easily

⁴These elements have been borrowed from ASCII encoding and represent acronyms for Start Of Header (SOH), Start Of Text (SOT) and End Of Text (EOT).

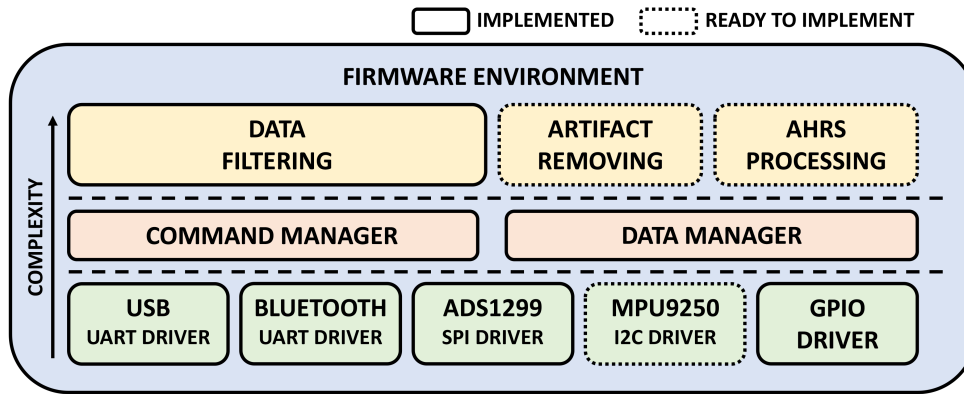


Figure 2.20: The overall structure of the implemented firmware with its layered layout to underline the hierarchy of the libraries (every individual box) that increases in complexity from the bottom towards up.

rehabilitated simply by appropriately recompiling the source code and reloading it on the microcontroller.

Starting from the bottom level we have the functionality for the most basic processes, which means the communication drivers between microcontroller and external peripherals. During the hardware design phase we have chosen the interpreters for USB and Bluetooth communication interfacing with the PIC32 through the UART serial standard, this the reason two separate serial drivers have been created for the independent management of the aforementioned communication devices. After them we have the driver that manages the exchange with A/D ADS1299 front-end which uses the SPI standard and the driver for the management of communication with the IMU MPU9250 through the use of the I2C standard (actually this device is disabled). Finally, for the sake of completeness, the library for the management of the microcontroller’s I/O ports suitable for the control signals, such as the status LEDs or the activation of analog power supplies.

In the upper level we find the routines that allow the connection between the interface drivers and the processing algorithms. Of particular interest, the state machine used for decoding and managing the commands that the system receives from the terminal (*Command Manager* in Fig. 2.20). During the decoding, the control over the integrity of the command packet also occurs through the markers described above; in the event that the system recognizes an anomaly in the structure of the packet, it’s excluded waiting for the next one and setting an error flag to trace the error occurred. Regarding the data, a shared memory allocation was created and accessible from both the remaining levels (*Data Manager* in Fig. 2.20). This is basically a data structure in which are stored temporarily the raw data of A/D conversion coming from the driver and also the subsequent results of their

processing carried out by the upper level, which will then be collected and managed by the USB/Bluetooth communication drivers.

Finally, we find the most interesting and complex part that includes the effective processing of signals, designed to clean up and prepare data for the subsequent processing on the connected terminal where the higher performances allow to perform much more complex calculations and eventually extrapolate further additional information. At the higher processing level we find all the algorithms that allow the user to process the acquired data. In this context we enter the most interesting part of the firmware design, as it relates to the particular choices made to try to extract the wanted information. It should be clear that this type of processing is not strictly necessary for systems of this nature, but it has been considered useful to give the user the possibility of reading already *clean* data, reducing the load of downstream processing. Such processing can therefore be enabled or disabled at the discretion of the user simply by sending appropriate commands. The two most important processes concerning the filtering will be described in more detail in the following paragraphs. Regards the AHRS, we won't deal with it in this work due to its particular complexity and the non-strict correlation with the EEG systems; the reader can anyway find numerous articles about this argument, such as [35] [28].

2.2.1 Filtering

In Par. 2.1.2 we mentioned the fact that analog input stages placed close the front-end ADS1299 are substantially first order RC low-pass filters; this base configuration helps to eliminate all the high-frequency disturbances beforehand and it doesn't represent a definitive solution at all. This is a pre-filtering phase which does not affect the useless signals in any way. Moreover, depending also on the applications in which the EEG system will be used, filter the signals permanently in an analogical way before the conversion does not appear to be a functional choice since the signals in their raw form can be useful to apply on them different types of analysis at a later stage. However, the adoption of a digital post-conversion processing is the optimal solution for a system which requires as much as flexibility as possible.

As we explained in Chap. 1, we are interested in the band between the ~ 4 Hz and the ~ 80 Hz composed by *theta*, *alpha*, *beta* e *gamma* waves. The final objective of the filtering is to reduce as much as possible the signal-to-noise ratio cutting all the disturbances which don't fit with the band of our interest. From an energy point of view, the most heavy disturbances are those at low frequencies,

particularly all the frequencies components very close to the continuous one (or DC), while those at high frequencies are present but with far lower energy contributions. Although conceptually it does not seem to be a problem, the use of filters in the post-processing of an EEG acquisition can be a real challenge for the designer who wants to keep the information content intact and still useful for his own analysis, without the risk of producing wrong results. The main real danger, indeed, is to introduce a distortion that deeply modifies the original signal. Obviously, it is not known how much more or less this distortion can be tolerated since it depends strictly on the type of final analysis on the data; but it is still a good form to keep it as low as possible. For this reason, some studies, as [33], even suggest to completely avoid the use of filters and to focus on working on raw data.

The introduction of distortion is the reason why it is better to avoid the use of a band-pass filter in order to isolate our band from disturbances at low and high frequencies as, as underlined in [37] and in other studies, it introduces significant distortions on the output signal. It is instead advised to use a high-pass filter and a low-pass in cascade: the first with a very narrow transition band, useful feature for studying evoked potentials (or ERP), while the second with a wider transition band, in order to minimize the total distortion introduced.

2.2.1.1 FIR and IIR

Digital filters can be divided into two groups: the ones under the name of *Finite Impulse Response* (FIR) and the ones which take the name of *Infinite Impulse Response* (IIR). Let's briefly look at their main characteristics keep in mind their use in electroencephalography.

The use of a FIR filter is appropriate when the phase characteristic should be flat. When the demands on the filter are not very high, this is the easy solution to go for. In the context of EEG measurements this filter could be used as high pass or low pass filters. The EEG signal is not degraded by a variable phase characteristic and yet a sharp fall-off can be attained by picking a filter with a high order, since a large delay is allowed for the off-line application. These filters are especially well suited if the phase characteristic of the signal is very important and can thus be used for coherence and synchrony measures.

- PROS Finite Impulse Response filters:
 - A FIR filter will always give a stable output, because it is non-recursive
 - A FIR filter has a delay that is constant over all frequencies; the signal shape will not be influenced by phase shifts

- CONS Finite Impulse Response filters:
 - A FIR filter is inefficient, it uses lots of input to calculate the output, therefore:
 - A FIR filter has a large delay

The use of an IIR filter is appropriate when, a small absolute delay is required or when strong requirements on amplitude characteristic are necessary. Where there is only one type of FIR filter, there are several types of IIR filters.

- PROS Infinite Impulse Response filters:
 - An IIR filter is very efficient, it uses only a few previous output values to calculate the current output, therefore:
 - An IIR filter has only a small delay
- CONS Infinite Impulse Response filters:
 - An IIR filter can become unstable, if coefficients are not well chosen
 - Because the requirement of causality and an infinite impulse response that converges to 0 for $n \rightarrow \infty$, the impulse response cannot be symmetrical. This implies a phase characteristic that is not constant over frequencies. Therefore, different frequencies will appear at the output with a different shift in phase. The shape of the output signal will change as a consequence of different phase shifts

The three most common IIR filters are the Butterworth, the Chebyshev and the Elliptic, and everyone has a specific characteristic for specific contexts.

The use of a Butterworth IIR filter is appropriate when a maximally flat pass- and stop-bands are important, when less stringent restrictions on fall-off and phase characteristics are allowed. Choice to put emphasis on fall-off or phase characteristics can be tuned by choosing an appropriate filter order. The phase characteristic of a Butterworth filter is poor, therefore synchrony or other phase related analysis are not recommended with this filter. An example of the use of Butterworth filters in EEG would be an on-line EEG frequency band analysis (theta, gamma, alpha, etc). The pass- and stop-bands are maximally flat, thus resulting in a quality output signal for the different frequency bands. Furthermore, a reasonably sharp fall-off can be reached. Care has to be taken in selecting the correct trade-off between fall-off and phase characteristic.

The use of a Chebyshev IIR filter is appropriate when some ripple in the pass-band is allowed and more emphasis is placed on good stop-band behavior and fall-off. The phase characteristic of a Chebyshev filter is poor. The use of this filter is recommended with intermediate frequency ranges e.g. alpha 1 vs. alpha 2.

The use of an elliptic IIR filter is appropriate when the fall-off is the very critical design criterion. The sensori-motor rythm (SMR) is a good example of such a critical design criterion. The SMR is a very specific rhythm of 12-14 Hz. For a quantification of the SMR –and only the SMR– a very narrow frequency band has to remain at the filter output, thus implying a very steep fall-off. Some waveform degradation has to be accepted (ripple, phase characteristic) to attain this sharp fall-off, but this is a small price to pay knowing that you analyze a true sensor-motor rhythm.

From this brief overview of the main differences between the FIR and IIR filters, we can already make choices for our system. Bearing in mind the limited processing and memory resources made available by our system: in [19] we can read that the PIC32MZ0512EFE064 in use has a maximum frequency of 200 MHz and a volatile data memory of 128 KB. These values are completely acceptable for the vast majority of applications but can become a limitation as soon as we deal with operations which involves a large amount of data. From this point of view the FIR filters can easily represent a problem if their order is very high (as often happens with particularly selective filters); with the same frequency characteristics, the IIR filters certainly represent a more suitable solution thanks to their lower computational weight. We can take as example the implementation of a high-pass filter designed through the MATLAB application *Filter Designer*. In Fig. 2.21 are shown the characteristics that can be set for the generation of the filter's coefficients. Fixed $A_{stop} = 80dB$, $A_{pass} = 1dB$, $F_{stop} = 3Hz$ and $F_{pass} = 4Hz$, the implementation of a FIR Equiripple filter generates 687 floating point coefficients while for a IIR Butterwhort filter requires only 126⁵. Considering that inside the program they become 4-byte floating-point numbers, it will be occupied a space of 2744 and 504 bytes respectively. This without any temporary variables used during code execution and only for one channel: in our particular case, using 8 channels and considering also the space occupied by the past values, necessary during the FIR execution, we easily arrive at about 45 KB of memory occupied only for the high-pass filtering.

Furthermore, in addition to a computational and memory's occupation advan-

⁵In the case of IIR filter, are used sections of the second-order which provide three coefficients to the numerator, three to the denominator and one factor of correction. For the implementation of the code see App. A.2.1

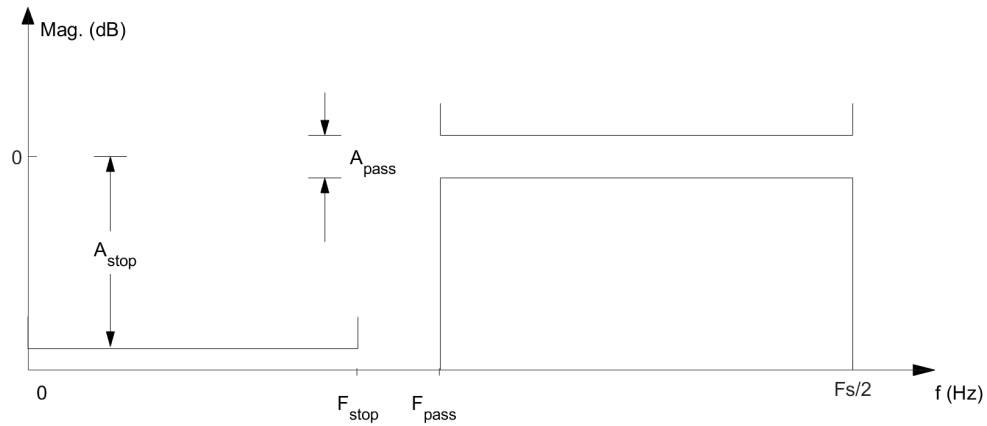


Figure 2.21: The characteristic of an high-pass filter as shown in the MATLAB's app *Filter Designer*.

tage, IIR filters have less delay, making them particularly suitable for real-time applications, as in our case. Always referring to the example above, we can assume that the response of an IIR filter is almost immediate while the FIR filter presents a delay in the response of about 1.4 seconds. The only sore point regarding the use of IIR filters is that their phase is non-linear with respect of the frequencies. This means having a greater distortion on the output signal than in some cases, depending on the types of analysis, it can represent a crucial issue. As far as we are concerned, we considered this defect less relevant since our initial intention is to analyze exclusively the Power Spectral Density (PSD) of the acquired signals, an analysis which takes in consideration only the amplitude of the frequency components. However, it is good to keep in mind that, in case of switching into an analysis in the time domain, the use of IIR filters could be a problem if their phase in the passband is not monitored.

2.2.1.2 The high-pass filter

We have seen how the IIR are the most suitable filters for our system thanks to their characteristics which are perfectly suited to a real-time acquisition. At this point, it became important to choose between the three main categories of IIR: Butterworth, Chebyshev and Elliptical. Due to their characteristics, the most used are the Butterworth filters, because of their flat trend in the pass-band, and the Elliptical filters which have a narrow transition band and a limited ripple in the pass-band. These characteristics of the Elliptical filter make it a perfect candidate to implement the high-pass filter, able to eliminate the low frequencies close to the DC component and trying at the same time to keep intact those following, which can convey useful information. However, as we will see in the Par. 2.2.1.3,

<i>family</i>	<i>type</i>	<i>band</i>	<i>f_c</i>
IIR	Elliptic	high-pass	1 Hz
IIR	Butterworth	low-pass	45 Hz

Table 2.2: The filters and their characteristics in the system.

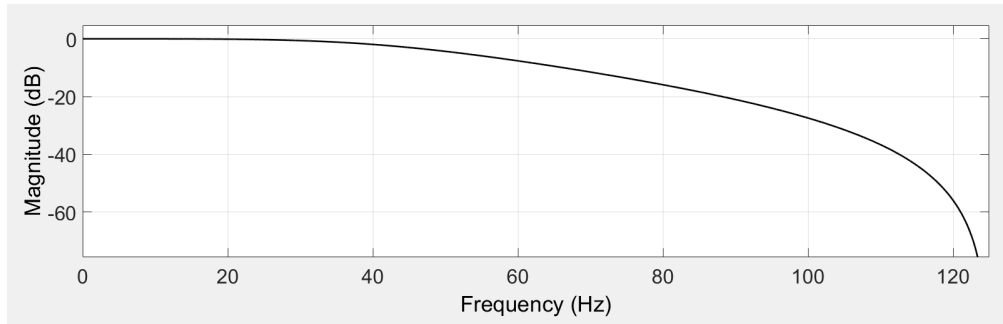
the Elliptical filter may not be entirely adequate as it introduces a longer delay than the Butterworth. Concerning the low-pass filter, however, we have already mentioned that their characteristics can be chosen with less rigidity, making the Butterworth, in this case, the best choice. In fact, if implemented with a low order, it contributes minimally to the introduction of distortions on the final signal.

Attention should, therefore, be focused more on the high-pass filter since its strongly selective characteristic can create problems of distortion. In literature, we can find a lot of discussions about which are the perfect features for this type of filters, but all often come to different results as they strictly depend on the type of analysis for which the EEG system is used. For example, in [30] and [31] it is highlighted, through a specific analysis of the various filtering techniques, how the wrong choice of the cutoff frequency of the high-pass filter can lead to artifacts that deviate from the correct interpretation of the signals; always from [30] and [31] the optimal cutting frequency which should not go beyond 0.1 Hz. These studies are based on the correct interpretation of the evoked potentials N400 and P600 related to semantic incongruity contexts (see [29]). Other studies, however, closer to our final target, put much weaker constraints on the filtering; in [40] they set the cutoff frequency to 1 Hz while in [34] to 2 Hz. In these last two cases, the analysis refers precisely to the behavior of the signals in the two states of mind of like and dislike. This is what interests us cause the distortion introduced by the filtering does not involve any problem since the analysis is based only on the Power Spectral Density and not in the time domain. We will see in Chap. 3 how, with our particular system, to limit the analysis only to the frequency domain can represent a limit.

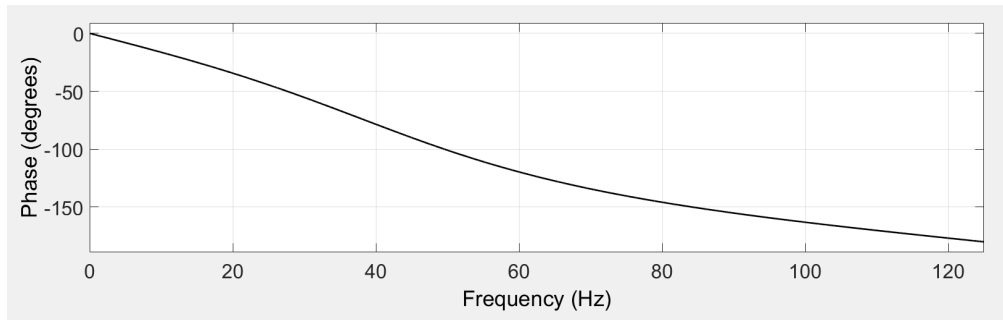
At the moment we follow the suggestion of [40] fixing the cutting frequency of the high-pass filter to 1 Hz and the low-pass ones to 45 Hz (Tab. 2.2) and controlling the effects of our choice on the real signals, in order to control the quality of the filtering.

2.2.1.3 Filtering effect

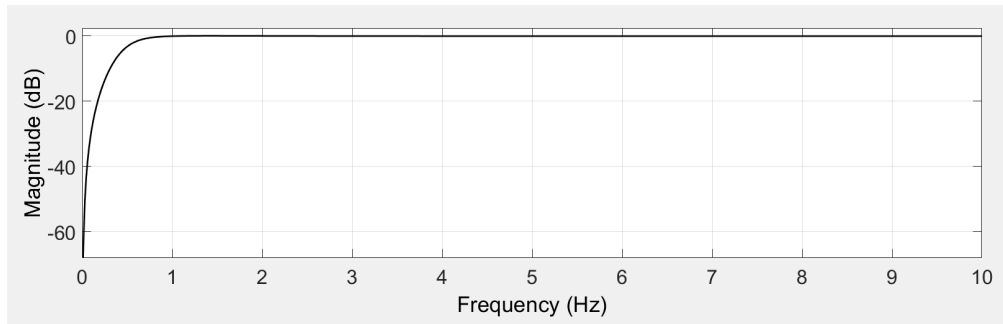
The effects of the use of high-pass and low-pass filters in cascade can only be evaluated in the practice. Given the adoption of IIR filters, it is indeed useful to understand in our specific case how far we have managed to keep under control the



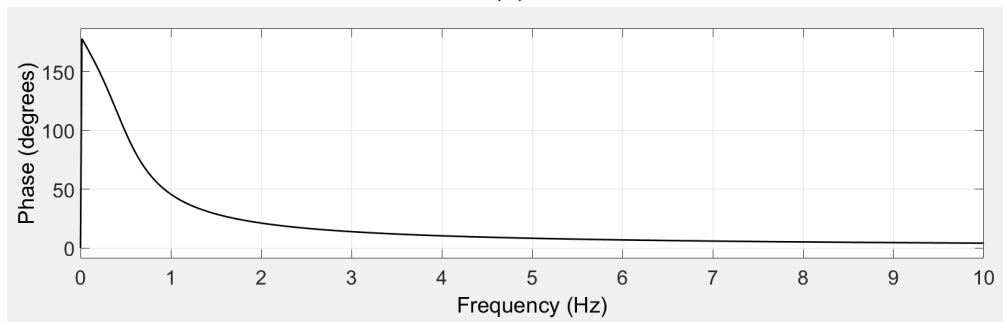
(a)



(b)



(c)



(d)

Figure 2.22: The filters' response in low-pass (a,b) and high-pass (c,d) case. For the second order IIR low-pass filter we've chosen a cut frequency at 45 Hz; in this case the phase response is almost linear in the pass-band. the second order IIR high-pass filter we've chosen a cut frequency at 1 Hz; here the phase response is more non linear in the lower frequencies of the pass-band, due to the narrow transition band.

distortion introduced by them, as it can lead to the presence of artifacts in case of analysis of the signals over time. In [37] what they always recommend to do is to test the effectiveness of the filters by directly comparing the filtered signals with the original ones, and eventually make the difference between them to get all the cut off components in the time domain. It must be said that the context in which this verification is made, is that of the auditory evoked potentials characterized by well known waves, especially N1, P1, N2 and P3 (see [29]), which have very particular trends. In these cases, it becomes easy to identify, if it is present, the effect of the distortion on the signal or the *trend* from which we want to extract the information. Our case doesn't concern this type of analysis, but what we still do is to observe the effect of the filters chosen on the signals acquired in real time in order to evaluate if there are large deviations.

First of all, what we did was to design the filters and make the appropriate observations in off-line mode through the MATLAB's Filter Designer application, to speed up the study and give the possibility to make any changes on-fly. In this regard, we have previously acquired a test signal taken from the Fp1 electrode of our system; the acquisition was set with a sample rate of 250*sps* (250Hz) for a duration of about 6 seconds, this means 1536 samples. We have recorded obviously raw data, without any kind of processing if not for the only one necessary to scale the output values in microvolt. The gain of the ADS1299 has been set to 1. The signal was acquired during a state of rest in which two types of common artifacts has been intentionally created: appears in a certain moment three peaks, each one corresponding to the blinking of the eye and a *step* due to a small displacement of the electrode. After its acquisition, the signal has been saved in the MATLAB environment where it was processed afterwards using a proper script.

Subsequently, we have implemented six filters:

1. Low-pass filter, IIR, Butterworth, 2nd order, 45 Hz cut-off frequency
2. Low-pass filter, IIR, Elliptic, 2nd order, 45 Hz cut-off frequency
3. High-pass filter, IIR, Butterworth, 2nd order, 1 Hz cut-off frequency
4. High-pass filter, IIR, Elliptic, 2nd order, 1 Hz cut-off frequency
5. High-pass filter, IIR, Butterworth, 2nd order, 0.1 Hz cut-off frequency
6. High-pass filter, IIR, Elliptic, 2nd order, 0.1 Hz cut-off frequency.

We wanted to keep the comparison between the use of Butterworth and the Elliptical for each type of filter and cutting frequency value. In particular, although

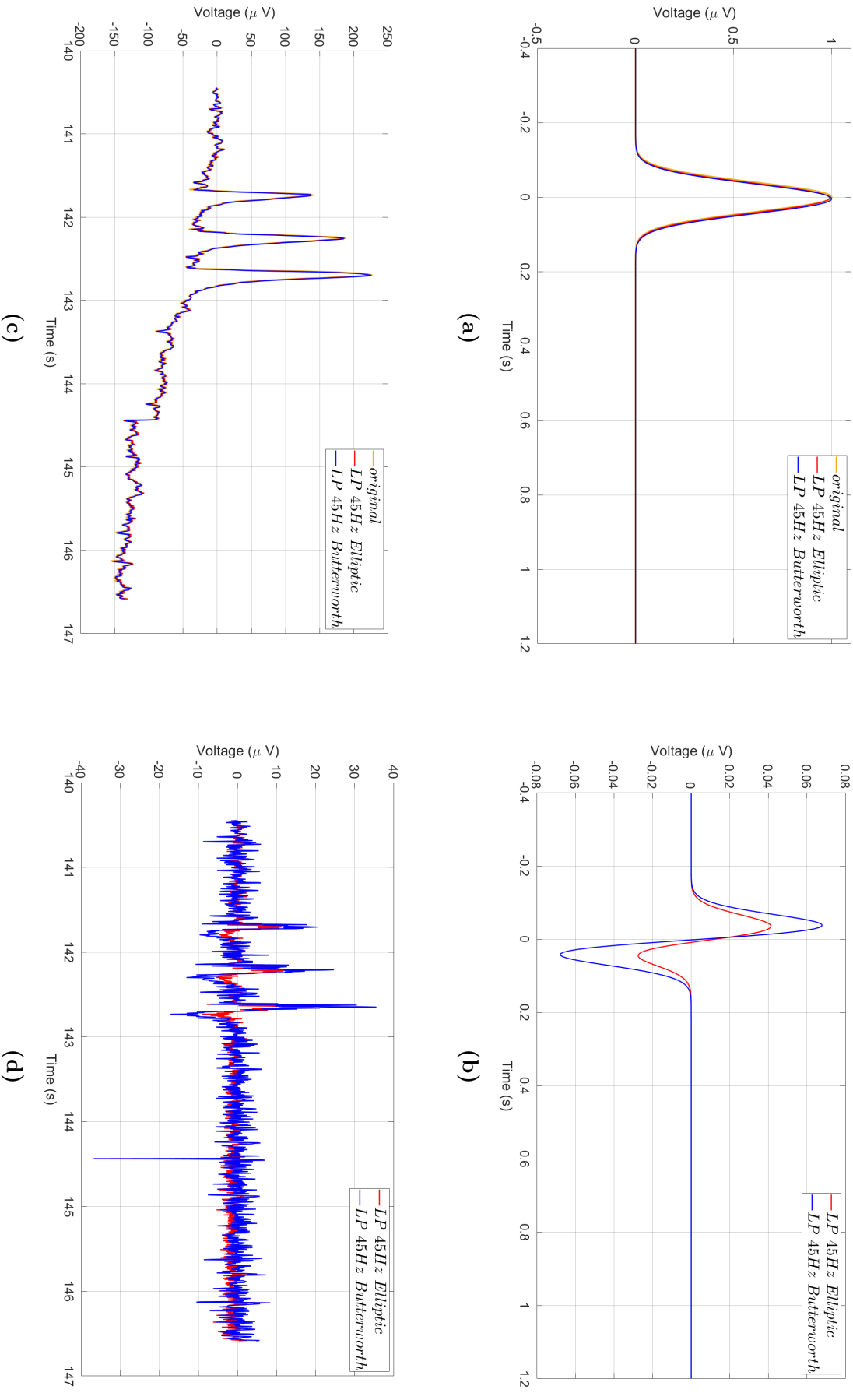


Figure 2.23: The low-pass filter effects. It introduces a very low distortion with a practically null delay. We can verify this both on the Gaussian test signal (a) and on the real test (c) where the outputs overlap; also observing in (b) and (c) we can confirm the actual low distortion. The amplitude of the oscillations, indeed, is an indication of the amount of distortion introduced: the greater the amplitude, the greater will be the distortion.

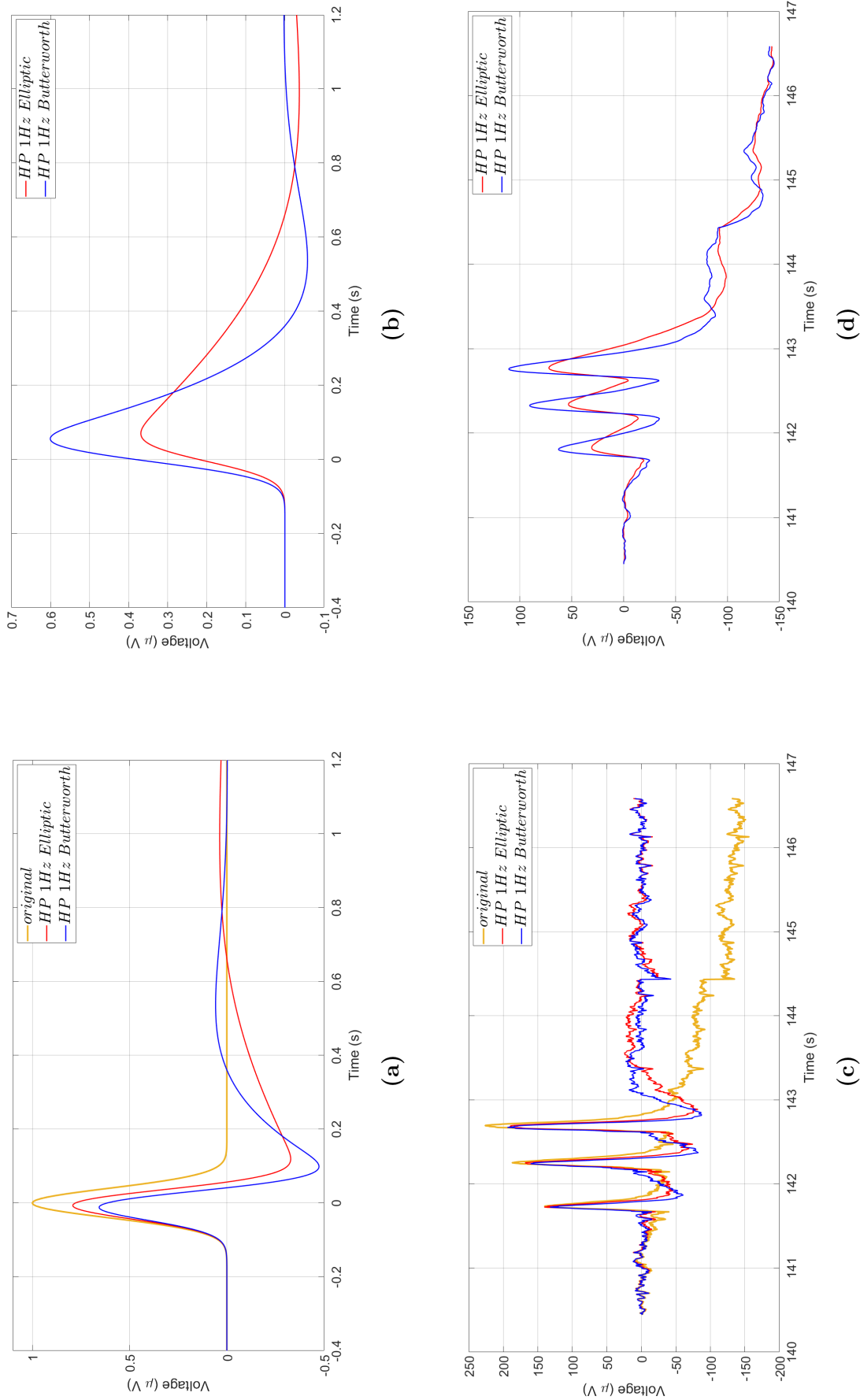


Figure 2.24: The high-pass filter effects. It introduces an evident distortion with some delay. We can verify this both on the Gaussian test signal (a) and on the real test (c); also observing in (b) and (c) we can confirm the actual distortion. The amplitude of the oscillations, indeed, is an indication of the amount of distortion introduced: the greater the amplitude, the greater will be the distortion.

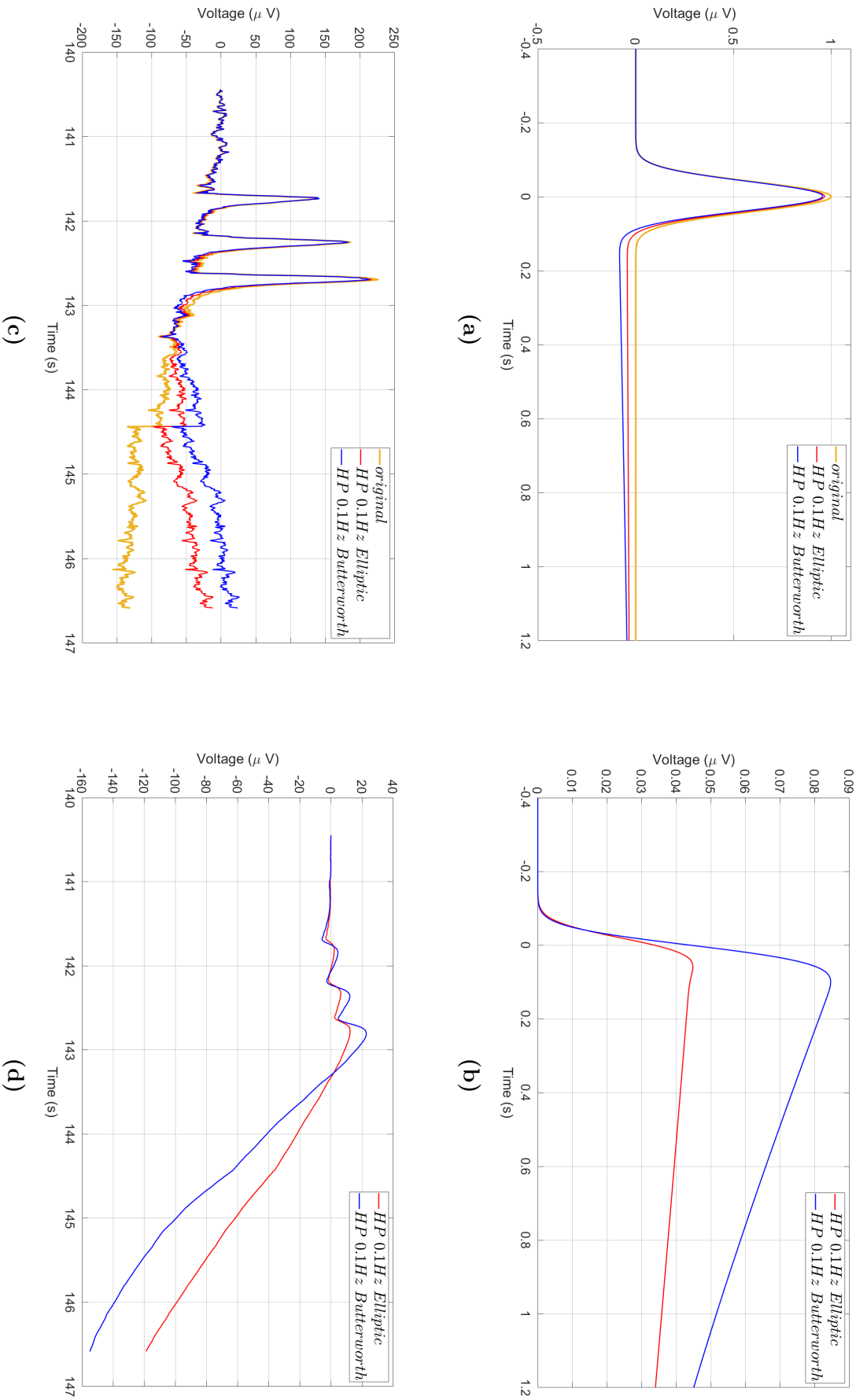


Figure 2.25: The 0.1 Hz high-pass filter effects. The choice of a cut-off frequency of maximum 0.1 Hz drastically reduces the distortion introduced by this type of filters, but at the expense of a much wider delay. In (b) and (d) the oscillations have a far lower amplitude than the high-pass filter at 1 Hz, and the results can be confirmed with the test function shown in (a) and (c): the peaks of the original waveforms are almost all preserved.

we are convinced about putting the cutoff frequency of the high-pass filters at 1 Hz, in any case, we wanted to test the effectiveness of the same filters with a cutoff frequency of 0.1 Hz, as suggested by [17] and [30].

The results of the six elaborations are grouped in Fig. 2.23, Fig. 2.24 and Fig. 2.25. For each elaboration, we illustrated a specific cut-off frequency and its comparison between the use of the Butterworth and the Elliptical. In the boxes (a) and (b) there are the effects of the filters on the Gaussian test signal, which is commonly used for this purpose due to its large spectral component; in this way, it is easier to consider the distortions and the delays introduced by the filters. In (a) are simply compared the outputs of the two filters with the original input signal, while in (b) it is made the difference between them in order to get an idea of the filtered components, of the delays and, in general, of the distortions introduced.

The first to be examined is the low-pass filter (Fig. 2.23). From the functional point of view, it is the most efficient because it introduces a very low distortion with a practically null delay. We can verify this both on the Gaussian test signal (Fig. 2.23a) and on the real test (Fig. 2.23c) where the outputs overlap; also observing in Fig. 2.23b and Fig. 2.23d we can confirm the actual low distortion having already observed the almost null entity of the heavy variations in the average trend of the curves. The amplitude of the oscillations, indeed, is an indication of the amount of distortion introduced: the greater the amplitude, the greater will be the distortion. The use of this filter, therefore, does not affect the final quality of the signal ⁶.

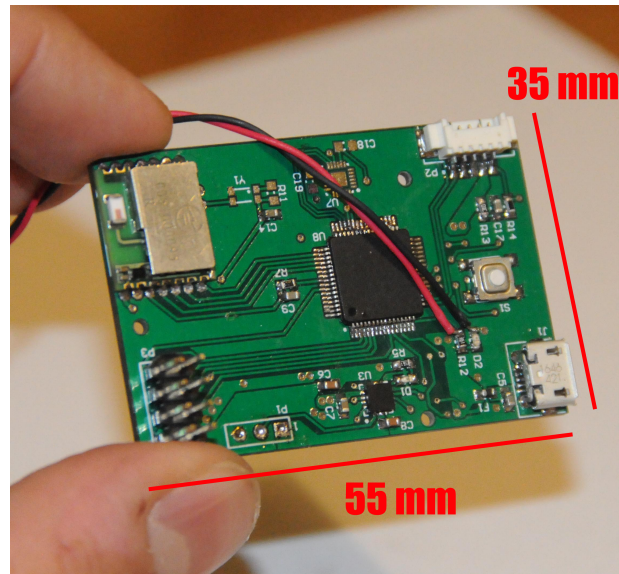
The second filter analyzed is the high-pass with a cut-off frequency at 1 Hz (Fig. 2.24). Here the distortion is certainly more evident and we can immediately notice it from the filter response to the Gaussian test signal in Fig. 2.24a. It is evident that the amplitude of the signal is considerably reduced provoking also an under-shoot which was not present originally, gradually stabilizing with a delay that differs according to the type of filter under examination. Indeed, we can observe considerable differences between the Butterworth and the Elliptical response. In the first one, although it has a lower delay, the distortion is visibly greater as confirmed in Fig. 2.24b. Also in the case of the real-time continuous signal, it would seem to have better characteristics considering how much time the signal takes to return to its originally state, but things changes as soon as we consider the distortion, since in Fig. 2.24d the oscillations in the Butterworth gap are wider. Starting from these considerations, the Elliptical filter has got a less significant

⁶The fact that the low-pass does not contribute to the distortion of the signal is given by its characteristic of being only second-order, which means a very low selectivity but still adequate for our purpose.

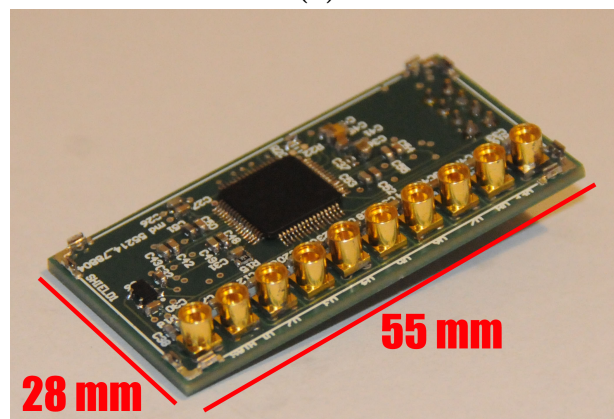
distorting characteristic than its competitor, to the detriment of a little larger delay. It is precisely this compromise which got us choosing the Elliptical filter for our system.

The third and last filter we are analyzing here is the high-pass filter with a cut-off frequency at 0.1 Hz (Fig. 2.25). This filter has been tested to clarify and confirm what has been shown in [17] and [30] and effectively, without explain why this value, the choice of a cut-off frequency of maximum 0.1 Hz drastically reduces the distortion introduced, but at the expense of a much wider delay. In Fig. 2.25b and Fig. 2.25d the oscillations have a far lower amplitude than the high-pass filter at 1 Hz, and the results can be confirmed with the test function shown in Fig. 2.25a and Fig. 2.25c: the peaks of the original waveforms are almost all preserved.

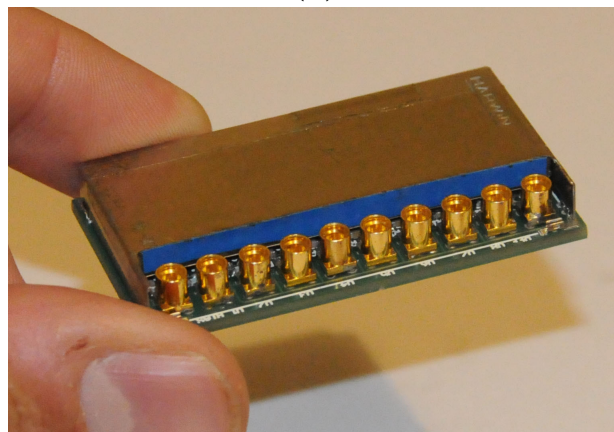
It has to be clear that the observations just made upon the filters we have chosen, do not lead to a precise confirmation about *which is the best filter*, but nevertheless we can have an idea of *which filter is more appropriate to be used for this analysis*. We must always keep clarity about which is the information we want to extract from the acquired signals. In our case, considering that it is the creation of a prototype, it would be ideal to give to the user the possibility to choose real-time which type of filter and characteristics he would like to adopt; which would not be a problem if the processing would take place on the terminal, but could become a problem if we would think about giving in charge of it to the on-board microcontroller, so that it would be more decisive an optimization of the code and occupation of memory.



(a)

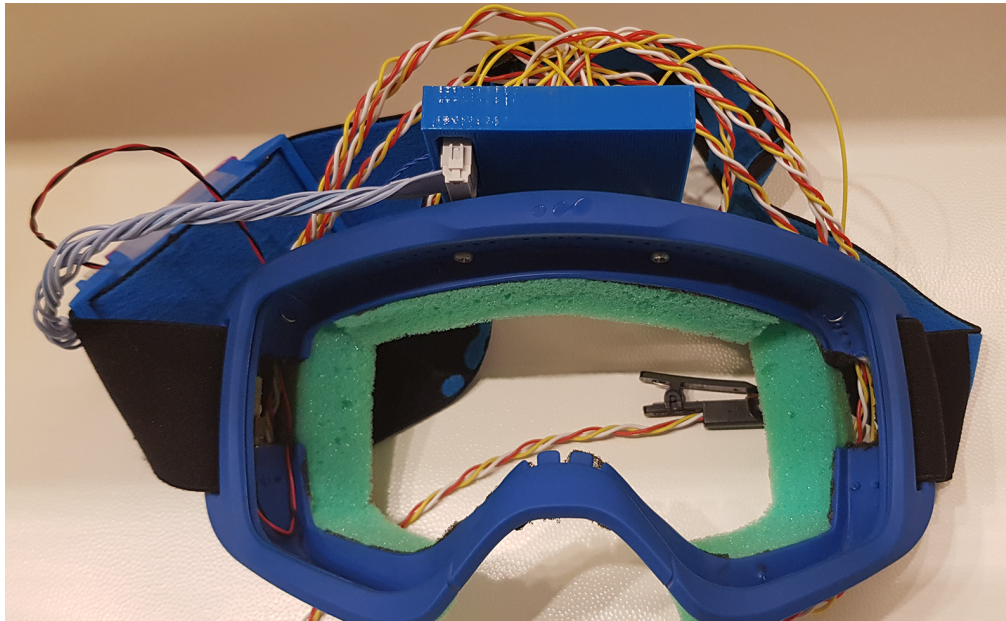


(b)

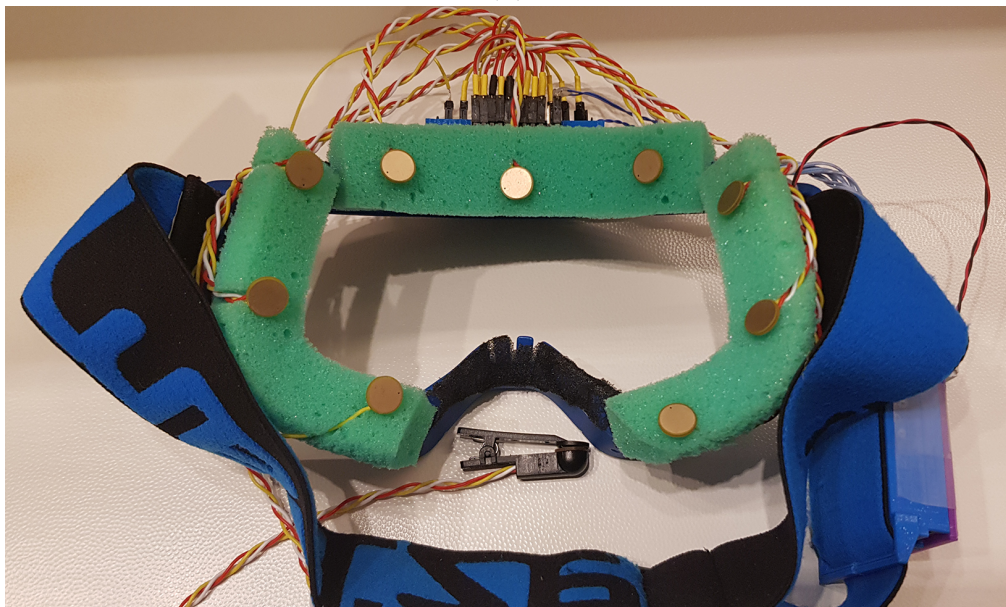


(c)

Figure 2.26: An overview of the VeeRg system's boards. In (a) the elaboration board which receives and processes the digitalized data coming from the analog-to-digital conversion. In (b) the acquisition board which is strictly analogue and has the specific front-end for bio-electrical signal acquisition, the ADS1299. In (c) the same board with the shielding.



(a)



(b)

Figure 2.27: An overview of the VeeRg prototype. In (a) the frontal side and in (b) the back side. The black clip is for the earlobe reference.

Chapter 3

Like and dislike recognition

For decades the interest of the research to identify and recognize the emotional states has always been high. So much so that over time we have been consolidating a branch of inter-disciplinary research that sees psychologists, neuroscientists, researchers of artificial intelligence, scholars of cognitive processes, etc. struggling with the analysis of all those processes that can objectively determine the mood of a person. The reason for this interest is inherent in its vast field of application that can range from pure commercial entertainment to the medical rehabilitation.

We can distinguish two main methodologies in the recognition of emotions. The first provides that the analysis is done on non-physiological signals such as facial expression or modulation of the vocal tone. This method proved to be the simplest to apply because it did not include the use of particularly complex instrumentation and data processing, at least until today where the current technology allows us to perform advanced analysis on video images. Its main problem, however, is given by the ambiguous facial expressions, easily controllable or not evaluable due to deficits such as paralysis. The second methodology for the recognition of emotions, on the other hand, is based on the analysis of the physiological signals coming from the inner part of our body and therefore apparently hidden from the outside. These signals are acquired through the use of techniques that have long been the exclusive heritage of medicine: the electroencephalogram (EEG) which allows the reading of brain activity in the form of variable electrical potentials, electromyography (EMG) that monitors and transforms the activity of the muscles still into electrical potentials, the electrocardiogram (ECG) that records the pattern of cardiac activity, the resistance of the skin (SR), the blood pressure and so on. It is important to underline that many studies relative the field of the emotion recognition use a methodology that is nothing but the fusion of the two described above, but are characterized by a very high systematic and computational complexity required

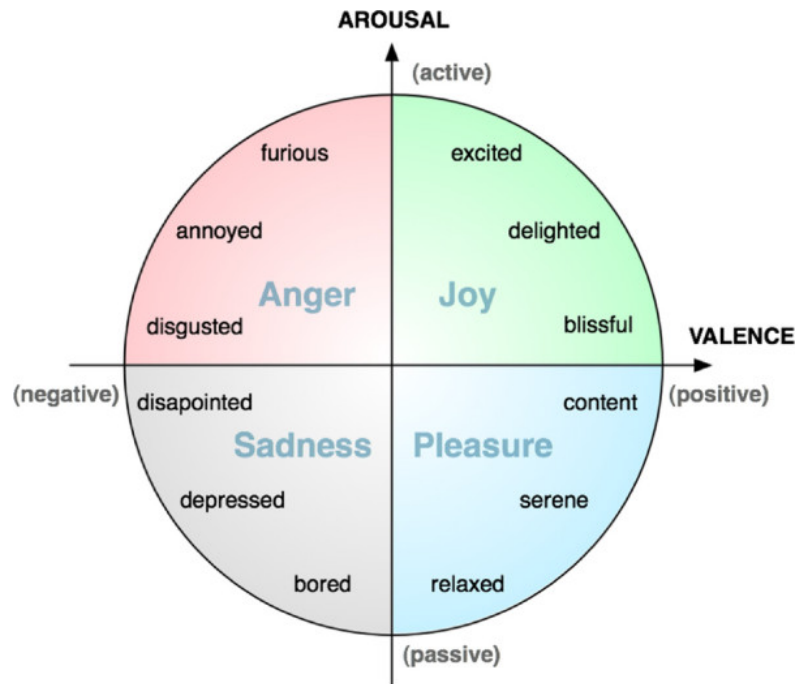


Figure 3.1: This is an example of the bi-dimensional emotional space defined by the arousal and valence values and described in [39].

only for very advanced analysis. Currently the methodology that uses only physiological signals is the one on which the attention of the greater part of the research community is being focused. The reason is mainly due to the strong diffusion of electroencephalographic systems on the market that, if properly designed, can also act as electromyographic systems. The fact that they have become the most used acquisition devices is due, however, not only to their low market price, but also to the fact that electroencephalographic systems have a high degree of practicality given their non-invasive characteristics. The possibility of acquiring brain signals through the use of surface dry electrodes placed on the epidermis (or in some cases even through contact-less capacitive electrodes) obtaining a good temporal and spatial resolution is the key to these systems.

Another very controversial subject concerns the way in which emotions can be described. There are two possible points of view: the discrete one and the dimensional one. Discrete classification is based on the fact that emotions can be seen as combinations of discrete and well-defined moods. For example in [22] are defined anger, fear, sadness, disgust, surprise, expectation, acceptance and joy. In [5] are shown the relationships between facial expression and emotion rendered by anger, disgust, fear, happiness, sadness and surprise. The dimensional point of view in the classification of emotions is the one that is usually used starting from a two-dimensional space: two concepts are used, the *valence* that represents

the degree of pleasure of the individual and which can vary between the negative and the positive, and the *arousal* that represents the grade of activation of the emotion that can vary from total calm to total excitation (see Fig. 3.1). The space can become three-dimensional if we also consider the concept of preference [38], or even four-dimensional if we add even further the concept of dominance [15].

Regardless of how an emotion can be described, it's in the interest of this work to focus on the acquisition of physiological signals through electroencephalography, since the intent is to integrate this system into a virtual reality viewer. Nowadays there are countless studies and researches that focus on the recognition of emotions through the EEG, and all propose different techniques. This context creates a lot of confusion when we enter into the merits, but in reality it is representative of a truly wide area in which there are many possible solutions to the same problem. The various studies in the recognition of emotions differ mainly from the type of analysis performed on the data. It is easy to come across terms such as *data mining*, *machine learning* or *deep learning*, which represent the evolution of all those techniques that lead a system to autonomously learn information that it will then use to make decisions under certain conditions. And it is precisely the case of the emotion recognition. Deep learning represents the evolution of neural networks which involves the use of various internal layers between the input interface and the output interface (hence the term "deep"), and can be seen as a particular type of machine learning; the two terms therefore can be confused because in both what is done is train the system in recognizing certain pattern in the input signals giving it a particular meaning to create decisional paths useful in the real-time prediction phase. For this reason, the training phase in which the system must analyze a large amount of data before it can be ready to operate in real-time contexts is of fundamental importance and this has a cost in terms of time. On the contrary, the data mining argument is different: it is proposed to look for precisely those patterns that will then be used in the various learning algorithms. It can be said that it represents the starting point of deep/machine learning. At its base there are nothing but elaborate statistical calculations which came from classical statistics.

This short introduction wants to demonstrate the reason for the high number of techniques used in the various studies. In [6], for example, propose a deep learning algorithm that learns features and at the same time classifies the emotions through a technique that makes use of three Restricted Boltzmann Machines (RBMs) layers; in [15] they consider the multimodal deep learning, in particular the technique called Bimodal Deep AutoEncoder (BDAE) which, according to the authors, is characterized by greater accuracy when compared with the others; in [36], on the other hand, they use a particular machine learning algorithm called Isomap. As

we can see, the techniques are endless and no one is better than the other a priori but its effectiveness is relative to the particular context within which the analysis of moods is carried out.

The present work does not want to go into the merits of deep or machine learning, certainly useful tools for the recognition of like or dislike mental status but at the same time too complex to be consumed in a complete manner. In our case we decided to stay at the lowest level: the pure statistical analysis in the domain of time and frequencies. The intention is to define results or basic considerations from which eventually start a deeper analysis on the potentiality of our VeerRg system.

3.1 Related research

Most of the numerous studies carried out on the recognition of emotional states, beyond the particular statistical analysis technique used, have all a common feature: the electroencephalographic system which is normally used is a complete or almost complete system. This means that the analysis carried out are based on considering the signals coming from the whole scalp. In fact, the most commonly electrode positioning used is the standard called 10-20 already seen in Par. 1.4 and in Fig. 1.3a which includes electrodes placed between the frontal and occipital part and between the two temporal ones. Obviously, more signals come from a distributed area of the scalp and more useful information are available to perform an accurate analysis. For example, in [14] the study was carried out using an EEG system with 10, 14, 18 and 32 channels comparing the differences between the different settings and highlighting how the use of a 32 system channels, although slightly, is to be considered more precise.

Obviously the use of a complete EEG system that covers the entire scalp goes beyond our purposes. The main VeerRg's characteristic is precisely that of blending into the virtual reality viewer without adding anything visible to it. Covering the whole area of the head would therefore not be possible; the only accessible points are the frontal ones, in the neuro-medical nomenclature Fp1, Fp2, F7, F8 and the central electrode we have called G (Fig. 1.3b). The use of only 5 electrodes for a reading of the brain waves, in order to extrapolate information about moods, represents a non-indifferent limit. Considering, for example, the fact that often in the acquisition of electroencephalographic signals turns out to be of fundamental utility to change the reference potential by taking the average of *all* the electrodes as substitute (common technique that goes under the name of Average Mean Ref-

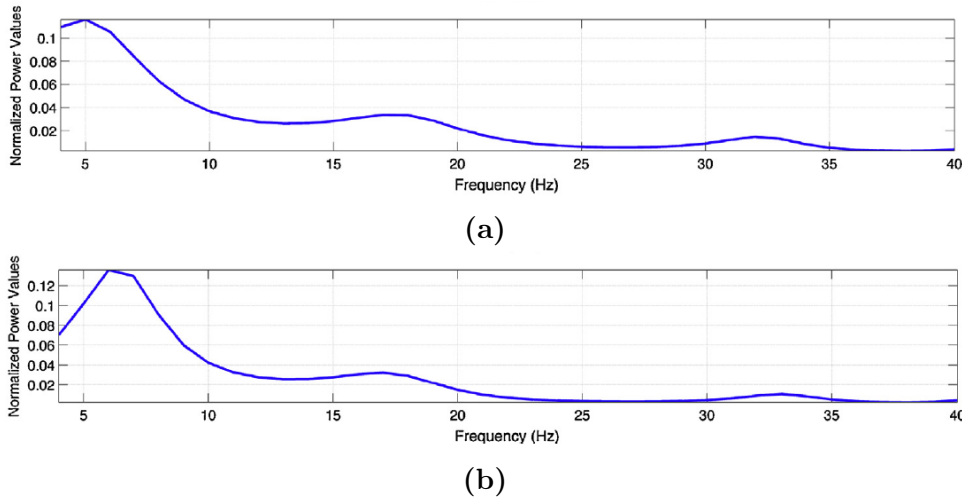


Figure 3.2: Example of Normalized Power Values (NPVs) for the signals coming from electrode F7 following the analysis in [40]. In (a) the case of like shows a higher activity in the band between 4 and 5 Hz respect the same band in the dislike case (b).

erencing, AMR), we understand how the VeeRg is limited in some aspects. This is the fundamental point from which the question arises: is it possible to recognize the status of like and dislike through only the use of frontal electrodes? The answer that has fueled hope came from two specific studies carried out to determine the cerebral activity in cases of like and dislike state of mind.

In [40] Yilmaz et al. performed an analysis of the electroencephalographic signals trying to understand which frequencies and channels were the most discriminating indicators in the process that leads an individual to a like or dislike state. The test proposed by them consists in the acquisition of EEG signals from 15 different subjects that have been asked to observe 16 images of shoes for 10 seconds and indicate in that time window whether they liked them or not. In this way, for every image the signals of all the channels have been clustered and marked with like or dislike. Once the data were collected from all 15 subjects, the Power Spectral Densities (PSD) were calculated for each EEG channel through the Burg method and then normalized to eliminate the inter-subject and intra-subject variability. These normalized spectral density values (Normalized Power Values, NPVs) were finally used as input data for an analysis technique that goes under the name of *logistic regression* where the two cases of like and dislike represent the binary output variables. The major advantage in using this technique is that the contributions of all the predictors are taken into account all at once avoiding misleading conclusions due to multiple tests. After completing the analysis, Yilmaz et al. finally determined the most discriminative components in the prediction of the status of like and dislike: with regard to the frequencies, the band that showed

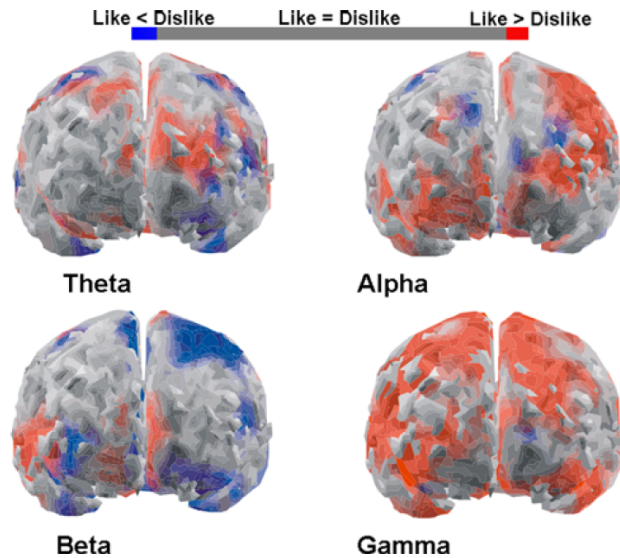


Figure 3.3: Brain's activity for different frequencies band (Theta, Alpha, Beta and Gamma) in case of like and dislike statement as analyzed in [34]. The figures represents the frontal lobe of brain.

the most influence in the determination of the two states was that ranging from 4 to 19 Hz, while the most significant channels are the frontal F7 and the temporal T6 (Fig. 3.2).

Also in [34] Vecchiato et al. wanted to analyze brain activity during the like and dislike states. To do this, they implemented a test that involves viewing a documentary intercut with old commercials and submitting it to 15 different subjects; at the end of the vision the tester was asked which of the commercials he had remembered and which ones they liked, linking the answers to the EEG data acquired during the respective spot. To analyze the recorded data, Vecchiato et al. used the technique known as Analysis of Variance (ANOVA). The results of the test revealed that during the display of advertisements that had been remembered and/or that had been pleasant, the activity of Theta waves is greater and localized in the left-frontal part of the cerebral cortex (frontal electrode F7) compared to the activity during the vision of forgotten commercials. A difference was also found in the activity of the Gamma waves this time however bilaterally in the frontal area (electrodes Fp1, Fp2, F7 and F8). The results for all the announcements are shown in (Fig: 3.3).

The two studies just described show how, at least in theory, the possibility of determining the mental state of like and dislike through VeeRg is actually real. In [40] the signals considered most discriminating are those belonging to the Theta wave band and coming from the frontal electrode F7, present in the VeeRg system.

In [34] this result is confirmed by emphasizing a difference of activity always in the Theta wave band located in the left-frontal area, with the addition also of Gamma wave band activity difference in the whole frontal area, practically the one completely covered by our VeeRg system.

3.2 Test definition and data recording

For the VeeRg we have developed a simple test inspired by those read in various studies on the tracking of emotions through EEG acquisition. The session for each test subject (10 in total) consists in placing him in front of a computer screen on which runs a graphical interface properly designed in LabView. Then a total of 20 images are shown spaced with a *pause* picture completely black. During the visualization it's possible to press a button through the computer's mouse to indicate if the image is liked or not. The button is only one because if the tester has not been pleased to see the image or remained in a state of indecision can simply avoid pressing it (button pressed = like; button not pressed = dislike/indecision). The duration of the image is 6 seconds, while for the *pause* one is 4 seconds. The acquisition of data coming from the EEG channels is performed only during the 6 seconds in which the image is displayed, then is collected in a numbered CSV file and marked with the like or dislike response given by the tester. At the end of test we have a total of 20 CSV files per subject divided between like and dislike. The analysis of the data is done later through scripts appropriately written in MATLAB.

Test guidelines	
Sample frequency	$250Hz$
EEG's electrodes	$Fp1, Fp2, F7, F8, G$
Image time window	$6s$
Relax time window	$4s$
N. of images per dataset	$20pics$
N. of dataset	$3(Tattoos, War/Cubs, Models/Growths)$

Table 3.1: The filters and their characteristics in the system.

In the design of the test we came across the very trivial problem of the image dataset to be used. In this regard, there are numerous studies such as [41] where the difficulty in classifying images according to the effect they have on the emotional state of a person is underlined, since not all people will react in the same way to the same image: some may find it pleasant, some not. For this reason they are even trying to find a relationship between the chromatic characteristics of the



Figure 3.4: Example of images for the War/Cubs test. To arise the *like* state of mind we used pictures of cubs (a) and to arise the *dislike* state we used picture of war instead (b).

picture and the emotions that it would evoke regardless of what it represents. Fortunately, however, our case is less complicated, since it is only a matter of deciding whether an image likes it or not. However, once we obtained an image dataset made available on the web as material for machine learning, we realized that the data collected and defined as like were quantitatively greater than the dislike of more than 80%, in our case less than 4 photos on 20 for each test session. This could have been a problem in the analysis phase because the minor sample would no longer have had a statistical value. For this reason we wanted to create three types of image datasets that go overboard with the objective division between pleasure and non-pleasure: the first is a set of tattoos images, in the second we have images of war and puppies (Fig. 3.4) and in the last dataset images of models and skin growth. With the last we wanted to put the subjects in a situation of objective dislike, although it should be noted that, even if in this case we have picture of models, not everyone has the same tastes in terms of them.¹

Another problem in defining the test was to understand the duration of an image. Even here, the opinions in the scientific community are several: in [13] a 30-second time window is used in the acquisition of EEG data; in [32] they find an improvement in the use of a time window of 4 seconds compared to one of 8; [25] fixes the duration of the rise of an emotion in 4 seconds; in [20] the comparison between a time window of 2 seconds and one of 4 seconds is won by the first; in [12] for the classification of four emotional states a 4 seconds time window was used. Fortunately, the studies highlight the absence of a strict minimum temporal limit.

¹It was interesting to see as, in the case of war and puppies images, most of the testers thought war images were pleasing even if they represented very bad moments; they actually appreciated the quality and meaning that picture brought with it. Another example that highlights the difficulty in selecting images.

Our initial concern was related to the fact that considering the final application of VeeRg in Neuromarketing where the response time of the EEG must respond to the fact that we want to know as soon as possible if a thing is pleasant or not, short time windows would have been insufficient to obtain acceptable results. In view of the consulted studies ([32]) we initially had the possibility to set a 4 seconds time window. This value is the result of a consideration made on the possibility of directly implementing the FFT of the signals on the microcontroller, which is optimized for a number of samples equal to a power of two; and in fact, sampling with a frequency of 250 Hz for about 4 seconds, 1028 samples (2^{10}) can be obtained. The additional 2 seconds bringing the total time to 6 seconds were added for redundancy in order to give the possibility to have a larger time window to perform correction (cutting off the artifacts) or simply to have a larger margin.

3.3 Analysis of data

The sample taken to perform the statistical analysis consists of 10 subject, 4 men and 6 women. For each of them were collected 20 acquisitions, or epochs, containing the signals coming from the 5 frontal electroencephalographic electrodes (Fp1, Fp2, F7, F8 and G). Every epoch contains 1536 samples since the duration of the picture is about 6 seconds (6s at 250 Hz). Altogether we have about 200 epochs for each type of test (Tattoos, War/Cubs, Models/Growths)². In these epochs we have the two groups related to the images that we liked and those not: for the Tattoos test we have 52 like and 142 dislike for a total of 194; for the War/Cubs test you have 100 like and 96 dislike for a total of 196; for the Models/Growths test we have 47 like and 153 dislike for a total of 200 (Tab. 3.2).

Test	n. like	n. dislike	total
Tattoos	52	142	194
War/Cubs	100	96	196
Models/Growths	47	153	200
After post-processing			
Tattoos	24	65	89
War/Cubs	51	49	100
Models/Growths	29	66	95

Table 3.2: The number of liked and disliked images for every test on a sample of ten people. With the post-processing the number of effective acquisitions was reduced.

²The number of final epochs in some cases is slightly lower because some have been discarded since they were not valid.

Once the data were collected, we wanted to carry out the analysis inspired by the methods adopted in [40], curious to compare the results to find or not a match. First we performed a post-processing on the signals collected eliminating the epochs where the presence of artifacts due to eye movement was evident. Following this cleaning the number of epochs available for analysis has been reduced: for the Tattoos test, 24 likes and 65 dislike remained for a total of 89 epochs; for the War/Cubs test, 51 like and 49 dislike remained for a total of 100 epochs; for the Models/Growths test there are 29 like and 66 dislike for a total of 95 epochs (Tab. 3.2).

Then, a script was created in MATLAB to automate the analysis of the current data. First of all, the script calculates the Power Spectral Densities for each epoch and normalizes it with respect to the power of the entire band we are going to consider (0-45 Hz). In this way we try to minimize the variability inter-subjects and intra-subjects obtaining for each epoch Normalized Power Values (NPVs) on which to base our analysis.

The first step was to compare the two cases of like and dislike through the NPVs of all the epochs and for each channel. Fig. 3.5-3.6-3.7 are the result of this comparison which, at first glance, would seem to highlight the significant differences in NPV trends between the like and dislike case. If we take as an example the Fig. 3.5a and the Fig. 3.5c we could notice a greater activity in the dislike, both at the low frequencies of the Theta band and in the medium/high frequencies that characterize the Beta band. In reality this difference is illusory due to the signifier greater number of epochs belonging to the dislike case (see Tab. 3.2). Also going to compare the average of all the NPV represented by the red curve would not seem to be significant differences. But things start to change when we analyze the power in the different bands. Fig. 3.5b and Fig. 3.5d show the distribution of the power values in the bands 4-8 Hz, 8-13 Hz, 13-20 Hz, 20-30 Hz and 30-42 Hz (Theta, Alpha, Beta-low, Beta-high and Gamma respectively). Also here the red circles indicate the average values of the powers in the band. In Tab. 3.3 the values of these averages are indicated for both the like and dislike cases and for all the three tests performed. In this context the difference between the two cases becomes clearer: in fact, even if only slightly, the average of the powers in the like case would seem to be almost always greater than those of the dislike cases. This would effectively confirm the actual presence of a greater brain activity when the subject had in front of himself an image of his liking.

In the second step of analysis, statistical elaboration has been carried out, using *logistic regression* to try and determine which are the most discriminating channels and frequencies for the recognition of the like or dislike state of mind. The

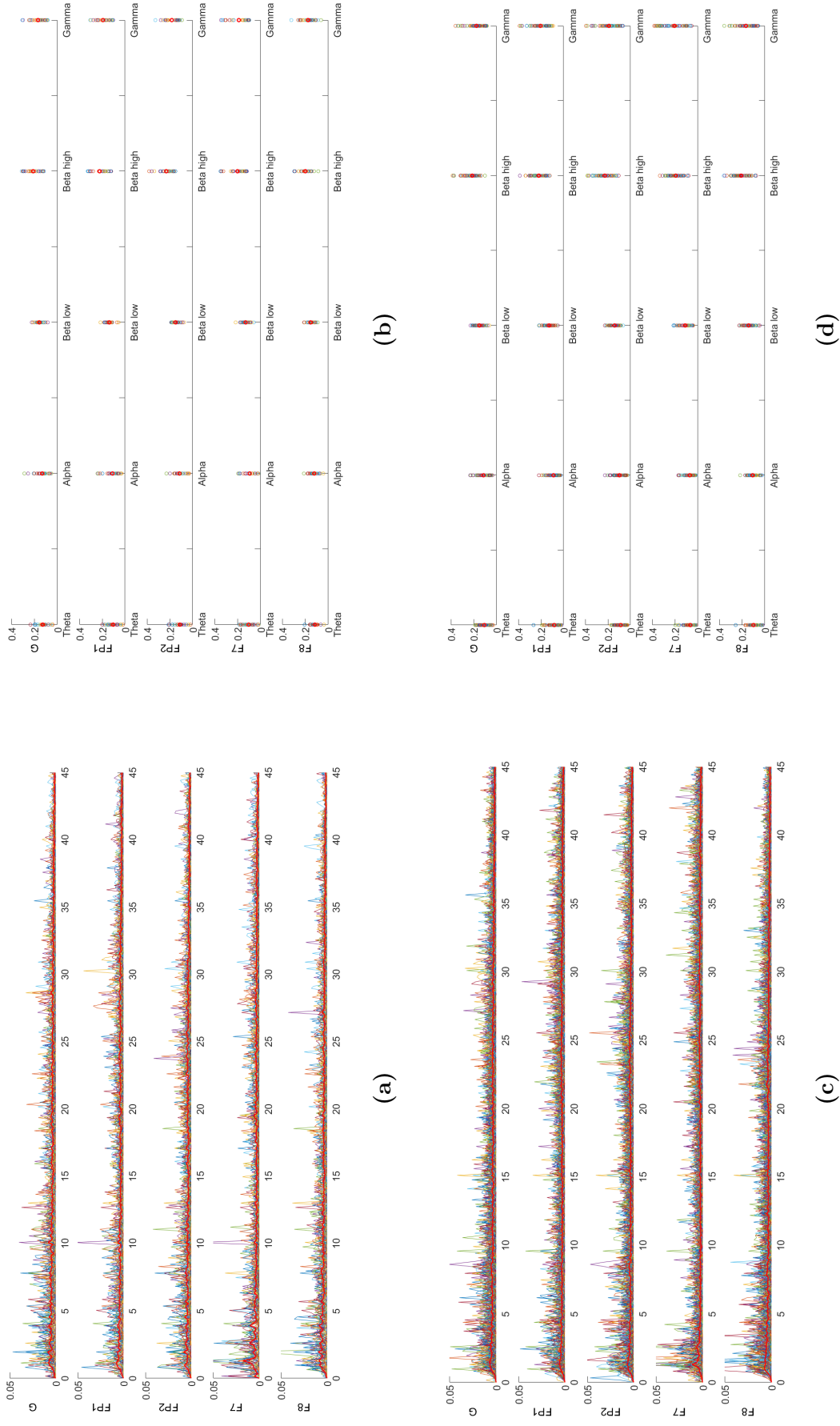


Figure 3-5: The Normalized Power Values (NPVs) of the Tattoo test are displayed for every channel and all acquisitions together. In (a) and in (c) there are the NPVs for the acquisitions marked as like and dislike respectively. In (b) and in (d) there are the values of the power in the Theta, Alpha, Beta and Gamma bands for all the acquisitions. The red line in (a) and (c) and the red circle in (b) and (d) represent the average.

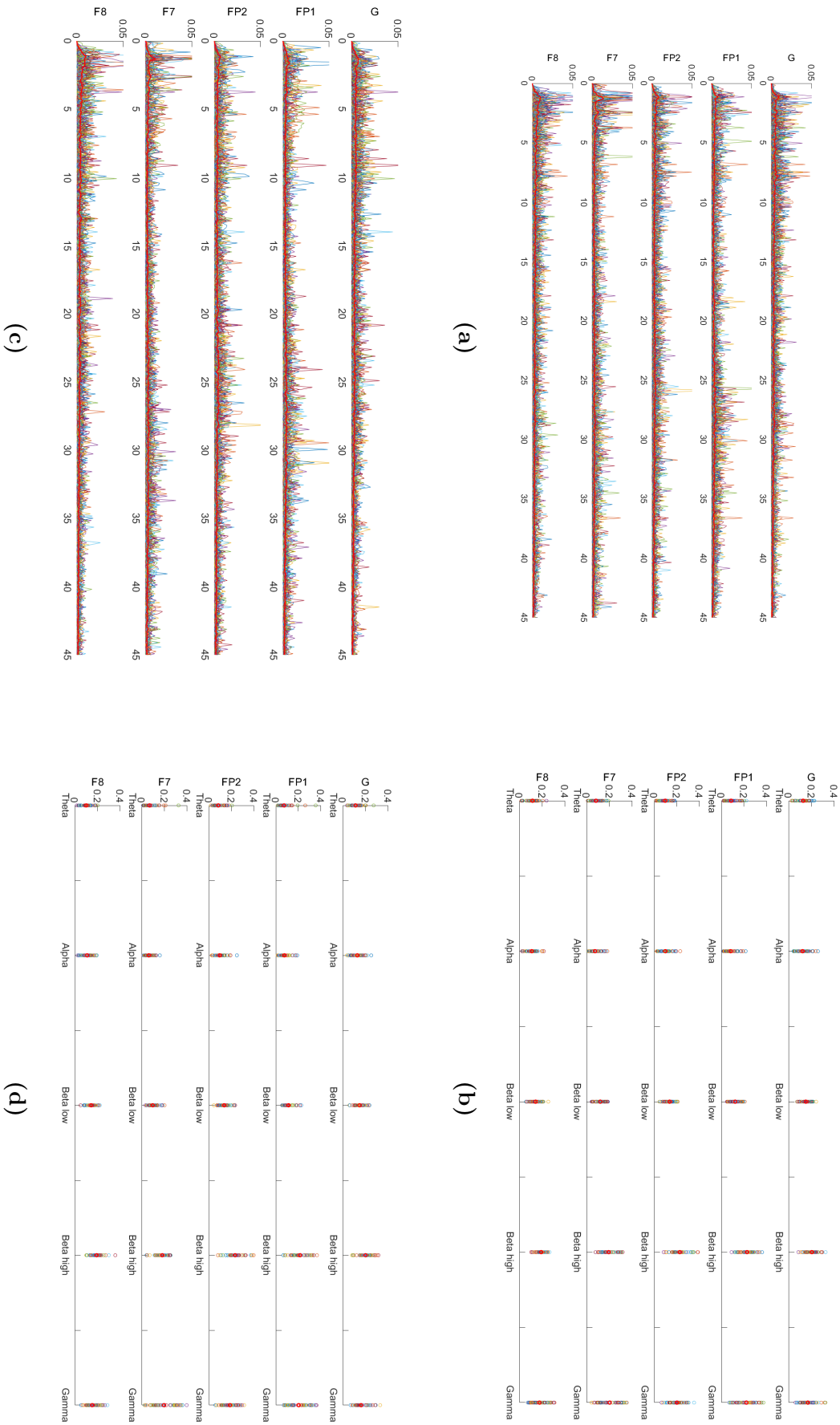


Figure 3.6: The Normalized Power Values (NPVs) of the Tattoo test are displayed for every channel and all acquisitions together. In (a) and in (c) there are the NPVs for the acquisitions marked as like and dislike respectively. In (b) and in (d) there are the values of the power in the Theta, Alpha, Beta and Gamma bands for all the acquisitions. The red line in (a) and (c) and the red circle in (b) and (d) represent the average.

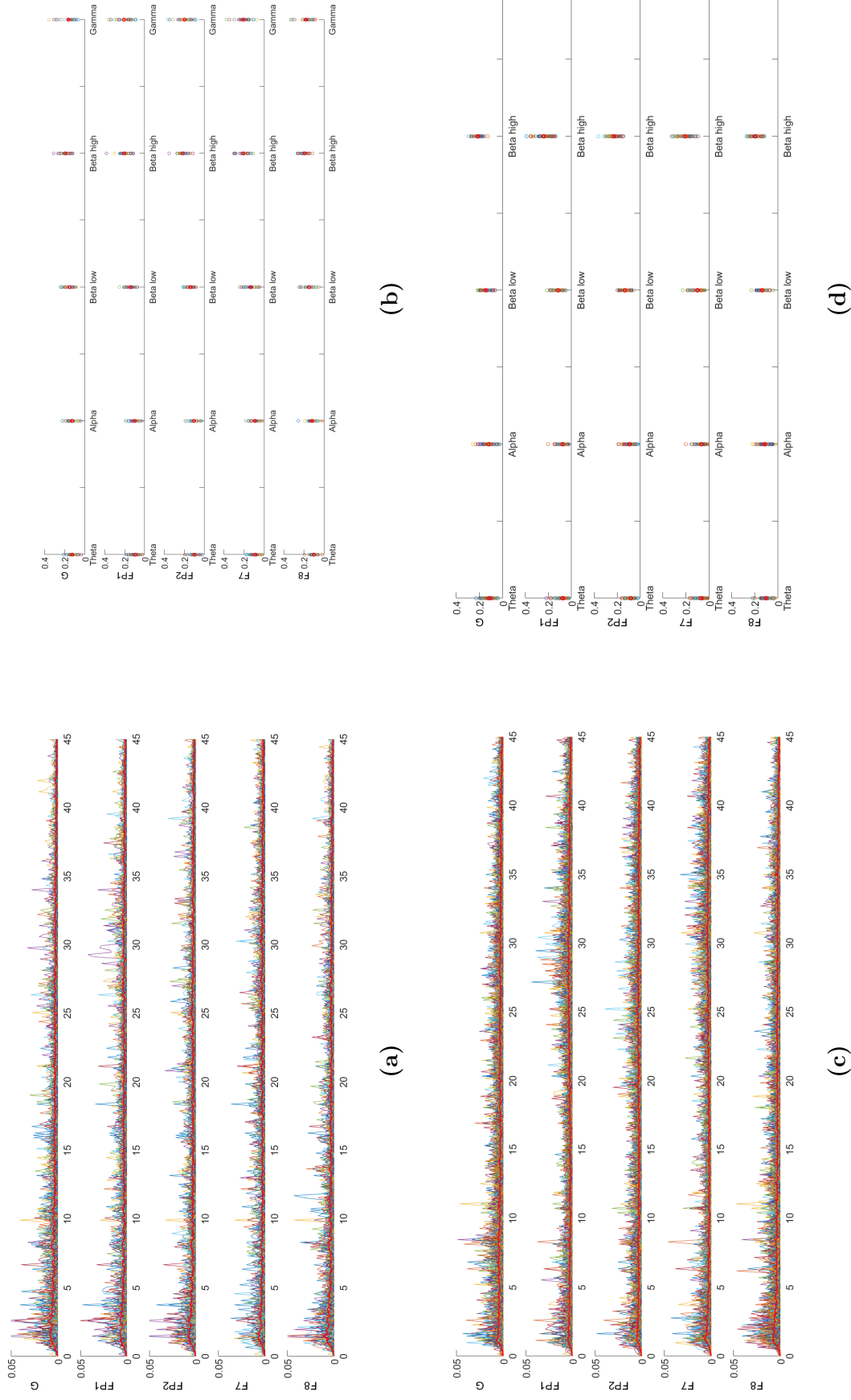


Figure 3.7: The Normalized Power Values (NPVs) of the Tattoo test are displayed for every channel and all acquisitions together. In (a) and (c) there are the NPVs for the acquisitions marked as like and dislike respectively. In (b) and (d) there are the values of the power in the Theta, Alpha, Beta and Gamma bands for all the acquisitions. The red line in (a) and (c) and the red circle in (b) and (d) represent the average.

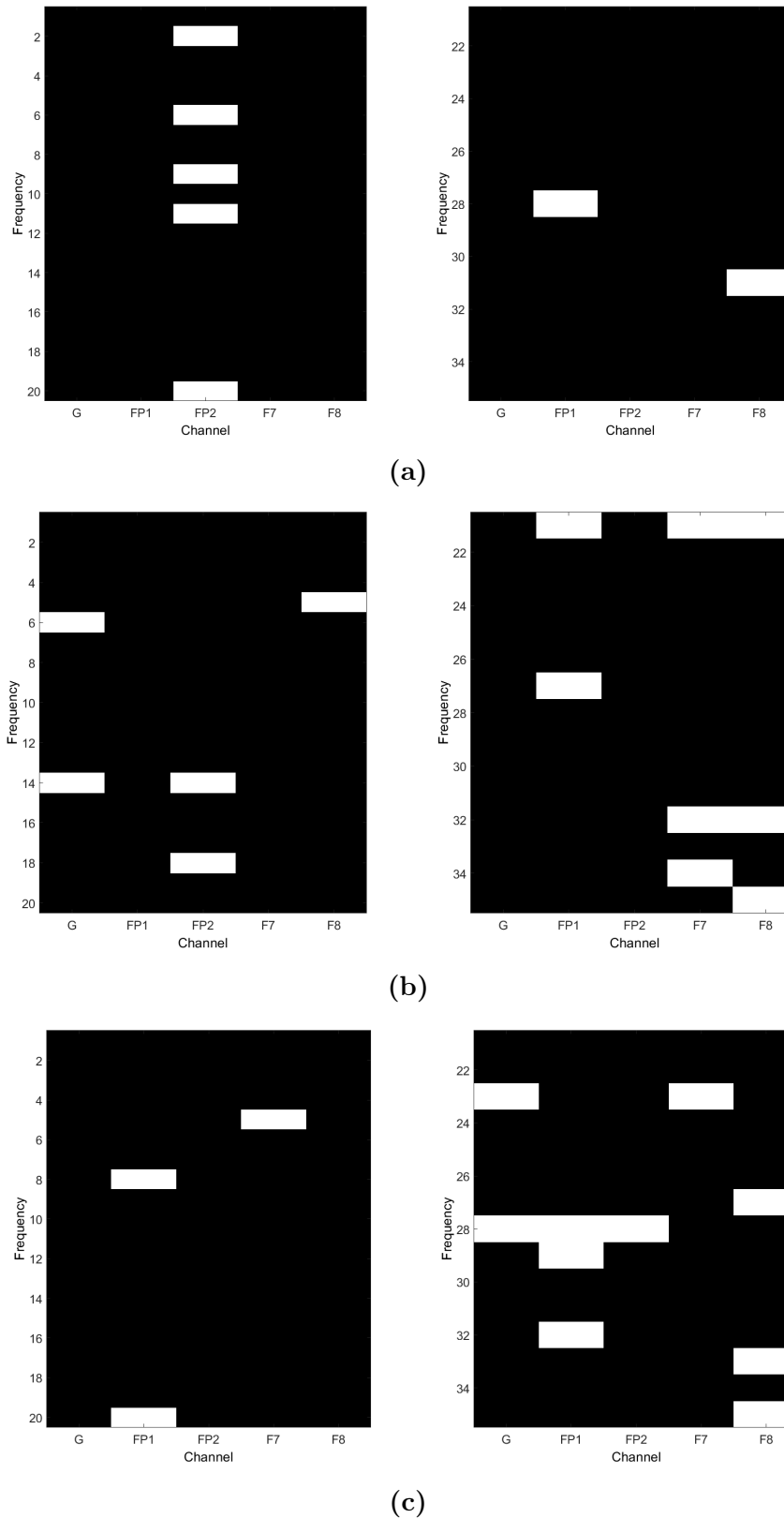


Figure 3.8: P-values of β parameters relative to every test: the Tattoo (a), the War/Cubs (b) and the Models/Growths (c). The white squares represent when the p-value is less than 0.05 (important p matrix) and the black ones when the p-value is greater. This representation helps to find which channels or frequencies are more discriminative to predict the like or dislike case.

		Like/Dislike				
	Theta	Alpha	Beta-low	Beta-high	Gamma	
G	0.12/0.10	0.13/0.11	0.15/0.15	0.21/0.21	0.16/0.17	
	0.12/0.11	0.12/0.12	0.15/0.14	0.20/0.20	0.16/0.16	
	0.12/0.11	0.12/0.12	0.15/0.14	0.19/0.21	0.16/0.19	
Fp1	0.10/0.08	0.10/0.08	0.13/0.12	0.22/0.21	0.19/0.20	
	0.08/0.07	0.08/0.07	0.12/0.11	0.22/0.21	0.22/0.20	
	0.09/0.07	0.09/0.07	0.14/0.11	0.20/0.23	0.20/0.23	
Fp2	0.11/0.08	0.11/0.09	0.14/0.14	0.23/0.22	0.18/0.19	
	0.09/0.08	0.09/0.09	0.13/0.13	0.22/0.23	0.20/0.18	
	0.09/0.08	0.10/0.09	0.13/0.13	0.21/0.22	0.19/0.22	
F7	0.10/0.06	0.09/0.07	0.13/0.11	0.20/0.19	0.18/0.20	
	0.08/0.06	0.07/0.06	0.12/0.09	0.19/0.18	0.20/0.19	
	0.08/0.06	0.09/0.06	0.13/0.10	0.20/0.20	0.20/0.24	
F8	0.11/0.09	0.12/0.10	0.15/0.14	0.19/0.20	0.17/0.16	
	0.11/0.10	0.10/0.10	0.14/0.14	0.19/0.19	0.17/0.15	
	0.10/0.10	0.11/0.11	0.14/0.13	0.19/0.19	0.17/0.18	

Table 3.3: The values in the table show the means of power in Theta, Alpha, Beta and Gamma bands for all channels. The triplets in the cells represent the three different test: Tattoo, War/Cubs and Models/Growths respectively. This table wants to highlight that the mean of power in the different bands is almost always higher in the case of like data.

procedure is the same as seen in [40]. Logistic regression represents a particular case of the more generic *Generalized Linear Model* (GLM) in which the dependent variables have a binomial distribution (like and dislike), as independent variables the NPVs and the *link* function the sigmoid that maps the real axis in values between 0 and 1. In the script created in MATLAB, logistic regression is implemented through the use of the *glmfit* function within the Statistical Toolbox. This function outputs the β weights of the respective predictors, which in our case are the NVPs that will compose the predictive model, together with the respective p-values which indicate their statistical validity. We have then a matrix of p-values in which the rows and columns represent the electroencephalographic frequencies and channels respectively. Using these p-values it is possible to determine the most discriminating frequencies and channels by observing where they are lower than 0.05 (high statistical value, error less than 5%). In applying logistic regression to our data, we had to divide the frequencies into two groups to make the *glmfit* function converge. The results are shown in Fig. 3.8.

The black squares indicate p-values greater than 0.05 while the white squares lower p-values. If we consider the method to choose the frequencies and channels

Test	Channel	Frequency (Hz)
Tattoos	<i>Fp2</i>	—
War/Cubs	<i>F7, F8</i>	21
Models/Growths	<i>Fp1, F8</i>	28

Table 3.4: The most discriminative channels and frequencies as the results of analysis with the logistic regression. Fixed a number of p -values more than 3 to determine the most discriminative component, we found three different results for the three different test.

used in [40], we must take as determinants those that have a number of p -values < 0.05 greater than 3. In our case, however, we have three different results for every types of tests . As summarized in Tab. 3.4 we have that in the Tattoo test the determining component is only represented by the *Fp2* channel. In the case of the War/Cubs test, on the other hand, the *F7* and *F8* signals are decisive along with the 21 Hz frequency. In the case of the Models/Growths test, the *Fp1* and *F8* channels together with the 28 Hz frequency.

These results are completely different from those found in [40] where the channels turn out to be *F7* and *T6* together with the 4 Hz frequency. They also differ between the different tests. Not entirely though. In fact this is true if one takes categorically for sure what comes out of the analysis through logistic regression. As far as we are concerned, in the War/Cubs and Models/Growths test cases the *F8* channel is decisive for both cases while the *Fp1* and *F7* channels are different but contiguous and therefore represent a circumscribed frontal area, the one on the left lobe; moreover, the frequencies that seem to be determinant, albeit different from the results of the study taken into consideration, are part of the same band, the Beta-high (20-30 Hz).

The analysis just made shouldn't be hastily indicated as wrong or useless, but must be taken as a starting point for a more thorough study on the possibilities made available by VeeRg in the detection of emotions that may be related to the sphere of pleasure or not.

The possibility, therefore, of identifying the status of like and dislike through the VeeRg system exists as we have been able to find is that:

- The most discriminating electrodes in the recognition of the like/dislike state of mind are the *Fp1*, *F8* and *F7*.
- The frequencies that results to be determinant belong to the Beta-high band (20-30 Hz).
- Considering the average of the powers in the different bands (Theta, Alpha,

Beta-low/high and Gamma) among all the acquisitions made, it appears to be greater in the case like rather than in the case of dislike.

These results must be considered in light of the fact that the test developed for our purpose can be improved by choosing a more appropriate image dataset or, better, by choosing to use videos; moreover, in order to have a greater statistical value, it is advisable to enlarge the number of subject from which the electroencephalographic signals can be acquired.

Conclusion

The realization of VeeRg has put us in front of numerous challenges, common to all those who have our own target: the recognition of emotional states, in particular that of pleasure. This is a vast subject if you start from scratch the designing of an EEG system to use it then in the analysis of brain activity, but on the other hand it is necessary if you want to have a completely flexible system for a complete integration with the viewers of virtual reality.

The biggest problem was to obtain electroencephalographic signals as clean as possible through an accurate analysis of the most common techniques used to reduce the onset of noise.

Starting from a design aimed at low-noise, we have generated analog references for the analog-to-digital conversion with a very low incidence of noise, obtaining a system with Input Referred Noise (IRN) of $0.97\mu V_{rms}$ and $5.79\mu V_{pp}$, values more than enough for this type of application.

We then addressed the typical Common-Mode issue in the acquisition of bio-electrical signals. An in-depth analysis of the typical technique of the Bias electrode (or Ground, or Feedback-loop) has shown what are the elements that improve the Common Mode Rejection (CMR) keeping it, at least theoretically (N/A), always below a certain limit. The development of these techniques led to the realization of an EEG system with a Power Spectrum Density (PSD) at rest (system worn in a relaxed position) that, already at low frequency, has a characteristic below the $1\frac{\mu V^2}{Hz}$ (-120dB).

Finally, the topic of filtering was introduced, useful but nevertheless dangerous, trying to define the risks that can be met if one is not aware of it. Depending on the type of application, the filters may be more or less useful as they introduce distortions that can severely change the results of a subsequent analysis.

At this point, with a working prototype in our hand,s we entered the delicate phase of our journey: the recognition of the status of like/dislike. A delicate phase because, although there are numerous studies to confirm the possibility and although such devices have already been proposed, the question is still widely open. Inspired by a research article, we have created a test for the collection of elec-

troencephalographic signals drawing from a sample of 10 subjects; subsequently, still referring to the methodology used in the article, we applied the *logistic regression* technique to determine which frequencies and EEG channels are the most determinant of the recognition of the like/dislike. At the end of the elaboration we discovered a slight difference in the power of the brain's waves between the two mental states and, as a result of the statistical analysis, we have obtained as discriminating elements the electrodes F7, F8 and Fp1 (standard position system) and the frequencies in the Beta-high band (20-30 Hz). These results, however, differ from those obtained in the article and that we expected to confirm.

However, even if our case deviates from what we expected, we must keep in mind that we are in an area not yet fully explored in which the studies and research will continue in the coming years to try to improve what we are already doing today. The possibility of the recognition of emotions through electroencephalography is possible and is a fact, but we have to consider that nowadays there aren't devices *on the market* able to do it, since they are all still in the embryonic stage. Prototypes that exist and work, but that can't keep high reliability in all the contexts in which they could be used.

The main problem is reduced in trying to get the bio-electric signals in the best way, without being contaminated by external interference or due mainly to sudden changes of the interface between the body and the system, in our case the skin/-electrode interface. It is our opinion that the main focus should be concentrated on the problem of acquisition, because it is obvious that with better and cleaner signals the analysis on it can lead to more significant results.

Appendix A

Schematics and Code

A.1 Schematics

In the following pages are available the schematics of the whole VeeRg system.

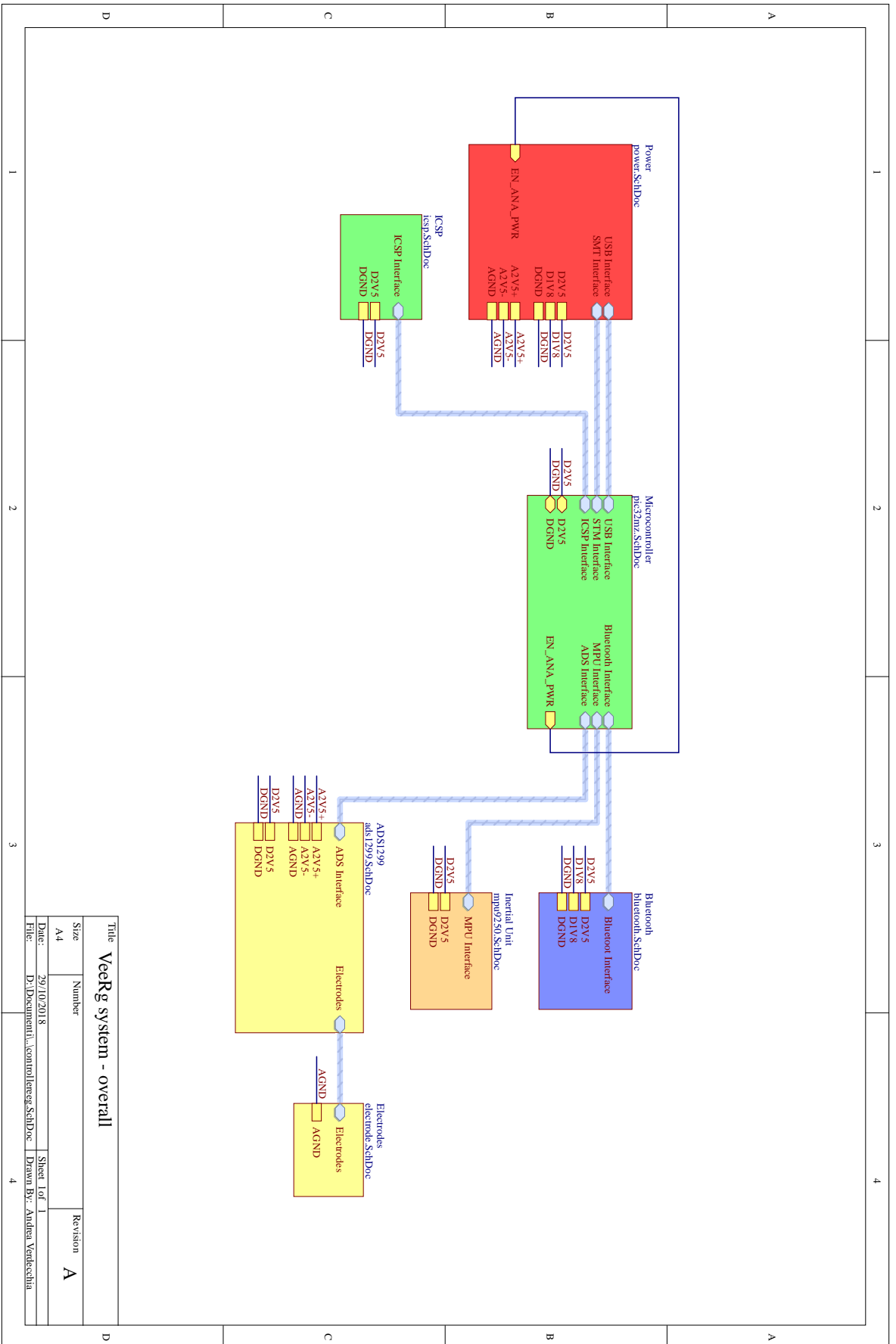


Figure A.1: Block schematic of overall VeerG system.

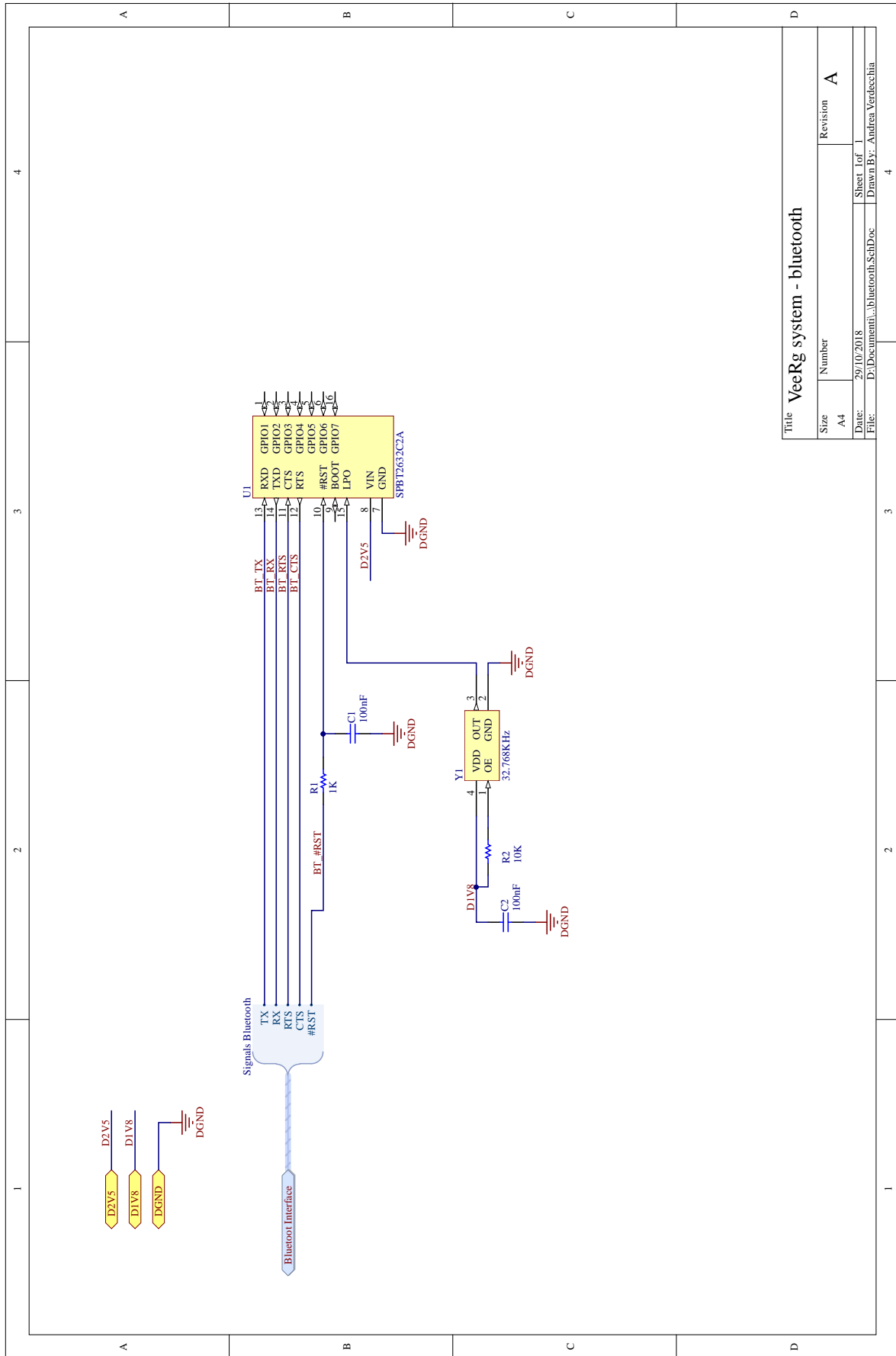


Figure A.2: Bluetooth block.

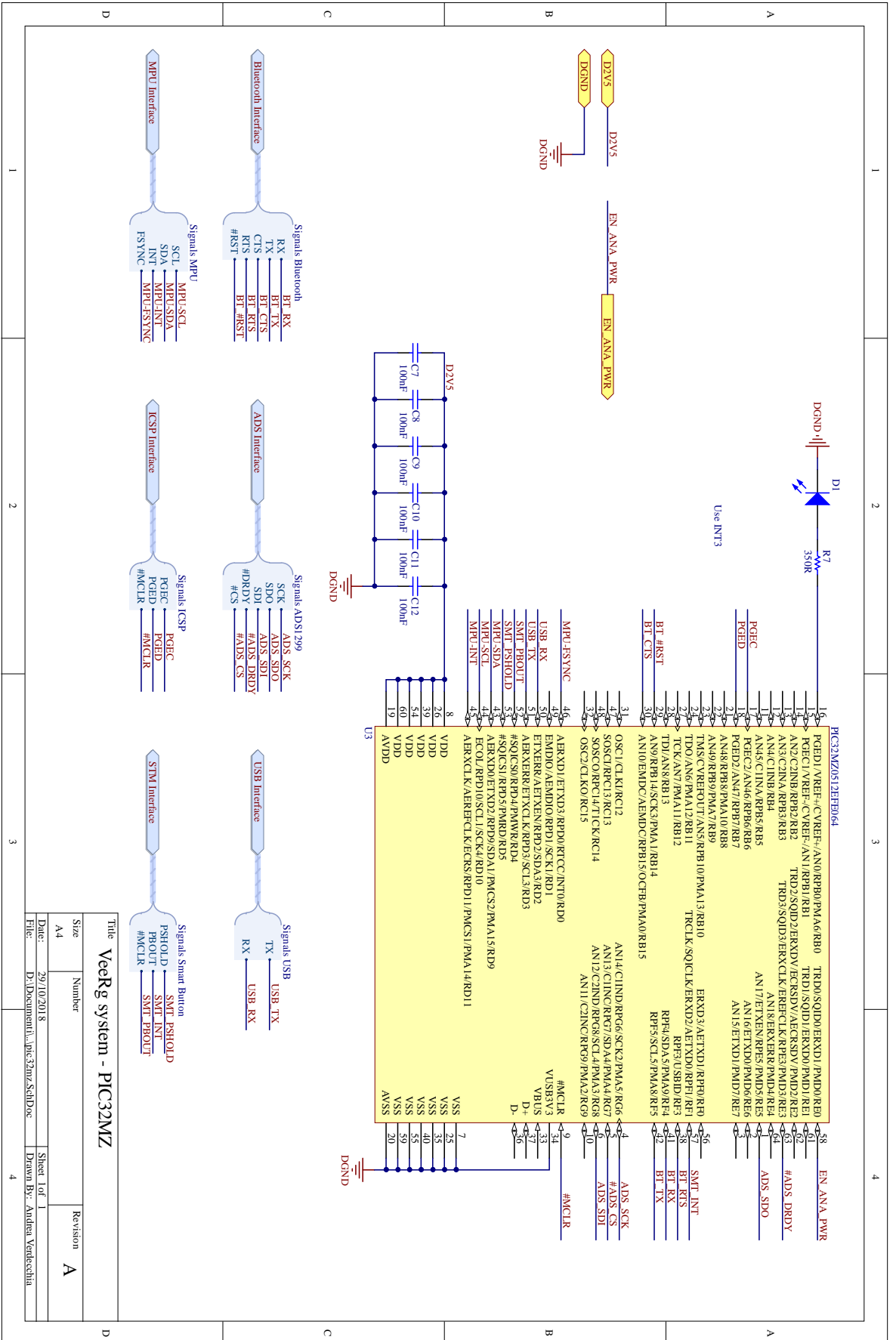


Figure A.3: PIC32MZ block.

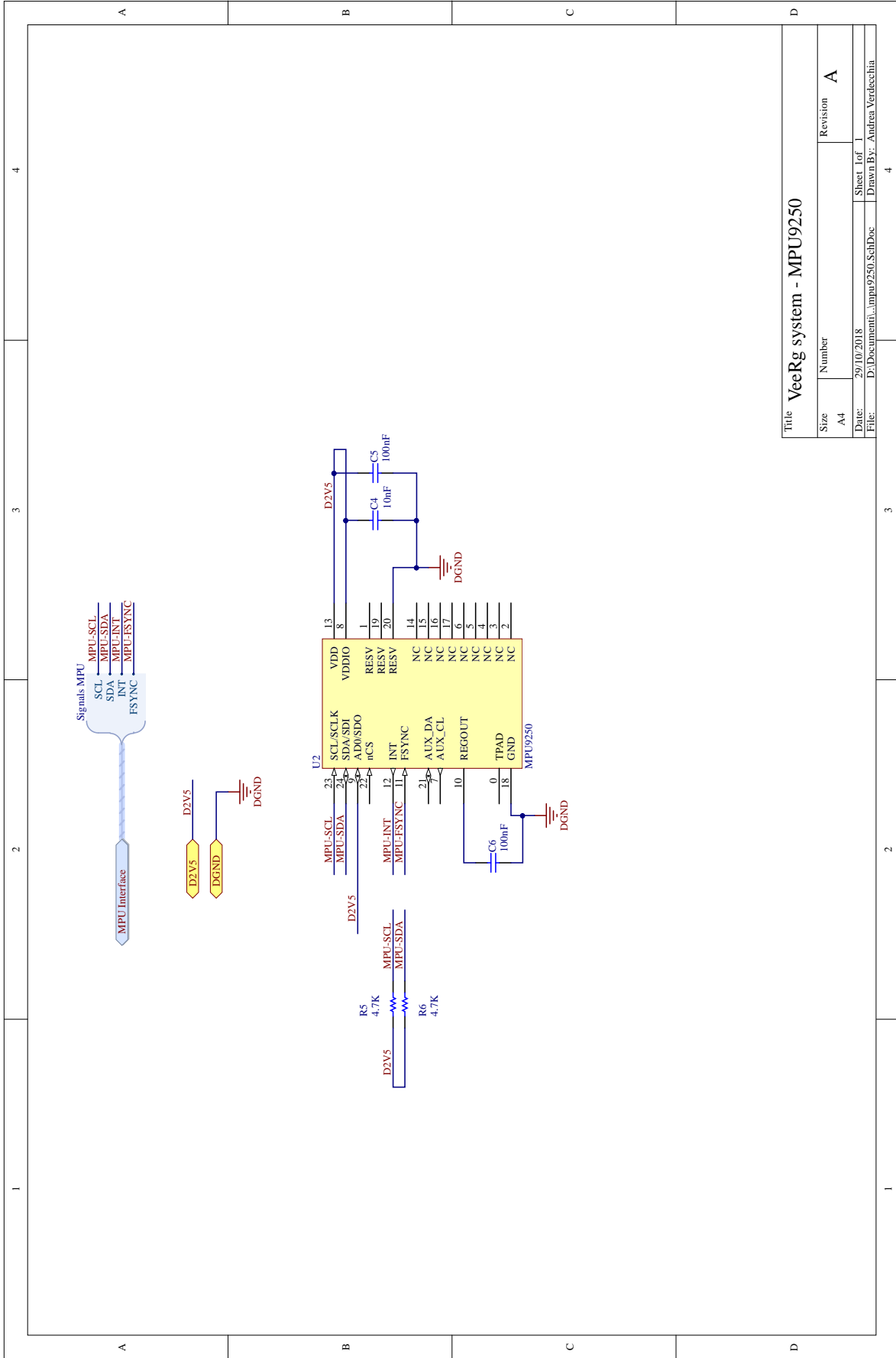


Figure A.4: MPU9250 block.

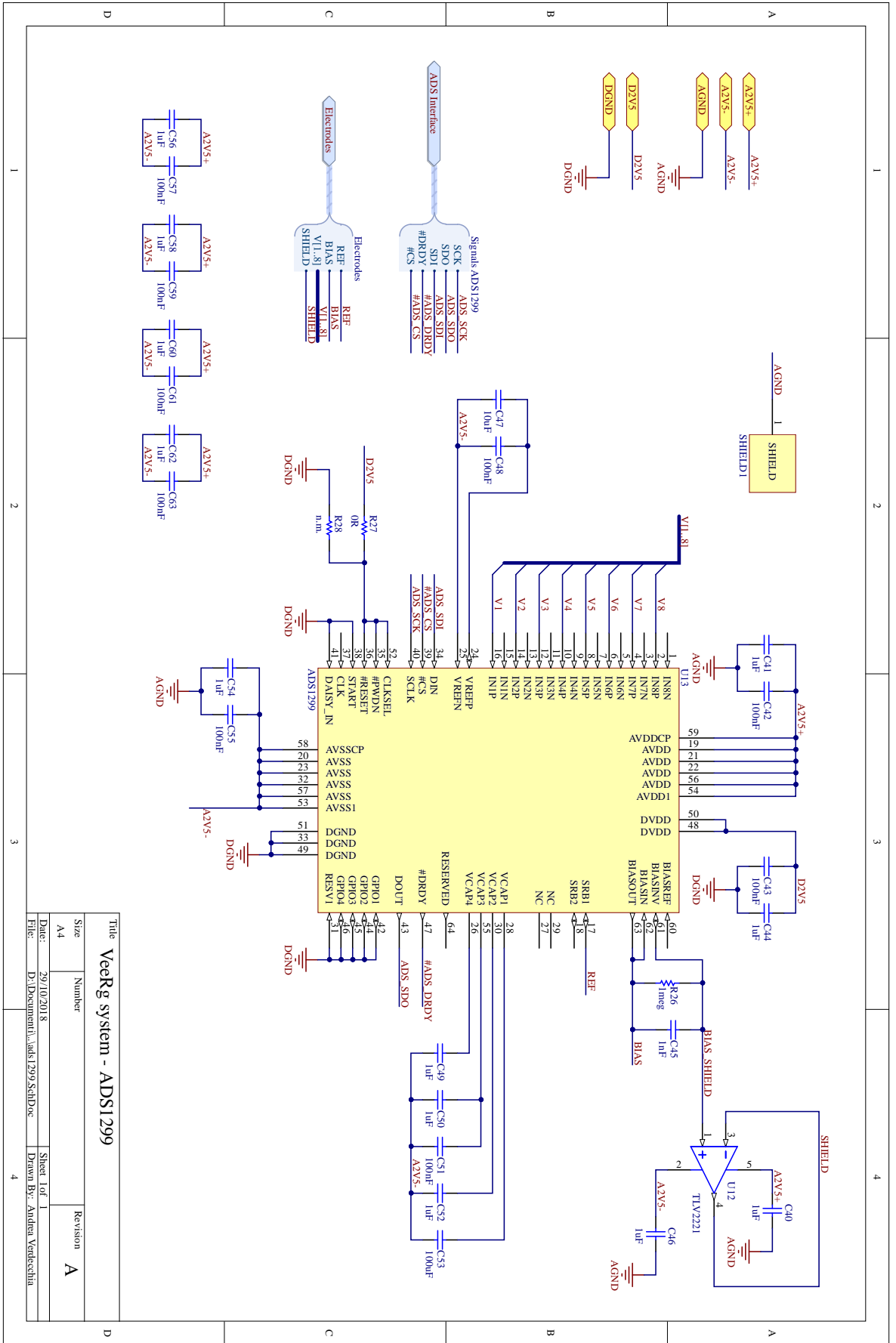
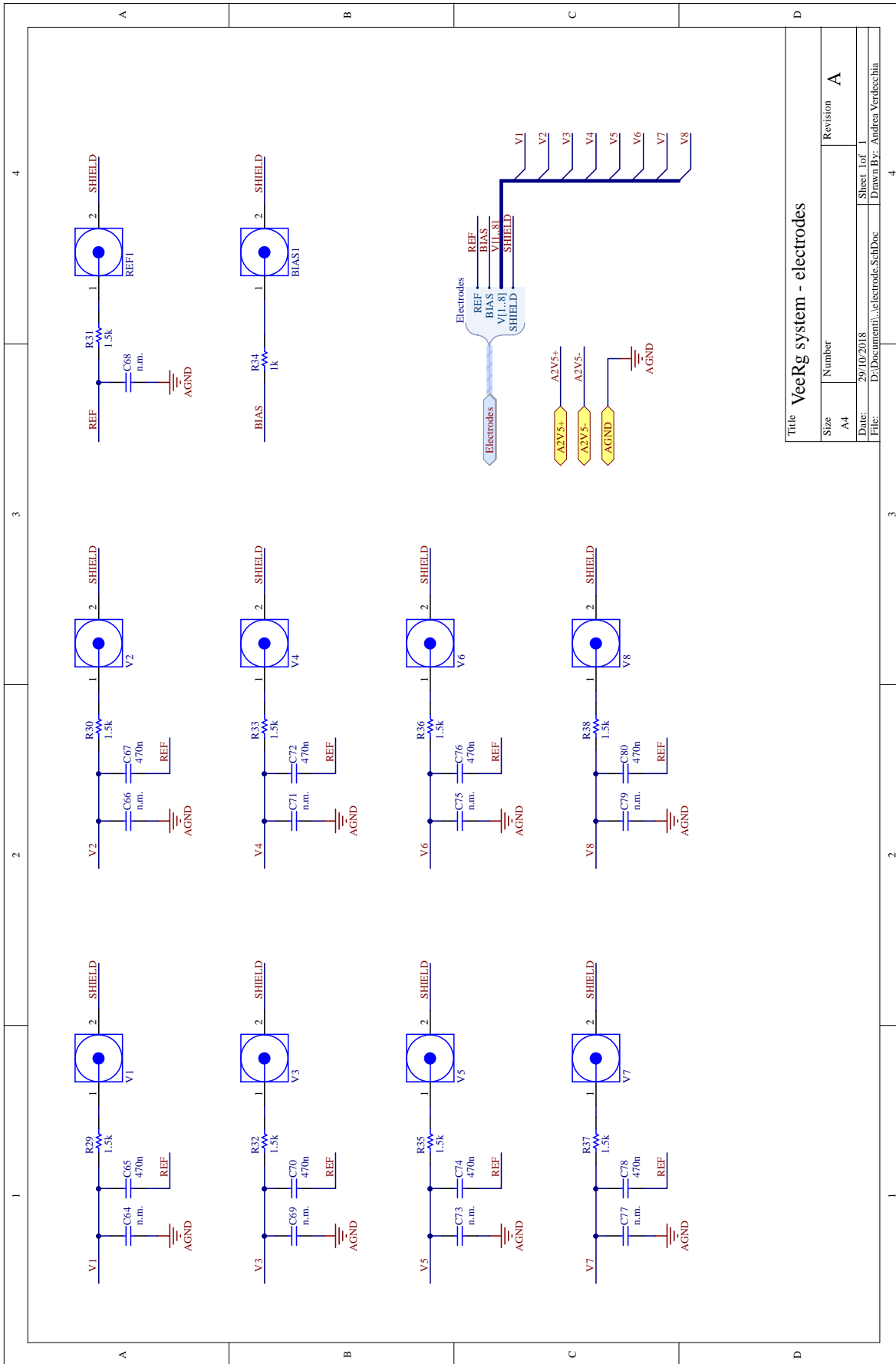


Figure A.5: ADS1299 block.



Title		VeeRg system - electrodes	
Size	Number	Revision	
A4		A	
Date:	29/10/2018	Sheet	LoF 1
File:	D:\Documenti\...electrode.SchDoc	Drawn By:	Andrea Verdecchia

Figure A.6: Electrodes block.

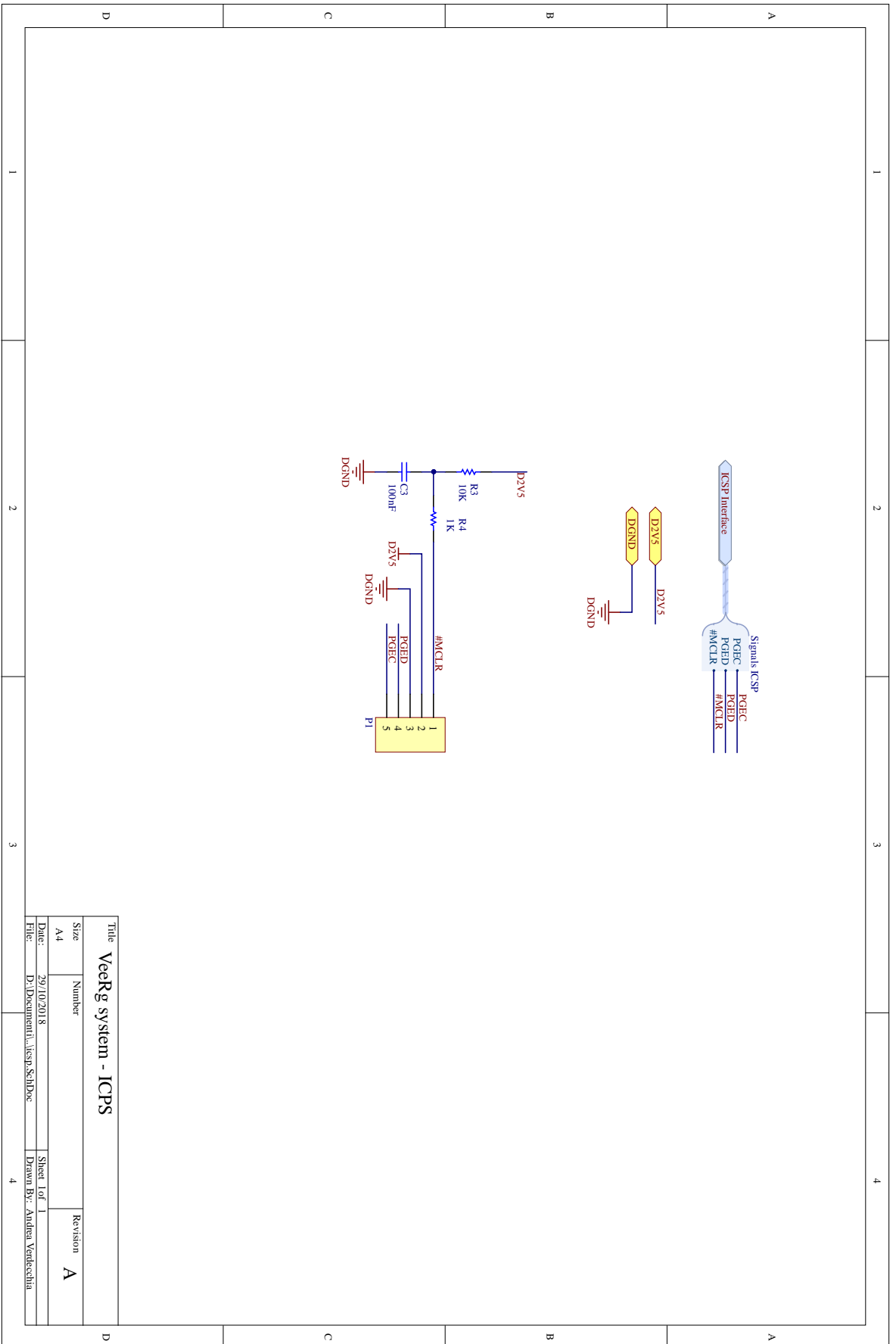


Figure A.7: ICSP block.

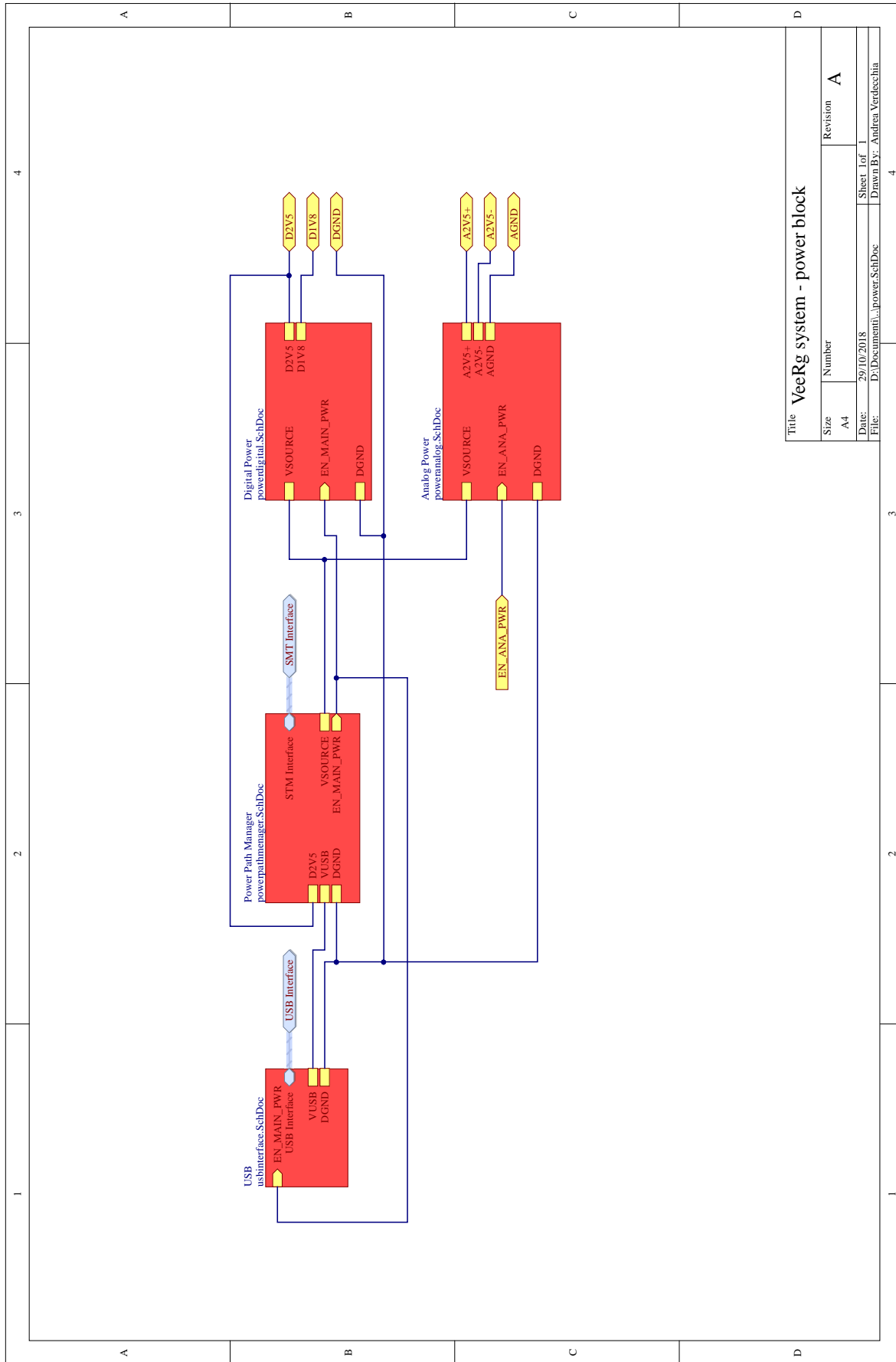


Figure A.8: Power block.

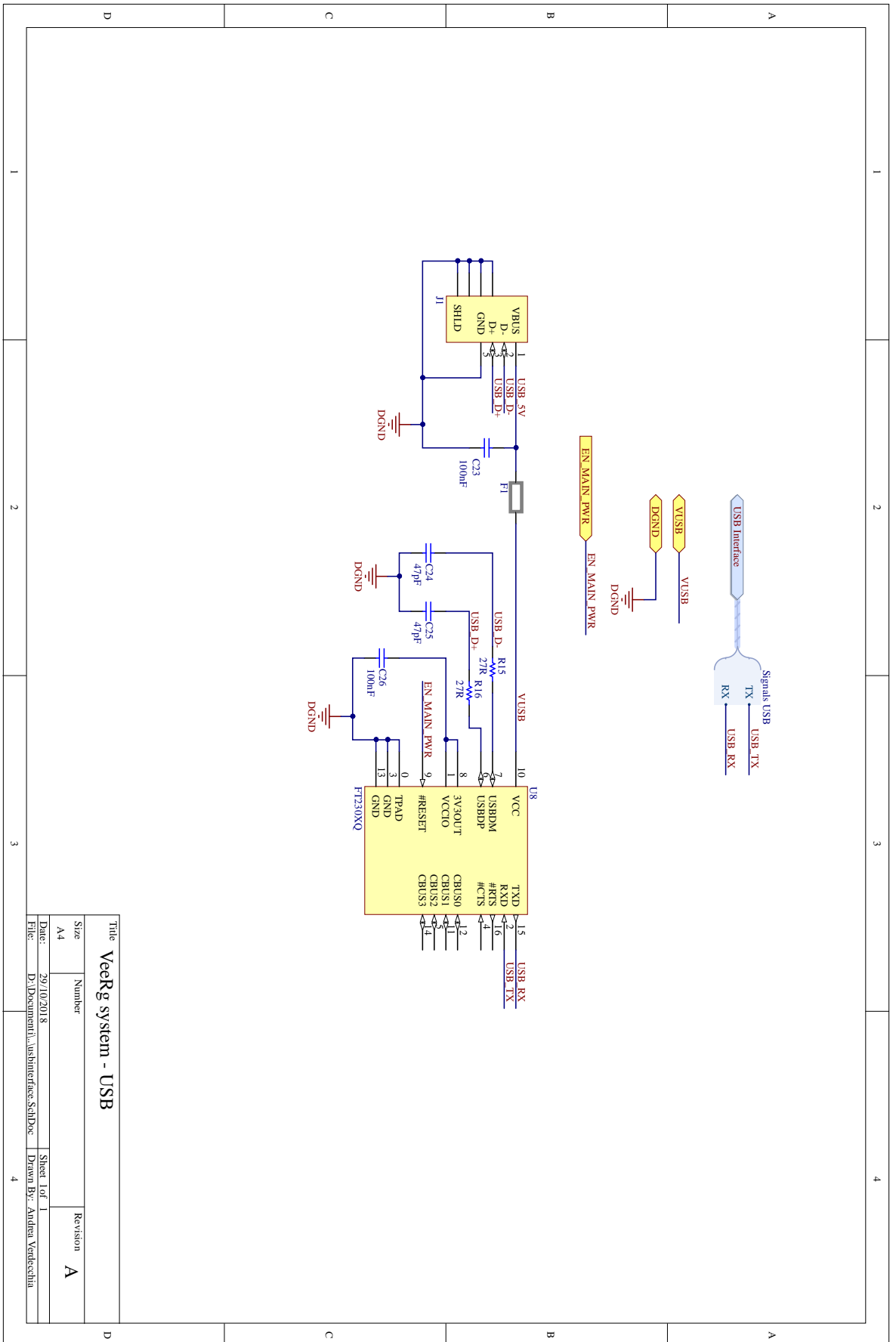


Figure A.9: USB interface block.

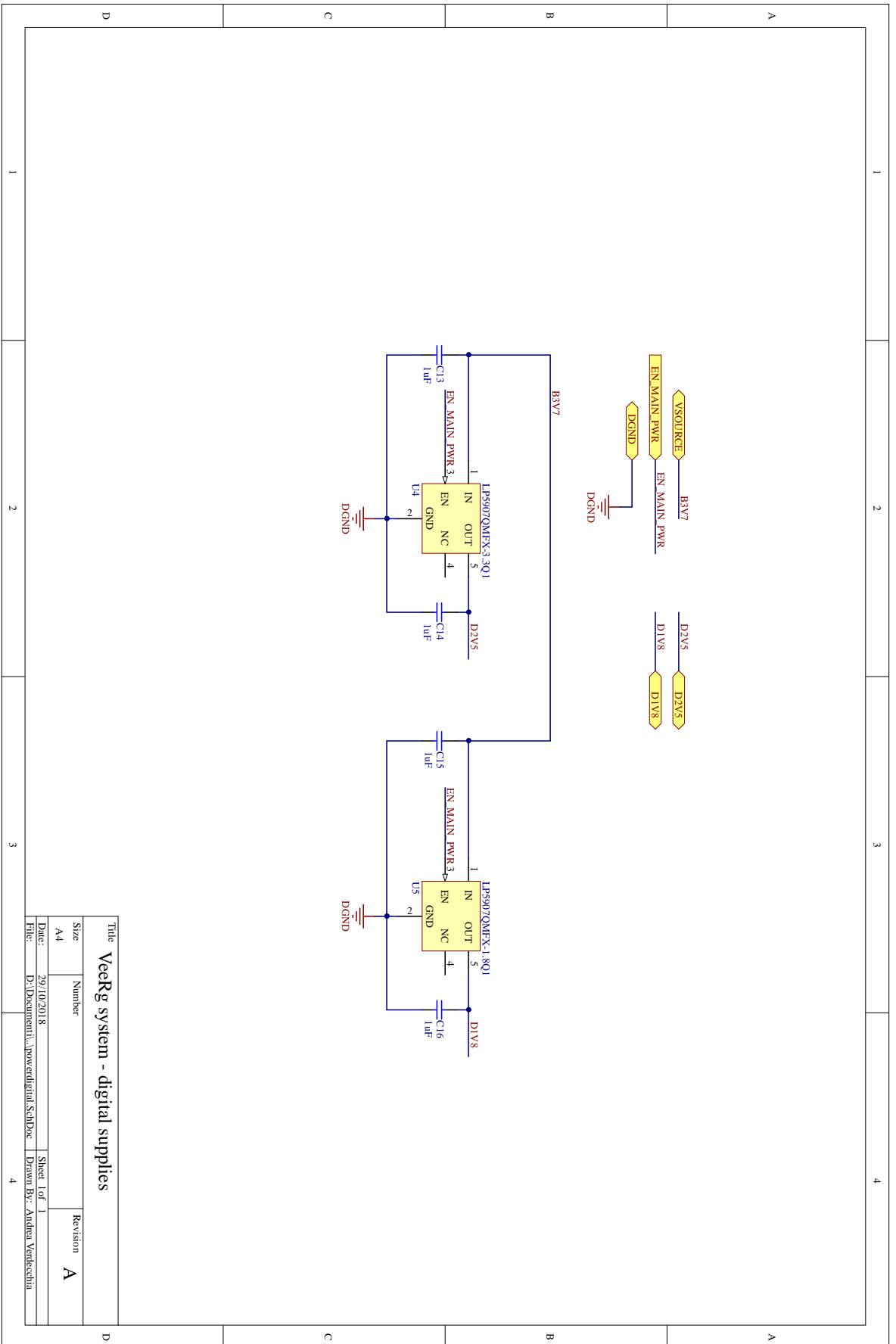


Figure A.11: Digital supplies block.

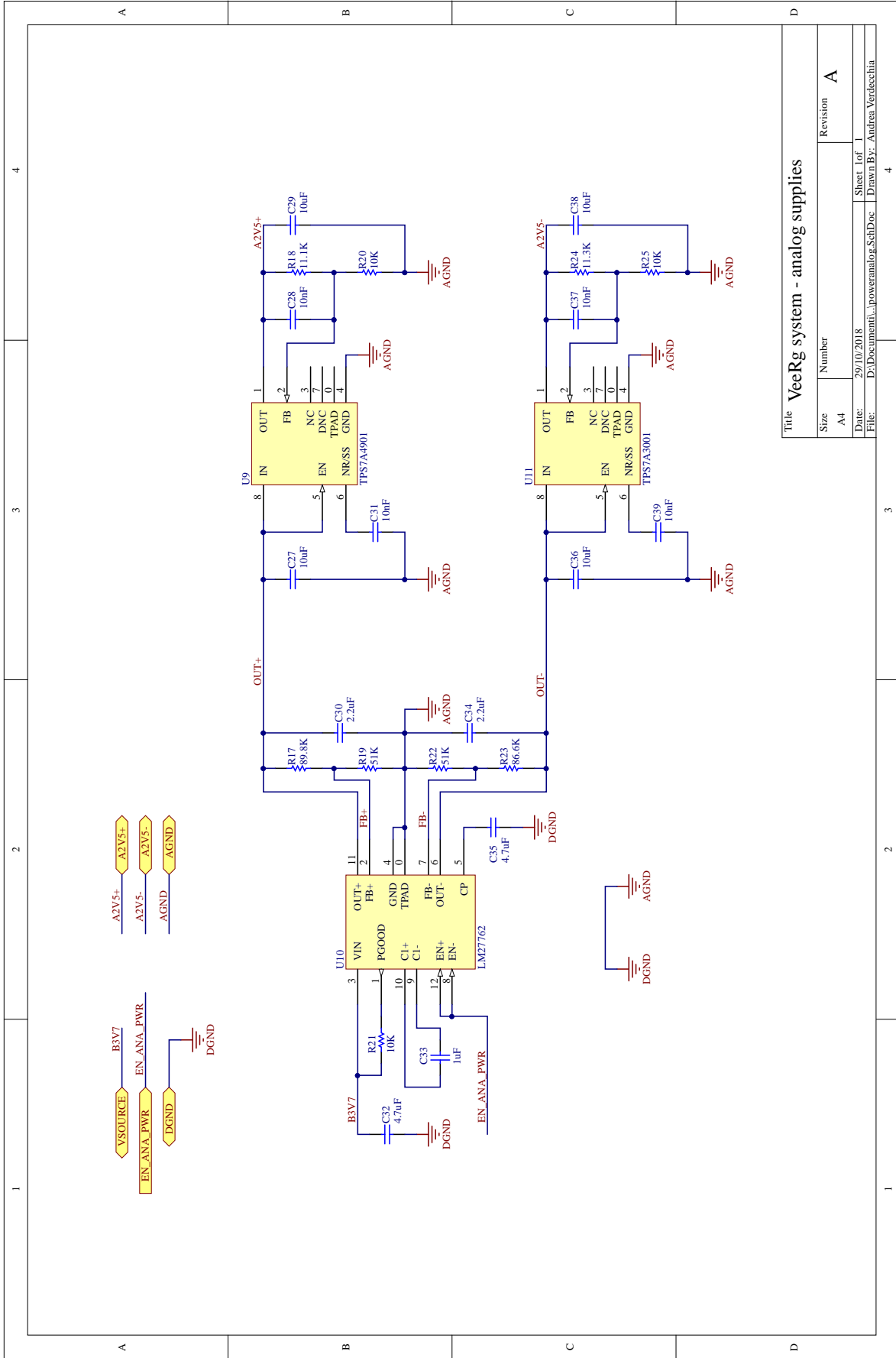


Figure A.12: Analog supplies block.

A.2 Code

A.2.1 Biquad filters

Following the code that implements a digital biquad filter in direct form 2 which requires only two delay registers. This type of filter is a second-order recursive linear filter containing two poles and two zeros.

```

1  /****
2  Function:
3  double Filter_IIR_Biquad_Sec( double, double *, double *,
   uint32_t )
4
5  Remarks:
6  See prototype in filters.h.
7  */
8
9  double
10 Filter_IIR_Biquad_Sec( double signal, double *coeffs, double *
   scaleValues, double *delayLine, uint32_t nSections )
11 {
12     uint32_t i, j;
13     double y = signal;
14     double w = 0.0;
15
16     for ( j = 0; j < nSections; j++ )
17     {
18         // The denominator
19         w = y;
20         for ( i = 0; i < 2; i++ )
21             w -= coeffs[ ( j << 2 ) + i ] * delayLine[ ( j << 1 ) + i
   ];
22
23         // The numerator
24         y = w;
25         for ( i = 0; i < 2; i++ )
26             y += coeffs[ ( j << 2 ) + i + 2 ] * delayLine[ ( j << 1 )
   + i ];
27
28         y *= scaleValues[ j ];
29
30         // Shift the register values
31         delayLine[ ( j << 1 ) + 1 ] = delayLine[ j << 1 ];
32         delayLine[ j << 1 ] = w;
33     }
34

```

```

35     return y;
36 }
37
38 /****
39 Function:
40 double Filter_HighPass( double, int32_t )
41
42 Remarks:
43 See prototype in filters.h.
44 */
45
46 double
47 Filter_HighPass( double x, uint32_t n )
48 {
49     return Filter_IIR_Biquad_Sec( x, highpassCoeff,
50         highpassScaleValues, highpassDelayLine[ n ],
51         NUM_IIR_BIQUAD_HIGHPASS_SECTIONS );
52 }
53
54 /****
55 Function:
56 double Filter_LowPass( double, int32_t )
57
58 Remarks:
59 See prototype in filters.h.
60 */
61
62 double
63 Filter_LowPass( double x, uint32_t n )
64 {
65     return Filter_IIR_Biquad_Sec( x, lowpassCoeff,
66         lowpassScaleValues, lowpassDelayLine[ n ],
67         NUM_IIR_BIQUAD_LOWPASS_SECTIONS );
68 }

```

A.2.2 Commands decoder

Following the implementation of command decoder which check the presence of markers to confirm the validity of incoming packet.

```

1
2 /****
3 Function:
4 void NGSC_CommandDecoder( uint8_t )
5

```

```
6  Remarks:
7  See prototype in NGSC.h.
8  */
9
10 void NGSC_CommandDecoder( uint8_t data )
11 {
12     static uint8_t tempCommand, tempChannelMask;
13
14     switch( commandDecoderState )
15     {
16         case NGSCCheckHeadingState:
17             if ( data == COMMAND_SOH )
18                 commandDecoderState = NGSCCheckStartOfPacketState;
19             else
20             {
21                 if ( NGSCVerbose )
22                     printf( "\nNGSC Error: Wrong packet" );
23                 commandDecoderState = NGSCCheckHeadingState;
24             }
25             break;
26
27         case NGSCCheckStartOfPacketState:
28             if ( data == COMMAND_STX )
29                 commandDecoderState = NGSCDecodeCommandState;
30             else
31             {
32                 if ( NGSCVerbose )
33                     printf( "\nNGSC Error: Wrong packet" );
34                 commandDecoderState = NGSCCheckHeadingState;
35             }
36             break;
37
38         case NGSCDecodeCommandState:
39             switch( data )
40             {
41                 case NGSCCommandCheckSPICommunication:
42                     tempCommand = NGSCCommandCheckSPICommunication;
43                     commandDecoderState = NGSCCheckEndOfPacketState;
44                     break;
45
46                 case NGSCCommandStartConversions:
47                     tempCommand = NGSCCommandStartConversions;
48                     commandDecoderState = NGSCCheckEndOfPacketState;
49                     break;
50
```

```
51  [.....]
52
53      case NGSCCommandFilterLowPassOn:
54          tempCommand = NGSCCommandFilterLowPassOn;
55          commandDecoderState = NGSCCheckEndOfPacketState;
56          break;
57
58      case NGSCCommandFilterLowPassOff:
59          tempCommand = NGSCCommandFilterLowPassOff;
60          commandDecoderState = NGSCCheckEndOfPacketState;
61          break;
62
63      case NGSCCommandFilterCombNotch500n:
64          tempCommand = NGSCCommandFilterCombNotch500n;
65          commandDecoderState = NGSCCheckEndOfPacketState;
66          break;
67
68      case NGSCCommandFilterCombNotch500ff:
69          tempCommand = NGSCCommandFilterCombNotch500ff;
70          commandDecoderState = NGSCCheckEndOfPacketState;
71          break;
72
73      case NGSCCommandFilterHighPass010n:
74          tempCommand = NGSCCommandFilterHighPass010n;
75          commandDecoderState = NGSCCheckEndOfPacketState;
76          break;
77
78      case NGSCCommandFilterHighPass010ff:
79          tempCommand = NGSCCommandFilterHighPass010ff;
80          commandDecoderState = NGSCCheckEndOfPacketState;
81          break;
82
83      case NGSCCommandReset:
84          tempCommand = NGSCCommandReset;
85          commandDecoderState = NGSCCheckEndOfPacketState;
86          break;
87
88      default:
89          if ( NGSCVerbose )
90              printf( "NGSC Error: Cannot decode command\r\n" );
91          tempCommand = 0;
92          tempChannelMask = 0;
93          commandDecoderState = NGSCCheckHeadingState;
94      }
95      break;
```

```
96
97     case NGSCChannelMaskState:
98         tempChannelMask = data;
99         commandDecoderState = NGSCCheckEndOfPacketState;
100        break;
101
102     case NGSCCheckEndOfPacketState:
103         if ( data == COMMAND_ETX )
104         {
105             Command_Received.command = tempCommand;
106             Command_Received.channelMask = tempChannelMask;
107             Command_Received.valid = true;
108             tempCommand = 0;
109             tempChannelMask = 0;
110             commandDecoderState = NGSCCheckHeadingState;
111
112             NGSC_CommandHandler();
113         }
114         else
115         {
116             if ( NGSCVerbose )
117                 printf( "\nNGSC Error: Wrong packet" );
118             tempCommand = 0;
119             commandDecoderState = NGSCCheckHeadingState;
120         }
121        break;
122
123     default:
124         if ( NGSCVerbose )
125             printf( "\nNGSC Error: Wrong state identifier" );
126         tempCommand = 0;
127         commandDecoderState = NGSCCheckHeadingState;
128    }
129
130    return;
131 }
```

List of Figures

1.1	Membrane potential.	8
1.2	Brain's waves classification.	9
1.3	10-20 electrodes' arrangement.	11
1.4	3D model for the placement of electrodes.	13
2.1	The main steps of workflow.	16
2.2	Overview of system's boards.	17
2.3	Background noise of the system.	19
2.4	Background noise of the system.	20
2.5	The body and the common mode noise.	21
2.6	The common mode effect.	22
2.7	The FL schematic.	24
2.8	Dependence of common mode signal from variable C_{bl} , C_{be} and C_{se}	25
2.9	The CM characteristic disjointed into the two contributions F and E	27
2.10	The effect of R_p on the f_{z1} value.	30
2.11	Electrodes mismatch schematic.	31
2.12	CM2DM in electrodes mismatch.	34
2.13	Single-ended and differential nput stages mismatch.	35
2.14	CM2DM in single-ended input stages mismatch.	37
2.15	CM2DM in differential input stages mismatch.	38
2.16	Stability in the feedback loop.	39
2.17	Instability in the feedback loop.	40
2.18	Simplified representation of the condition necessary between A and $1/\beta$ to keep stability.	42
2.19	The data and command packets.	44
2.20	The overall structure of the implemented firmware.	45
2.21	Example of characteristics of an high-pass filter.	50
2.22	The filters' response in low-pass and high-pass cases.	52
2.23	The low-pass filter effects.	54

2.24	The high-pass filter effects.	55
2.25	The 0.1 Hz high-pass filter effects.	56
2.26	Overview of system's boards.	59
2.27	Overview of systems.	60
3.1	Arosual and valence space in emotion classification.	62
3.2	Example of NPVs in case of like and dislike statment.	65
3.3	Brain's activity for different frequencies band in case of like and dislike statement.	66
3.4	Example of images for the War/Cubs test.	68
3.5	Normalized Power Values of the Tattuo test.	71
3.6	Normalized Power Values of the War/Cubs test.	72
3.7	Normalized Power Values of the Models/Growths test.	73
3.8	P-values of β paramenters relatives to every test.	74
A.1	Block schematic of overall VeeRg system.	82
A.2	Bluetooth block.	83
A.3	PIC23MZ block.	84
A.4	MPU9250 block.	85
A.5	ADS1299 block.	86
A.6	Electrodes block.	87
A.7	ICSP block.	88
A.8	Power block.	89
A.9	USB interface block.	90
A.10	Power path manager block.	91
A.11	Digital supplies block.	92
A.12	Analog supplies block.	93

Manuals

- [7] Texas Instruments. *-36V, -200mA, ULTRALOW-NOISE, NEGATIVE LINEAR REGULATOR*. URL: <http://www.ti.com/lit/ds/symlink/tps7a3001-ep.pdf>.
- [8] Texas Instruments. *ADS1299-x Low-Noise, 4-, 6-, 8-Channel, 24-Bit, Analog-to-Digital Converter for EEG and Biopotential Measurements*. Rev. C. URL: <http://www.ti.com/lit/ds/symlink/ads1299.pdf>.
- [9] Texas Instruments. *Improving Common-Mode Rejection Using the Right-Leg Drive Amplifier*. URL: <http://www.ti.com/lit/an/sbaa188/sbaa188.pdf>.
- [10] Texas Instruments. *LM27762 Low-Noise Positive and Negative Output Integrated Charge Pump Plus LDO*. Rev. B. URL: <http://www.ti.com/lit/ds/symlink/lm27762.pdf>.
- [11] Texas Instruments. *TPS7A49 36-V, 150-mA, Ultralow-Noise, Positive Linear Regulator*. Rev. E. URL: <http://www.ti.com/lit/ds/symlink/tps7a49.pdf>.
- [19] Microchip. *PIC32MZ Embedded Connectivity with Floating Point Unit (EF) Family*. Rev. E. URL: <http://ww1.microchip.com/downloads/en/DeviceDoc/60001320E.pdf>.

Articles

- [2] C. Assambo et al. “Determination of the Parameters of the Skin-Electrode Impedance Model for ECG Measurement”. In: (2007).
- [4] Joann Difede and Hunter G. Hoffman. “Virtual Reality Exposure Therapy for World Trade Center Post-traumatic Stress Disorder: A Case Report”. In: *CyberPsychology and Behavior* 5.6 (2004).
- [6] Yongbin Gao, Hyo Jong Lee, and Raja Majid Mehmood. “Deep learning of EEG signals for emotion recognition”. In: *2015 IEEE International Conference on Multimedia and Expo Workshops (ICMEW)* (2015).
- [12] Zhang J. et al. “ReliefF-Based EEG Sensor Selection Methods for Emotion Recognition”. In: *Sensors* 16.10 (2016).
- [13] Nitin Kumar, Kaushikee Khaund, and Shyamanta M. Hazarika. “Bispectral Analysis of EEG for Emotion Recognition”. In: *Procedia Computer Science* 84 (2016), pp. 31–35.
- [14] Mi Li et al. “Emotion recognition from multichannel EEG signals using K-nearest neighbor classification”. In: *Technology and Health Care* 26 (2018).
- [15] Wei Liu, Wei-Long Zheng, and Bao-Liang Lu. “Emotion Recognition Using Multimodal Deep Learning”. In: *Neural Information Processing* (2016), pp. 521–529.
- [16] M. A. Lopez-Gordo, D. Sanchez-Morillo, and F. Pelayo Valle. “Dry EEG Electrodes”. In: *MDPI - Sensors* (2014).
- [17] Burkhard Maess, Erich Schröger, and Andreas Widmann. “High-pass filters and baseline correction in M-EEG analysis”. In: *Journal of Neuroscience Methods* 266 (2016), pp. 164–165.
- [18] I. Marshall and J. M. Neilson. “Mains interference in ECG recording”. In: *Journal of Medical Engineering and Technology* 8.4 (1984), pp. 177–180.

- [20] Zeynab Mohammadi, Javad Frounchi, and Mahmood Amiri. “Wavelet-based emotion recognition system using EEG signal”. In: *Neural Computing and Applications* 28.8 (2017), pp. 1985–1990.
- [21] R. Pallas-Areny. “Interference-rejection characteristics of biopotential amplifiers: a comparative analysis”. In: *IEEE Transactions on Biomedical Engineering* 35.11 (1988), pp. 953–959.
- [23] Albert Rizzo et al. “Virtual Reality Exposure for PTSD Due to Military Combat and Terrorist Attacks”. In: *Journal of Contemporary Psychotherapy* 45.4 (2015), pp. 255–264.
- [24] Barbara O. Rothbaum et al. “Virtual reality exposure therapy for Vietnam veterans with post-traumatic stress disorder”. In: *The Journal of Clinical Psychiatry* 68.8 (2001), pp. 617–622.
- [25] Levenson R.W. et al. “Emotion and autonomic nervous system activity in the Minangkabau of west Sumatra”. In: *Journal of Personality and Social Psychology* 62.6 (1992), pp. 972–988.
- [28] Zhongbin Su et al. “AHRS Design based on STM32 and MEMS Sensors”. In: *International Journal of Control and Automation* 8.7 (2015), pp. 55–66.
- [29] Shravani Sur and V. K. Sinha. “Event-related potential: An overview”. In: *Industrial Psychiatry Journal* 18.1 (2009), pp. 70–73.
- [30] Darren Tanner, Kara Morgan-Short, and Steven J. Luck. “How inappropriate high-pass filters can produce artifactualeffects and incorrect conclusions in ERP studiesof language and cognition”. In: *Psychophysiology* (2015).
- [31] Darren Tanner et al. “On high-pass filter artifacts (they’re real) and baseline correction (it’s a good idea) in ERP-ERMF analysis”. In: *Journal of Neuroscience Methods* 266 (2016), pp. 166–170.
- [32] Nattapong Thammasan, Ken-Ichi Fuki, and Masayuki Numao. “Application of deep belief networks in EEG-based dynamic music-emotion recognition”. In: *International Joint Conference on Neural Networks* (2016).
- [33] Rufin VanRullen. “Four common conceptual fallacies in mapping the time course of recognition”. In: *Frontiers in Psychology* 365.2 (2011).
- [34] Giovanni Vecchiato et al. “Changes in Brain Activity During the Observation of TV Commercials by Using EEG, GSR and HR Measurements”. In: *Brain Topography* 23 (2010), pp. 165–179.

- [35] Li Wang, Zheng Zhang, and Ping Sun. “Quaternion-based Kalman Filter for AHRS Using an Adaptive-step Gradient Descent Algorithm”. In: *International Journal of Advanced Robotic Systems* (2015).
- [36] Xiao-Wei Wang, Dan Nie, and Bao-Liang Lu. “Emotional state classification from EEG data using machine learning approach”. In: *Neurocomputing* 129 (2014), pp. 94–106.
- [37] Andreas Widmann, Erich Schröger, and Burkhard Maess. “Digital filter design for electrophysiological data – a practical approach”. In: *Journal of Neuroscience Methods* 250 (2015), pp. 34–46.
- [38] Haiyan Xu and Konstantinos N. Plataniotis. “Affective states classification using EEG and semi-supervised deep learning approaches”. In: *2016 IEEE 18th International Workshop on Multimedia Signal Processing (MMSP)* (2017).
- [39] Ashkan Yazdani et al. “Multimedia content analysis for emotional characterization of music video clips”. In: *EURASIP Journal on Image and Video Processing* (2013).
- [40] Bülent Yilmaz et al. “Like/dislike analysis using EEG: Determination of most discriminative channels and frequencies”. In: *Computer Methods and Programs in Biomedicine* 113 (2014), pp. 705–713.
- [41] Quanzeng You et al. “Building a Large Scale Dataset for Image Emotion Recognition: The Fine Print and the Benchmark”. In: *Association for the Advancement of Artificial Intelligence* (2011).

Books

- [3] Cédric Assambo and Martin J. Burke. *Low-Frequency Response and the Skin-Electrode Interface in Dry-Electrode Electrocardiography, Advances in Electrocardiograms - Methods and Analysis*. Richard Millis, 2012.
- [22] Robert Plutchik. *Emotions and life : perspectives from psychology, biology, and evolution*. 1st. American Psychological Association, 2003.
- [26] American National Standard. *Ambulatory electrocardiographs*. Arlington (VA): Association for the Advancement of Medical Instrumentation, 1999.
- [27] International Electrotechnical Commission Standard. *Medical electrical equipment*. International Standards et al., 2008.

Other References

- [1] Sharad Agarwal. *Advertising with and without social messages: insights from neuro marketing*. FPM - IIM Ranchi. 2013.
- [5] Paul Ekman. “Handbook of Cognition and Emotion”. In: ed. by Power-M. Dagleish T. 1999. Chap. Basic emotions.